UNIVERSIDAD DE INVESTIGACIÓN DE TECNOLOGIA EXPERIMENTAL YACHAY

Escuela de Ciencias de la Tierra, Energía y Ambiente

TÍTULO: ASSESSMENT OF SOLAR RADIATION IN THE ANDEAN REGION OF ECUADOR USING SATELLITE ESTIMATES AND GROUND MEASUREMENTS

Trabajo de integración curricular presentado como requisito para la obtención del título de Geóloga

Autor:

Ortiz Pulgarin Karen Belén

Tutor:

PhD – Pineda Ordoñez Luis

Urcuquí, Julio del 2022

SECRETARÍA GENERAL
ESCUELA DE CIENCIAS DE LA TIERRA, ENERGÍA Y AMBIENTE
CARRERA DE GEOLOGÍA
ACTA DE DEFENSA No. UITEY-GEO-2022-00005-AD

En la ciudad de San Miguel de Urcuquí, Provincia de Imbabura, a los 1 días del mes de julio de 2022, a las 13:00 horas, en el Aula S_CAN de la Universidad de Investigación de Tecnología Experimental Yachay y ante el Tribunal Calificador, integrado por los docentes:

Presidente Tribunal de Defensa	Mgs. CARLOSAMA MOREJON, FELIPE JAVIER
Miembro No Tutor	Mgs. PEREZ ROA, RICHARD ANSELMI
Tutor	Dr. PINEDA ORDOÑEZ, LUIS EDUARDO , Ph.D.

Se presenta el(la) señor(ita) estudiante **ORTIZ PULGARIN, KAREN BELEN**, con cédula de identidad No. **0105707376**, de la **ESCUELA DE CIENCIAS DE LA TIERRA, ENERGÍA Y AMBIENTE**, de la Carrera de **GEOLOGÍA**, aprobada por el Consejo de Educación Superior (CES), mediante Resolución **RPC-SE-10-No.031-2016**, con el objeto de rendir la sustentación de su trabajo de titulación denominado: **ASSESSMENT OF SOLAR RADIATION IN THE ANDEAN REGION OF ECUADOR USING SATELLITE ESTIMATES AND GROUND MEASUREMENTS** , previa a la obtención del título de **GEÓLOGO/A**.

El citado trabajo de titulación, fue debidamente aprobado por el(los) docente(s):

Tutor	Dr. PINEDA ORDOÑEZ, LUIS EDUARDO , Ph.D.

Y recibió las observaciones de los otros miembros del Tribunal Calificador, las mismas que han sido incorporadas por el(la) estudiante.

Previamente cumplidos los requisitos legales y reglamentarios, el trabajo de titulación fue sustentado por el(la) estudiante y examinado por los miembros del Tribunal Calificador. Escuchada la sustentación del trabajo de titulación, que integró la exposición de el(la) estudiante sobre el contenido de la misma y las preguntas formuladas por los miembros del Tribunal, se califica la sustentación del trabajo de titulación con las siguientes calificaciones:

Tipo	Docente	Calificación
Tutor	Dr. PINEDA ORDOÑEZ, LUIS EDUARDO , Ph.D.	8,2
Miembro Tribunal De Defensa	Mgs. PEREZ ROA, RICHARD ANSELMI	8,9
Presidente Tribunal De Defensa	Mgs. CARLOSAMA MOREJON, FELIPE JAVIER	9,4

Lo que da un promedio de: **8.8 (Ocho punto Ocho)**, sobre 10 (diez), equivalente a: **APROBADO**

Para constancia de lo actuado, firman los miembros del Tribunal Calificador, el/la estudiante y el/la secretario ad-hoc.

ORTIZ PULGARIN, KAREN BELEN
Estudiante

Firmado electrónicamente por:
KAREN BELEN ORTIZ PULGARIN

Mgs. CARLOSAMA MOREJON, FELIPE JAVIER
Presidente Tribunal de Defensa

Dr. PINEDA ORDOÑEZ, LUIS EDUARDO , Ph.D.
Tutor

Firmado electrónicamente por:
LUIS EDUARDO PINEDA ORDONEZ

Mgs. PEREZ ROA, RICHARD ANSELMI
Miembro No Tutor

Firmado electrónicamente por:
RICHARD ANSELMI

TERÁN ROSALES, ANDREA YOLANDA
Secretario Ad-hoc

Firmado electrónicamente por:
ANDREA YOLANDA TERAN ROSALES

AUTORÍA

Yo, **KAREN BELEN ORTIZ PULGARIN**, con cédula de identidad 0105707376, declaro que las ideas, juicios, valoraciones, interpretaciones, consultas bibliográficas, definiciones y conceptualizaciones expuestas en el presente trabajo; así cómo, los procedimientos y herramientas utilizadas en la investigación, son de absoluta responsabilidad de la autora del trabajo de integración curricular. Así mismo, me acojo a los reglamentos internos de la Universidad de Investigación de Tecnología Experimental Yachay.

Urcuquí, Julio del 2022.

_____

Karen Belén Ortiz Pulgarin

CI: 0105707376

AUTORIZACIÓN DE PUBLICACIÓN

Yo, **KAREN BELEN ORTIZ PULGARIN**, con cédula de identidad 0105707376, cedo a la Universidad de Investigación de Tecnología Experimental Yachay, los derechos de publicación de la presente obra, sin que deba haber un reconocimiento económico por este concepto. Declaro además que el texto del presente trabajo de titulación no podrá ser cedido a ninguna empresa editorial para su publicación u otros fines, sin contar previamente con la autorización escrita de la Universidad.

Asimismo, autorizo a la Universidad que realice la digitalización y publicación de este trabajo de integración curricular en el repositorio virtual, de conformidad a lo dispuesto en el Art. 144 de la Ley Orgánica de Educación Superior

Urcuquí, Julio del 2022.

_____

Karen Belén Ortiz Pulgarin

CI: 0105707376

Dedicatoria

Para mi Mimicha y mi Meme, que desde donde quiera que estén, sigan conmigo.

Para mi Geme, Albis, quien es mi otra mitad y mi fuerza, sin vos no hubiese llegado a ningún lado.

Para mi ma, toda mi familia y amigos.

Karen Belén Ortiz

Agradecimientos

Este es un pasito más en mi vida y quiero agradecer a todas las personas que me encontré en este camino. Todos fueron parte de mí y ahora les pertenece un pedacito de mi corazón.

A quien siempre ha estado conmigo, mi luz y mi fuerza en todo momento, mi Geme Albis, gracias por los abrazos, por contestar mis llamadas de madrugada, por ser mi lugar seguro y mi paz, gracias por ser mi soulmate estos 24 años y por haberme apoyado en mis cosas locas siempre.

A mi moms, que siempre sacrifica sus sueños para que yo pueda soñar, que siempre calmó mi ansiedad, aun estando lejos, gracias mami por todo, la vida no me va a alcanzar para devolverte todo lo que has hecho y haces por mí. A mi pa, gracias por tus consejos y por darme fuerza.

A mi Lolis, que, sin tener responsabilidad de nada, me ayudó y me ayuda en lo más difícil de la vida, gracias por cuidarme cuando ni yo mismo puedo hacerlo.

A mi Mimicha y mi Meme, que volaron lejos, pero nunca se fueron. Gracias por hacer de mí una mujer sensible, fuerte y generosa. Gracias mis dos ángeles por estar presentes en cada momento importante de mi vida, gracias por su infinito cariño y gracias por los mejores consejos.

A mis tíos, quienes siempre han estado a mi lado, en lo bueno, malo y triste, Moca, Maño, Willy, Katty, Marcia, Lupis, Fer, Jorge y Mañis. A mis primos, son mi vida.

A mis amigos, gracias por estar en mi vida y llenarme de felicidad. Esto no hubiera sido lo mismo sin ustedes. Gracias Erika por dejarme entrar en tu vida, por convertirte en mi conciencia, en mi pañuelo de lágrimas y en mi seguridad, gracias por abrirme las puertas de tu casa y enseñarme lo que es una amistad sincera, gracias también por convertirte en una hermana que busca lo mejor para mí. Mauro y Daniela, gracias a ustedes pude salir de mis peores momentos, gracias por siempre tenderme una mano, por abrazarme en los momentos más indicados y por no irse nunca, son los mejores amigos que la U me dio. A Danny y Amanda, quienes estuvieron y están desde el primer día que esto empezó, gracias por todas las risas. Gracias a mi compa de estudio de unos cuantos semestres, con quien compartimos un montón de cosas, risas, lágrimas y enojos, gracias Chavo porque la U hubiese sido aburrida sin tus chavadas y sin tu amistad. A mi GeoFamily, ustedes son la prueba de que los amigos son la familia que uno escoge, gracias por las sesiones de estudio, de estrés y de fiesta, gracias María, Jorgito, Profits, Joshua, Negris, Marito, Andy. A mis amigos de Tics, que estuvieron para ayudarme a entender esta vida de programas, algoritmos y cerveza, Bryan, Andy, Henry, Sagu, Steven. La vida no sería lo mismo sin mi Bri y sin mi galapaguito Alex, llegaron a mi vida de manera inesperada y se quedaron para siempre dentro de mi corazón.

Gracias a mi profe Luis Pineda, por la infinita paciencia y por instruirme en este proceso.

Gracias a todas las personas que conforman Yachay Tech, que nunca dudaron en tenderme un mano cuando se presentó algún inconveniente. Gracias a toditos los profes que tuve la suerte de conocer desde los de nivelación hasta los del fin de mi carrera. Gracias Andre por ser el ángel en nuestra escuela y siempre salvarnos de líos. Gracias al cuerpo docente de la escuela de Ciencias de la Tierra, Energía y Ambiente, que sin pensarlo dos veces nos entregaron todos sus conocimientos y su amistad, para que nos formemos como profesionales, pero sin olvidar nuestro lado personal.

A veces las palabras no expresan todo el cariño que uno siente por personas tan increíbles como ustedes, pero quiero que sepan, que cuando yo mire atrás, ustedes serán mi soporte para poder dar el siguiente paso. Infinitas gracias.

Karen Belén Ortiz

RESUMEN

La ubicación del Ecuador representa un gran potencial solar pero debido a la falta de información o datos el uso de este tipo de recurso es limitado. Este estudio tiene como objetivo validar los datos satelitales de radiación solar global y radiación neta obtenidos de Climate and Metereologic Satellite Application Facilities (CM SAF) de la Organización Europea para la explotación de satélites meteorológicos con datos de estaciones meteorológicas de la superficie terrestre de las provincias de Azuay, Chimborazo y Pichincha. También busca obtener los resultados de radiación neta en la parte Andina del Ecuador. Los datos de radiación solar en el período de estudio (2016 a 2018) fueron suministrados por el Instituto de Investigación Geológico y Energético (IIGE) y por la Secretaría de Ambiente del Distrito Metropolitano de Quito (DMQ). Se realizó un análisis de los datos de las estaciones terrestres y satelitales para proceder con la validación. Se aplicaron los comparativos estadísticos entre la información de cada una de las doce estaciones del INER y las cinco estaciones del DMQ y los datos satelitales mediante el uso de diferentes paquetes computacionales disponibles en el software de análisis estadístico R. El resultado comparativo entre los datos satelitales y terrestres de radiación solar global indica que los datos satelitales en escala mensual pueden ser usados siempre y cuando se realice una corrección de sesgo. En promedio el valor del sesgo entre los datos terrestres y satelitales en los dos conjuntos de datos es alrededor del 47% en las provincias estudiadas. Por otro lado, los resultados de la validación de radiación neta muestran que es relativamente confiable usar los datos de cada una de las variables del Balance de Energía Solar en Superficie para obtener la radiación neta debido a que los resultados de la comparación estadística se encuentran dentro de los rangos de error aceptables. Este estudio ha permitido determinar las características particulares del balance radiativo en la sierra ecuatoriana. En las zonas con intensa radiación solar global se presenta una radiación neta alta y constante, mientras que, en zonas de menor altitud, la radiación neta decrece. El albedo y la nubosidad son parámetros que deben ser analizados de manera individual debido a que son parámetros claves en la obtención de la radiación neta.

Palabras clave: radiación solar, radiación neta, datos satelitales, validación.

ABSTRACT

The location of Ecuador represents a great solar potential but due to the lack of information or data the use of this type of resource is limited. This study aims at validating satellite data of global solar radiation and net radiation obtained from Climate and Metereologic Satellite Application Facilities (CM SAF) of the European Organization to exploit meteorological satellites with data from meteorological stations on the ground surface of the provinces of Azuay, Chimborazo, and Pichincha. It also seeks to obtain the results of net radiation in the Andean part of Ecuador. Solar radiation data in the study period (2016 to 2018) were provided by the Instituto de Investigación Geológico y Energético (IIGE) and by the Secretaría de Ambiente del Distrito Metropolitano de Quito (DMQ). An analysis of the data from ground and satellite stations was performed to proceed with the validation. Statistical comparisons were made between the information from each of the twelve INER stations, the five DMQ stations, and the satellite data using different computer packages available in the statistical analysis software R. The comparative result between satellite and terrestrial data of global solar radiation indicates that the satellite data on a monthly scale can be used as long as a bias correction is made. The bias value between ground and satellite data in the two data sets is about 45%.

On the other hand, the results of the net radiation validation show that it is relatively reliable to use the data of each of the variables of the Surface Solar Energy Balance to obtain the net radiation because the results of the statistical comparison are within the accepted errors ranges. This study has allowed us to determine the particular characteristics of the radiation balance in the Ecuadorian highlands. In areas with intense global solar radiation, net radiation is high and constant, while net radiation decreases in lower altitude regions. The albedo and cloudiness are parameters that should be analyzed individually because they are critical parameters in obtaining the net radiation.

Keywords: solar radiation, net radiation, satellite data, validation.

LIST OF FIGURES

LIST OF TABLES

LIST OF EQUATIONS

Chapter 1

Introduction

Energy is the core for the development of life and the world itself. Over the years human beings have been increasing energy consumption to carry out their activities, work, and production. In 2018, fossil fuels represented 84.70% of all primary word energy consumption and the percentages were distributed as follows in 2018: oil with 33.62%, followed by coal with 27.21%, and gas by 23.87% (Dudley, 2018). The main problem with the use of these energy sources is the direct impact on the environment. For example, the high amounts of carbon dioxide (CO_2) and other greenhouse gases emitted into the atmosphere due to the combustion of resources are overheating the planet. Population growth and economic development increase energy consumption; while energy consumption from these non-renewable resources increases, the environmental impact of such activities is observed (Dincer, 1998). To prevent such ecological problems and have a steady energy source to satisfy human requirements, there is a need to find alternative energy sources and technologies to guarantee energy supply in a sustainable and environmentally acceptable way.

The Sun is the closest star to the Earth. It is considered the primary energy source, being the engine that generates the meteorological, climatic, and biological phenomena of our planet. This energy propagates in the form of electromagnetic radiation with different wavelengths. Solar radiation refers to the Sun's energy reaching the Earth's surface. Solar radiation has been recorded on the ground by various meteorological facilities in order to provide reliable data for solar resource assessment. These surface data represent the most accurate records of solar radiation and are also essential for validating satellite-based models which are rapidly becoming the most widely used data for resource assessment (Polo et al., 2016). Different parameters are used to measure the amount and type of solar radiation that reaches the Earth. The most common is global horizontal irradiance (GHI), which is the total incident short-wave radiation received by a horizontal surface (Urraca et al., 2017).

GHI is comprised of three components: direct beam, diffuse, and ground-reflected radiation (Perez et al., 1990). Direct radiation describes the amount of radiation captured by the surface of the atmosphere without any interruption. Diffuse radiation describes the process in which solar radiation reaching the surface of the earth's atmosphere is scattered from its original

direction by molecules in the atmosphere. The reflected radiation is radiation reflected by the earth's surface. The sum of these three radiations corresponds to the total or global radiation received by a surface (Carl, 2014). The location, atmospheric effects, and topography of a place affect solar radiation's amount reaching the surface. In order to obtain reliable solar radiation data, multiple meteorological agencies have historically recorded solar radiation data. The most common one is the GHI or the total short-wave incoming radiation received by a horizontal surface (Polo et al., 2016).

Accurate and precise knowledge of the local solar resource is a prerequisite for successfully deploying any solar energy system. In order for the solar resource to be used in any activity ranging from agriculture to the generation of electricity, quantitative knowledge of resource availability is needed. Fundamental aspects such as short and long-term behavior and solar energy variability help to characterize it. The most important factor that determines the solar resource at the level of the earth's surface is the presence of clouds (Wang et al., 2018). Therefore, the modern way of estimating solar irradiation uses models based on satellite images to obtain information on cloud cover. These models must be adjusted and validated using quality-controlled ground radiation measurements (Suarez, 2017).

High-quality solar surface radiation data are essential for proper monitoring and analysis of the Earth's radiation balance and climate system. They are also crucial for the efficient planning and operation of solar energy systems (Sanchez-Lorenzo et al., 2013). However, well-maintained surface measurements are scarce in many regions of the world including oceans. Thus, satellite-derived information is the exclusive source of observation. This emphasizes the important role of satellite-based surface radiation data (World Metereological Organization, 2008). Solar radiation data are relevant for agricultural research and applications such as estimating reference evapotranspiration and crop water requirements. It is also important for energy planning, as solar radiation data allow a correct evaluation of thermal and photovoltaic systems in plants whose factor capacity is linearly correlated with solar irradiance (Meza & Yebra, 2016).

Solar radiation data is used in the calculation of the energy balance or net energy of the earth's surface. Net radiation is a fundamental parameter that governs the climate of the lower layers of the atmosphere and depends on the structure and composition of the atmosphere, cloud cover, albedo, emissivity, temperature, humidity and soil properties. (Salcedo et al., 2001). It is also the driving force behind several physical, dynamic and biological processes, such as soil and air heating, photosynthesis, and evapotranspiration, the latter being used to optimize crop quality and yield and water resource planning (Geraldo-Ferreira et al., 2011); and its

current use in the conversion of this energy into photovoltaic and thermal (Gueymard & Myers, 2008). Solar radiation that reaches the earth's atmosphere can be considered constant for meteorological purposes, despite slight changes in Earth's position relative to the Sun and solar activity cycles. As it passes through the atmosphere, solar radiation is attenuated depending on the atmospheric components and the presence of gases and clouds (Polo, 2010). The determination of the Earth's radiation balance is essential for modeling studies in the field of atmospheric sciences. In particular, expressing the energy balance on a regional scale is necessary to estimate the local variation of meteorological, climatic, hydrological and biological processes (Laine et al., 1999). In recent years, the radiation balance has been studied using information obtained from soft and ground data. Despite its importance, net radiation is measured with a limited number of standard weather stations because net radiometers are expensive instruments and require constant care in the field (Geraldo-Ferreira et al., 2011).

However, there is uncertainly or great variability in measurements of this renewable resource and therefore, in this regard, it is necessary to find data analysis methods that help to ascertain the whole spectrum of variables used to characterize this resource (Suarez, 2017). Both terrestrial and satellite measuring instruments are used to quantify radiation at the surface. Most of the surface instruments that record radiometric information do so based on the measurement of solar brightness and surface radiation (Augustine et al., 2000).

The satellite images allow covering larger regions. This indirect estimation of solar radiation can be carried out using two models: physical and statistical. The two models are based on an energy balance between the radiation that reaches the atmosphere and the radiation that is reflected by the satellite. The physical model of satellite images takes into account parameters such as absorption, spread, and albedo. On the other hand, the statistical models are based on regressions between the measurements and the information recorded by the satellite. Based on these satellite data, historical estimates of solar radiation can be generated. An important step in the estimation of solar radiation for either method is the validation of satellite data against surface measurements; this latter usually provide data related to other meteorological variables such as temperature, humidity, wind speed, among others, that are used to estimate the balance of solar radiation (Suarez, 2017). Nowadays, due to technological development, the evaluation of solar resources is carried out using data obtained with meteorological satellites, the same ones that help to analyze the components of solar radiation in larger territories. These methodologies have been evolving during the last 30 years, reaching advances in remote sensing and other techniques (Byrne et al., 2015).

In this thesis project, we validate satellite based estimates against surface solar radiation measurements in order to study the solar radiation resource. Furthermore, this work aims at examining energy radiation balances in selected locations in the Andes of Ecuador to contribute to a better understanding of this resource.

1.1. Problem Statement

Approximately the radiant power that reaches the earth is 1353 W/m^2. However this value does not represent the radiant power that reaches the earth's surface due to the influence of atmospheric phenomena such as: reflection in clouds and absorption of gases from the atmosphere (Olcoz Larrayoz et al., 2014). The average annual solar energy potential for the Ecuadorian territory ranges from 183 to 195.83 Wh/m^2 (Vaca et al., 2019). Ecuador has great stability in terms of annual radiation perceived since it remains almost constant throughout the year. The "Atlas Solar de Ecuador" (CONELEC, 2008) reflects the indices of global, diffuse, and direct radiation in the country (Table 1). Solar radiation indices show very low variability between the months of highest and lowest irradiation. The annual average value of global radiation in Ecuador is approximately 183 W/m$^{2\text{-}}$day

Table 1: *Diffuse, Direct and Global Radiation Values*

Month	Diffuse Radiation (Wh/m^2)	Direct Radiation (Wh/m^2)	Global Radiation (Wh/m^2)
JANUARY	122.08	94.17	183.75
FEBRUARY	129.16	76.25	186.66
MARCH	125.00	90.42	194.16
APRIL	118.33	85.42	181.66
MAY	106.66	101.67	178.33
JUNE	101.25	105.00	172.50
JULY	102.92	111.66	179.58
AUGUST	110.83	112.50	192.50
SEPTEMBER	111.66	127.50	207.08
OCTOBER	116.25	117.50	203.75
NOVEMBER	112.08	130.41	205.83
DECEMBER	112.50	126.66	201.66

Note: Retrieved from CONELEC. (2008). Atlas solar del ecuador. *Conelec*, 1–51. http://www.conelec.gob.ec/archivos_articulo/Atlas.pdf

Due to the great abundance of green energy resources such as solar, hydraulic, geothermal, eolic and biomass; Ecuador's energy matrix has potential to harness these sources and bring benefit to society. They are characterized as being economically viable, and particularly solar radiation plays an important role in surface meteorological conditions, energy balance and its applications.

Even though Ecuador has great solar potential, this type of resource in the energy matrix is low. As an example, in the Ecuadorian electricity matrix, the energy generated by photovoltaic solar technology covered only 0.14% of the national demand in 2016 (ARCONEL, 2020). There are few studies in the country dedicated to the assessment of this resource, but also there are not enough surface data that can be used for such studies. Many meteorological stations do not measure solar radiation, they just register other variables such as precipitation, pressure, and temperature (Meza & Varas, 2000).

In Ecuador's case, the scientific need to have accurate solar energy balances is paramount when understanding local hydro-meteorological and biological processes as well as starting engineering projects based on the use of solar resources. The information on the solar resource in Ecuador would be the basis for many projects that seek to use this type of energy. As previously mentioned, the low coverage of the stations and the lack of meteorological information in the national territory makes it necessary to use another source of information to improve the temporal resolution and spatial cover of surface radiation, such as satellite images. Satellite solar radiation data are usually erroneous due to their resolution, while surface data are more accurate, the only disadvantage of this type of direct measurements is the small number of stations in the territory and the lack of continuous records. On the other hand, satellite images help to know the solar resource from an hourly scale to an annual scale with a resolution of approximately 1-2 km over a specific area (Paulescu et al., 2013).

Nevertheless, satellite data cover large areas and can reach those areas of the territory with a challenging access, so they are useful in both short- and long-term monitoring. In order to use satellite data for solar resource monitoring and assessment in Ecuador, it is necessary to validate these data with ground measurements.

1.2. Objectives

2.1.1. General Objectives

The objective of this study is to assess the potential of solar radiation estimates to obtain surface energy balances and identify the potential and drawbacks of satellites products as a primary source of information for solar radiation in the highlands of Ecuador.

2.1.2. Specific Objectives

- To evaluate satellite products of solar radiation by validating the Surface Incoming Short-wave Radiation (SIS) satellite data and Net Radiation obtained from Climate and Meteorological Satellite Application Facilities (CM SAF) against the Global Horizontal Irradiation (GHI) data obtained from ground stations on a daily and monthly scale.
- To calculate the Surface Energy Balance using the variables obtained from CM SAF, the CM SAF Cloud, Albedo and Surface Radiation dataset from AVHRR data – second edition of Cloud, Albedo and Radiation Data (CLARA-A2).

Chapter 2

Theoretical Framework

2.2.   Solar Radiation

The Earth's atmosphere is considered a great thermal machine whose source of energy is the electromagnetic radiation coming from the Sun and which has its origin in nuclear reactions. These reactions take place in the sun's nucleus as a result of the continuous transformation of hydrogen into helium (Volpe, 2014).

The Sun represent the primary source of energy for the atmosphere, it behaves like a black body. That is, it absorbs and radiates energy at the highest possible rate for a given temperature. Considering a solar temperature of 6000°K, 73.5 X 10^6 J/sm^2 are obtained. From a series of calculations, it can be shown that the amount of energy that reaches the upper layer of the atmosphere is approximately 1353 Wh/m^2. This amount is called the solar constant (Wald, 2018).

The energy emitted by radiation is divided into different wavelengths; thus, solar radiation is divided into 9% ultraviolet radiation, 45% visible light, and 46% infrared radiation. The maximum index of wavelengths is between 0.2 µm and 4 µm with a maximum at 0.5 µm (Figure 1) (Nicol & Concepci, 2019). The spectrum of solar and infrared radiation has been divided into short and long wave radiation, with the aim of having a simple classification that allows differentiating the wavelength, thus, the short wavelength represents the solar radiation (Caldwell et al., 1989).
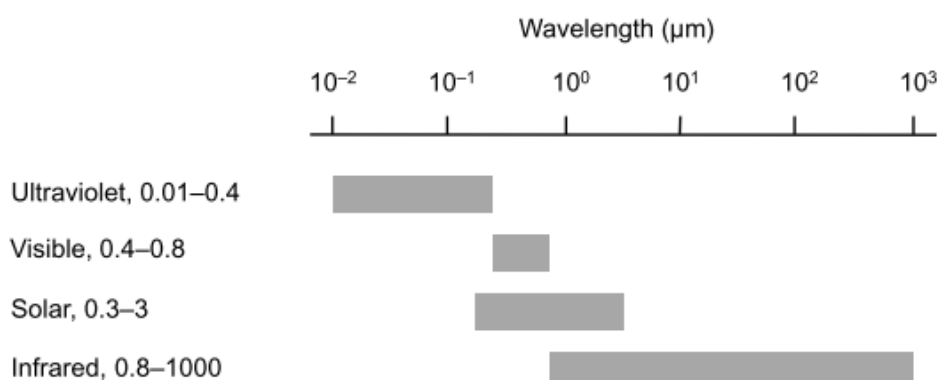

Figure 1. *Common wavelength bans in the spectrum of electromagnetic radiation.*

Retrieved from: (Munkhammar, 2019).

2.2.1. Irradiance and Insolation

Irradiation is the amount of radiant energy that reaches a given surface in a given time. On the other hand, irradiance is an instantaneous measure of solar energy in a given area; its units are W/m^2. Insolation represents a measure of accumulated energy measured in an area during a defined time period: hourly, daily, monthly, or annually. Insolation is measured in KWh/m^2. Therefore, irradiance is power, and insolation is defined as energy (Wald, 2018). By combining these two concepts, irradiance measurements can be defined, interpreted, and studied, for example, direct normal irradiance (DNI), extraterrestrial irradiance (Ea), diffuse horizontal irradiance (DHI), global horizontal irradiance (GHI) (Vignola et al., 2019).

2.2.2. Incoming Solar Radiation

The spectral distribution of solar energy that falls on the Earth's atmosphere is relatively constant, while the solar radiation that falls on the Earth's surface varies according to the distribution of solar radiation in space and the components that make up the Earth's atmosphere. Atmospheric effects, including absorption and dispersion; local variations in the atmosphere, such as water vapor, clouds, and pollution; latitude of the place; and the season of the year and the time of day have various impacts on the solar radiation received at the earth's surface. These changes include variations in the total received power, the spectral content of the light, and the angle from which the light strikes a surface. Furthermore, a key change is that the variability of solar radiation in a particular location increases dramatically. Effects such as cloudiness, seasonal variations and the length of the day are responsible for the existence of a noticeable variability in the solar radiation flux (Garg & Prakash, 2000). According to studies, in desert regions there is low variability, as a consequence of local atmospheric phenomena such as the presence of clouds. Equatorial regions have little variability between seasons. As a consequence of this variability, two radiant energy flows are generated: extraterrestrial solar radiation and global solar radiation. The flux of solar radiation that falls on a horizontal plane located at the outer edge of the Earth's atmosphere is known as extraterrestrial solar radiation. Instead, the flux of solar radiation that passes through the Earth's atmosphere and falls onto a horizontal surface of the Earth is known as global solar radiation (Liu & Jordan, 1960). The intensity of extraterrestrial solar radiation that the earth receives from the sun varies according to the distribution of solar radiation in space.

Atmospheric effects have various impacts on solar radiation on the Earth's surface. The main consequences are the reduction of the power of solar radiation by absorption, scattering and

reflection in the atmosphere; the change in the spectral content of solar radiation due to greater absorption or scattering of some wavelengths; the introduction of a diffuse or indirect component in solar radiation; and local variations in the atmosphere (such as water vapor, clouds, and pollution) that have additional effects on incident power, spectrum, and directionality (Liu & Jordan, 1960).

It has been found that most of the heat and light from the Sun falls on the equatorial regions and only a small part goes to the polar areas. This uneven heating of the earth's surface produces a complex circulation of the elements that make up the atmosphere, which move from the warmer regions to the colder ones (Wald, 2018). Through the study of these phenomena it is possible to conclude that there are certain meteorological variables, which, together with influencing atmospheric parameters, produce notable variations in the amount of global solar radiation within which the temperature and atmospheric pressure are considered (Allen, 2009).

The atmosphere is mostly transparent to incoming solar radiation. Considering that 100% of solar radiation reaches the top of the atmosphere, only 25% reaches the Earth's surface directly and 26% is scattered by the atmosphere as diffuse radiation towards the surface, this makes 51% of radiation reaches the earth's surface. 19% is absorbed by clouds and atmospheric gases. The other 30% is lost to space, of this the atmosphere disperses 6%, the clouds reflect 20% and the ground reflects the other 4%. Then the solar radiation that reaches the atmosphere can be scattered, reflected or absorbed by its components. This depends on the wavelength of the transmitted energy and the size and nature of the substance that modifies the radiation (Liou, 2002).

2.2.3. Outcoming Terrestrial Radiation

The 51% of the solar energy that reaches the top of the atmosphere, reaches the surface of the Earth directly or indirectly and is absorbed into the ground. Most of this energy is re-radiated into the sky. But since the Earth has a much lower temperature than the Sun, Earth's radiation is emitted at much longer wavelengths than short-wave solar radiation. Terrestrial radiation is emitted at wavelengths between 1 and 30 µm, within the infrared range of the spectrum, with a maximum at 10 µm, which is why it is also called long-wave radiation or infrared radiation. The atmosphere is transparent to short-wave radiation from the Sun, but it absorbs long-wave terrestrial radiation, therefore the atmosphere is not heated by solar radiation, but is heated from the ground upwards. The further you are from the surface of the Earth, the colder it is, this explains the decrease in temperature with height in the troposphere (Liou, 2002).

2.2.4. Position of the Earth relative to the sun and Temporal and geographical variations in solar energy availability

The solar radiation that is available on the earth's surface per unit area and time, depends on the following factors:

- Latitude: The solar radiation that reaches the earth's surface or a certain receptor depends on where the receiver is located, since the level of solar radiation is different for each of the different terrestrial latitudes; the solar position with respect to the reception point is variable throughout the day and which will determine the angle of incidence of the solar rays on the earth's surface (Rubio et al., 2015)

- Cloudiness: The atmospheric conditions are important, since the radiation will not be the same in cloudy or clear sky conditions, and the orientation of the receiving plane which will witness a more or less direct incidence, depending on the inclination and azimuth of the receptor with respect to the Sun (Rubio et al., 2015)

- Aerosols: The atmospheric aerosol is formed by a set of suspended particles in the atmosphere; tropospheric aerosol is responsible for reducing solar radiation levels significantly in regions that are polluted. The distribution of solar radiation by aerosol effects can reduce solar irradiation at the surface for long wavelengths. Stratospheric aerosol also affects solar radiation levels that reach the surface indirectly, through its effect on stratospheric ozone chemistry (Carl, 2014).

- Seasons: The change of the seasons throughout the year occurs due to the peculiarity that the Earth's axis of rotation is inclined with respect to the plane of the orbit, this causes the Sun's rays to strike differently than what throughout the year in each hemisphere (Nikolov & Petrov, 2014).

- Albedo and altitude: The reflectivity of the ground influences solar radiation both in diffuse radiation, as well as in direct radiation. Albedo data usually have values of less than 10% for vegetation, but they vary for ice and can reach values of 7 to 75% and for snow they reach a value of 20 to 100%. High reflectivity is of great importance in the geographical and seasonal distribution of solar radiation, specifically in cold climates (Nikolov & Petrov, 2014). The levels of solar radiation depend a lot on the altitude above sea level, since the reduction of the layer of air that remains above. Likewise, solar radiation rises with the altitude of the place approximately 10% for each kilometer of elevation. As in meteorological conditions, places higher above sea level receive more solar radiation than those at sea level (Rubio et al., 2015).

The inclination with which the waves of solar radiation impinging on a surface is even more important than the amount of total energy that reaches the atmosphere. The induction will

cause the energy to spread over a large area, decreasing or increasing its intensity (Olmo et al., 1999). The same point of the Earth's surface receives the rays with a different inclination due to the inclination of the Earth's axis of rotation for its plane of orbit around the sun and its spherical shape. Depending on the time of year the energy incident on a square meter of horizontal surface varies considerably. In summer, the sun's rays fall at a greater angle concerning the horizontal, which means that the rays are perpendicular in the areas near the equator in the central hours of the day. In a time period, the incident solar energy is greater in the day's central hours than the sunrise's hours (Wald, 2018).

The axis of rotation of the Earth is 23.45°, and it points to the same place. That produces that one of the hemispheres is more illuminated during the middle of the year. June 21 corresponds to the summer solstice that marks when the northern hemisphere is brighter, while the winter solstice makes the most significant difference in favor of the southern hemisphere (Figueira & Angel, 2015). Midway between the solstices are the equinoxes, where Earth's axis of rotation is perpendicular to the Sun and the Northern and Southern Hemispheres receive equal amounts of radiation (Figure 2) (Munkhammar, 2019). As a result, we can distinguish five areas on Earth: Two polar zones above 66.5° latitude, two temperate zones between 23.45° and 66.5° latitude and an equatorial zone between 23.45 degrees North and South.

The polar zones are characterized because the days are too long in summer, and some last 24 hours. On the other hand, the days in winter are short, and some nights last 24 hours. The energy received is scarce because the height of the sun is lower. The equatorial zone is characterized because the duration of the day and night is constant. Therefore, the solar radiation received is constant and high. In the summer and winter solstices, respectively, the sun is set vertically. Temperate zones are known as transition zones, where the duration of the day and night varies (Zuñiga & Crespo del Arco, 2021)

A key meteorological factor in understanding the distribution of radiation on Earth is the presence of a low-pressure belt at the equator. High cloudiness occurs throughout the year, resulting in a higher absorption capacity of the atmosphere. There is a heat transfer between the equator and the poles, which is why the equatorial and tropical areas are not warmer, and the high latitudes are not as cold. The displacement of the air masses causes this energy flow to work related to convective movements in the intertropical zone and atmospheric disturbances of medium latitudes (Zaror, 2002).
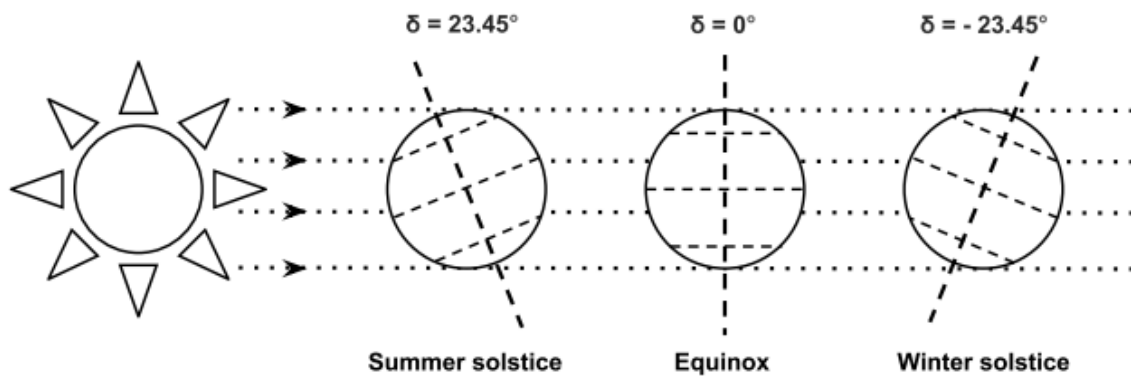
Figure 2. *Earth's tilt relative to the Sun at three particular points in time. Earth's tilt with respect to the direction of incident solar radiation is shown at the summer solstice, the equinoxes and the winter solstice. The corresponding declination (the angle between the Sun's position and the equatorial plane) is shown.*

Retrieved from: (Munkhammar, 2019)

2.3. Earth's Energy Balance

A complicated energy balance is maintained on the earth's surface between incoming short and long wave radiation and outgoing short and long wave radiation. The average amount of energy that the Earth receives is 340J/m^{2}s, which results from dividing the solar constant (1397 J/m^{2}s) by 4. This energy goes through a series of processes and transformations within the climate system that an energy balance model usually represents. Radiant solar or short-wave energy is transformed into sensible heat, latent energy (involving different water states), potential energy, and kinetic energy. Almost one third of the incident solar energy is reflected back into space, while the rest is absorbed in the atmosphere, by oceans and in inorganic and organic matter on Earth. The. The percentage reflected is called albedo. On the other hand, the radiation that reaches the Earth, transmitted by the atmosphere, does so in two ways, direct radiation, and diffuse radiation. The absorbed solar energy drives meteorological and hydrological processes such as winds, waves and ice melting, and it fuels photosynthesis in the biosphere. The diffusion of radiation is the redistribution of energy in the atmosphere since the molecules transmit it by dispersing it. Due to this process, the sky appears illuminated (Battan, 1979).

The whole earth's atmosphere must emit energy to compensate for the incoming energy. The total outgoing energy must be equal to the incoming energy (340 J/m^{2}s) to maintain energy balance (Wald, 2018). The total radiation balance is maintained balanced by long-wave

radiation emitted from the Earth's surface. Greenhouse gases allow for a cycle in which part of the radiation leaves the Earth's surface, and another part radiates back to Earth (Munkhammar, 2019).

The Energy Balance at the surface level can be defined as the way in which the net radiation is distributed in the different biophysical processes present. According to the basic law of conservation of energy (Figure 3). The balance energy equation is the following:

$$S \downarrow (1 - \alpha) + L \downarrow - L \uparrow + H + LvE + G = 0 \qquad (1)$$

And summarizing the radiation fluxes:

$$NR + H + LvE + G = 0 \qquad (2)$$

Where,

NR: Net Radiation

α: albedo

S↓: Surface incoming short-wave radiation or Global Radiation

L↓: Surface downwelling long-wave (atmospheric counter-radiation)

L↑: Outgoing long-wave radiation (terrestrial emission)

H: Sensible heat flux

LvE: Latent heat flux

G: Soil heat flux

Very little of the energy gained by net radiation is stored in the ground G. Most of this energy is emitted as turbulent fluxes of sensible and latent heat. The energy fluxes associated with photosynthesis, heat storage and advection are often neglected in the practice. The soil heat flux G must be determined, in order to carry out an analysis of the impact that the atmosphere produces on the soil's behavior, in this way, the soil heat flux represents the border between the atmosphere and the soil. Obviously, the calculation accuracy of G is conditioned by the calculation accuracy of NR. This balance varies throughout the day and depends on the specific characteristics of the earth's surface (Van den Broeke et al., 2011).
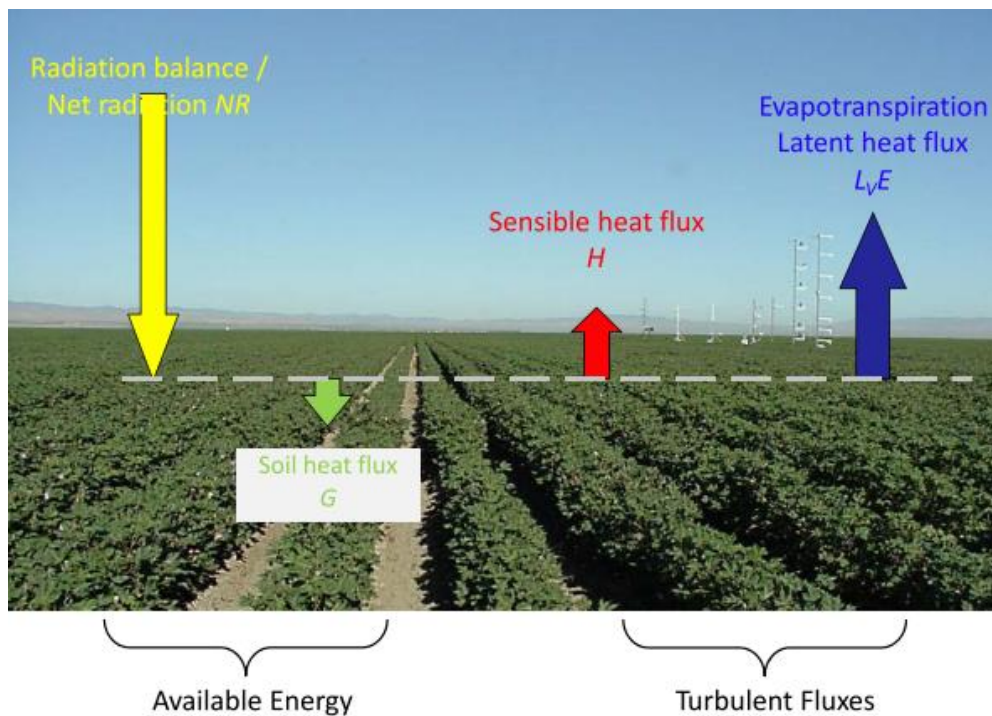
Figure 3. *Surface Energy Balance*

Retrieved from: (Van den Broeke et al., 2011).

2.3.1. Net Radiation

The estimation of net radiation is fundamental when analyzing soil-vegetation-atmosphere interactions in different areas such as agronomy, agriculture, environmental engineering. This radiation is the effective or available energy provided by the sun to ensure soil and air heating and evaporation of surface water (An et al., 2017). The net radiation is the net result of the contributions of short and long wave radiation entering and leaving the surface (Figure 4). It can be determined either by direct measurement or by calculation. Net Radiation is expressed as:

$$NR = S \downarrow (1 - \alpha) + L \downarrow - L \uparrow \ (Wm^{-2}) \tag{3}$$

Where:

α: albedo

S: Surface incoming short-wave radiation

L$\downarrow$: Surface downwelling long-wave radiation

L$\uparrow$: Outgoing long-wave radiation
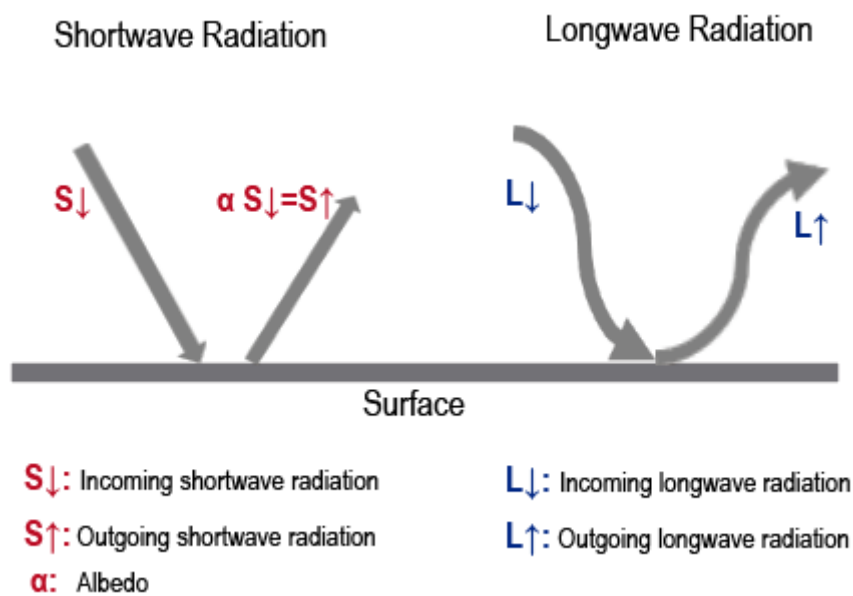
Figure 4. *Net Radiation Budget and it's components.*

2.4. Solar Radiation Data

The availability of solar radiation is considered to be discontinuous due to meteorological events taking place on Earth, which makes its use difficult and limits its competitiveness about other renewable sources. To be able to identify the availability of the resource, it is necessary to analyze different geographic, astronomical, geometric, physical, and meteorological factors (Saffaripour & Mehrabian, 2009). The analysis of all the phenomena that arise when the radiation reaches the earth, allows the evaluation of this resource. The evaluation of solar radiation can be carried out using different methodologies, such as the recording of measurements made in the areas under study, the processing of satellite data and images or the use of physical irradiation calculation models (Chamorro et al., 2015).

2.4.1. Ground Measurements

The meteorological stations placed in strategic points of the territory, instrumentally measure the amount of solar radiation that enters the Earth's surface. These measurements are accurate and provide necessary solar data to be used in the conversion of the solar resource for multiple applications. The sensors that directly record surface radiation information are mainly actinographs, pyrheliometers, pyranometers and heliographs. The pyranometer is an instrument used to measure direct and diffuse global solar radiation on a horizontal surface at an angle of 180 degrees. The measurement is made from the heating difference of two black and white sections on a flat disk (Benavides et al., 2017). When the device is exposed to solar

radiation, the black section increases in temperature compared to the white section. This temperature difference can be detected electronically from the generation of an electrical voltage proportional to the incident solar radiation. In Ecuador, this tool is used mainly for the collection of solar radiation data.

2.4.2. Satellite Data

The Earth is continuously monitored by a large number of meteorological satellites, which are usually classified according to the height of their orbit. In recent years, a series of databases with information on solar energy resources have been developed, this has led to the situation that several different databases exist in parallel, each with a different focus, with different spatial coverage and different times and resolutions (Trentmann et al., 2020).

The observed solar radiation measurements have incorrect spatial and temporal availability, so geostationary satellite information or polar-orbiting over time may be the solution to this problem. Remote sensing would be an alternative to obtain homogeneous solar radiation data in space and time that can be used directly in subsequent applications (Liang, 2004)

In the article Best Practices Handbook for the Collection and Use of Solar Resource Data for Solar Energy Applications, the authors mention several key considerations to consider when looking for sources of solar radiation data. These are: The period of a data record, these solar resources may be available over an average period of 30 years, most databases contain climate time series from the period 1981 to 2010, but will be updated to the period 1991 to 2020 because these periods are updated every ten years. The temporal resolution depends on the type of data. For example, these series can vary from 1-second, hourly, daily, weekly, monthly and annual samples. The units in which these databases present their solar data are generally W/m^2 or the integrated power kWh/m2. Daily irradiance should be expressed in kWh/m^2. Spatial coverage varies according to the availability of satellites; data can be displayed from the region of a station, a city, province, country, continent to a global perspective. Spatial resolution ranges from 3km by 3km to 10km by 10km, depending on pixel size. The variability of solar resource data depends mainly on GHI and DNI data. Data availability can be public, for purchase or licensed (Sengupta et al., 2021).

Chapter 3

Study Area, Data and Methods

This study involves two main parts. The first one corresponds to the validation of the satellite data by comparison with surface data. The validation uses the SIS satellite data retrieved from CM-SAF and GHI surface data corresponding to 26 INER (Instituto Nacional de Eficiencia Energética y Energías Renovables) meteorological stations provided by the Instituto de Investigación Geológico y Energético (IIGE) and to 5 meteorological stations provided by the Distrito Metropolitano de Quito (DMQ) and the information of surface measurements of Net Radiation in the Zhurucay zone, Azuay Province.

In the second part Surface Energy Balances are computed. These balances are useful to record the amount of solar radiation that interacts with the surface. Therefore, they are a great tool to understand the timing and distribution of solar radiation on the Earth's surface and also to carry out solar radiation studies. A correct evaluation of the solar resource depends on the quantity and quality of information available. This section describes the study area, the data used, as well as the applied methodology.

3.1. Study Area

Ecuador is located in the equatorial zone, as a consequence the duration of the day and night is nearly constant. Therefore, the solar radiation received is constant and high. In the country the attenuation of solar radiation by the atmosphere is influenced, both in space and in time by the marine currents, the cold of Humboldt, the warm of El Niño, the great semi-permanent anticyclones in the Atlantic and in the Pacific, the change of position throughout the year of the high pressure areas, the equatorial zone and the Andes mountain range (Baigorria et al., 2004). The factors that determine the climate and its variations correspond to those that affect the rest of the country mainly geographical and meteorological factors, among which the following stand out: latitude, orography (relief-altitude set) and the presence of the Pacific Ocean (Nikolov & Petrov, 2014).

Solar irradiation is constant and of great magnitude all the time. Although two climatological seasons can be defined in the year, this does not imply that the angle of incidence of solar irradiation varies, as is the case of countries located to the north or south of the globe and that have four climatic seasons. Sunny days are often appearing throughout the year regardless

of the season, the variation between the two seasons is mostly in the rainy precipitation. Roughly, in summer (dry season) sunny days are presented with a lot of wind and in winter (wet season) sunny days are followed by heavy rainfall in the afternoon mainly. The differences lie in the proximity to the sun at each time of the year. In the months of July and August the planet Earth is at the closest position to the Sun within its orbit (summer), while in January and February at the farthest point from the Sun within its orbit (winter) (CONELEC, 2008). Because beam irradiance is nearly perpendicular to the country throughout the year, the entire national territory receives a large amount of solar energy; the irradiation intensity varies by several aspects but mainly by the cloudiness of each location particularly in the winter (rainy) season.

Ecuador presents a complex topography due to the presence of the Andes Mountains, in addition to other minor mountain systems with the presence of alternating valleys and ridges, as consequence there is a great variation in climatic conditions. It is divided into three main climatic regions: the western coastal part, which is about 200 km wide in Ecuador, the mountain chain of the Andes, which runs from north to south, with peaks that exceed 6,000 m, which geographically and climatologically separate the coastal zone from the Amazonian lands. In Ecuador this area is known as the Central or Andean Region and the Amazonian basins, also known as the Eastern Region or Oriente. A humid region that is crossed by numerous rivers that flow into the Amazon (Emck, 2007).

The in-year distribution of solar radiation based on the topographic characteristics of Ecuador varies across the different climatic regions as follows:

- Andean Region: During the first 6 months of the year, radiation remains at 4.4 Kwh/m^2-day, while in the following months the radiation increases reaching 4.8 Kwh/m^2-day, the average annual radiation for this region is approximately 4.5 Kwh/m^2-day (CONELEC, 2008).
- Coast Region: During the months of June and July the lowest radiation values, around 3.2 kWh/m^2-day are observed, with the maximum radiation in the months of March and April 4.2 kWh/m^2-day with an average of 3.5 kWh/m^2- day (CONELEC, 2008),
- Amazon region: the lowest radiation occurs from January to June with values of 3.5 kWh/m^2-day, the following months (August November) there are radiation values of 4.2 kWh/m^2-day with an annual average of around 3.8 kWh/m^2-day (CONELEC, 2008).

With latitudes between 0°S and 3°S, the areas of Pichincha, Azuay and Chimborazo provinces lies within the circum planetarian belt of ~±10° where the net radiation balance at the top of the atmosphere is year-round positive (McGregor & Nieuwolt, 1998). Because of their location,

these provinces have excessive radiation from the sun's altitude during the day, and radiation is excessively absorbed, dispersed, and reflected in the atmosphere and surface compared to high latitudes. These low latitudes are characterized by their daily temperatures higher than the average annual, monthly amplitude (Emck, 2007).

Among the databases containing satellite data available for Ecuador are National Aeronautics and Space Administration (NASA) Surface meteorology and solar energy, global solar atlas, National Renewable Energy Laboratory (NREL), CMSAF Cloud, and albedo and Surface radiation. In the article "Assessment of the Solar Resource in Andean Regions by Comparison between Satellite Estimation and Ground Measurements: Study Case of Ecuador", the authors use the data from NREL (NSRDB) to perform the validation, being this to our knowledge the most recent study on this topic (Ordonez et al., 2019).

3.1.1. Solar Seasons in Ecuador

As is already known, in Ecuador, there are no thermal seasons, a division of the year by seasons caused by the Sun is visible. During July, average temperatures are recorded by the low position of the Sun, and the presence of precipitation from the west occurs with the Sun passing the zenith. For these reasons, in the Interandean region, the seasons of the year are differentiated, and water-thermal changes are recorded. These rainy climate changes mean that the maximum daily temperatures are low than on clear days. Radiation indices at these latitudes show that the relationship between the elevation of the sun and the supply of solar energy is not closely related, which shows consequences on the magnitude of solar energy flows, and this also causes solar radiation seasons to be different from astronomical solar seasons (Echegaray-Aveiga et al., 2018).

For the present study, three provinces of Ecuador were considered in which solar radiation is measured and recorded daily, monthly and annually in meteorological stations. The provinces of Azuay, Chimborazo and Pichincha were considered and are located in the Andean part of the country. For the calculations of the net radiation Azuay, Chimborazo and Pichincha are considered. (Figure 5).
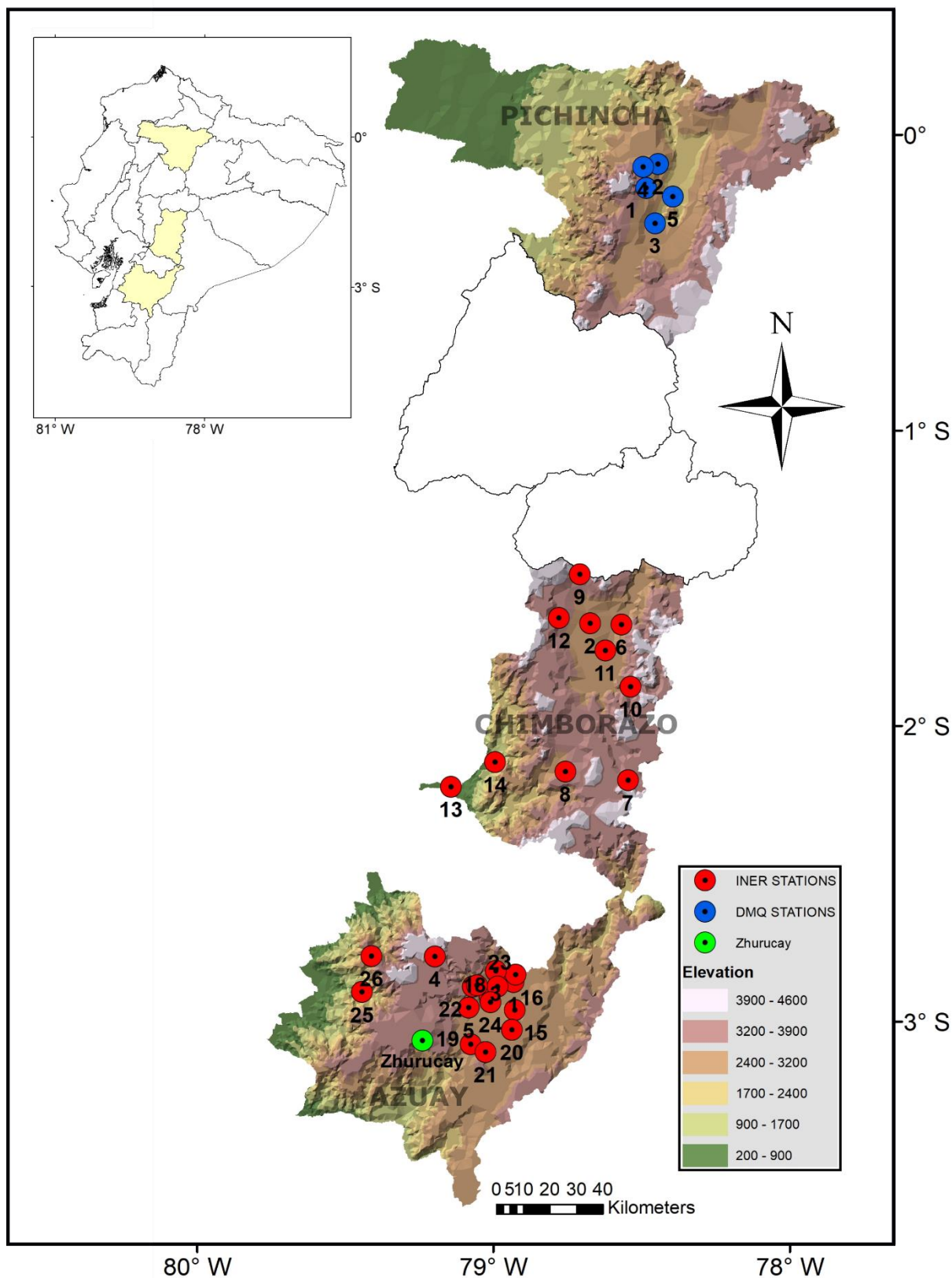
Figure 5. *Study area, Azuay, Chimborazo and Pichincha provinces and location of the 26 IIGE (INER) and DMQ superficial stations.*

3.2.   Datasets

3.2.1. Solar Radiation Data

3.2.1.1.   Satellite Data

CM-SAF products

The European Organization for the Exploitation of Meteorological Satellites (EUMETSAT) has Satellite Application Facilities (SAF) to ensure satellite-based data development and retrieval. They are intended to improve the quality and processing of data from meteorological satellites in the field of meteorology and climatology. The SAF on Climate Watch (CM SAF, http://www.cmsaf.eu/) provides high-quality records for climate applications on both a European and global scale for some products (Woick et al., 2002).

The Satellite Application Facility on Climate Monitoring (CM SAF) develops, produces, archives and disseminates satellite-data-based products to support climate monitoring. The product suite mainly covers parameters related to the energy & water cycle and addresses many of the Essential Climate Variables. The CM SAF produces Climate Data Records (CDR), which are time series of measurements of sufficient length, consistency, and continuity to determine climate variability and change (Woick et al., 2002).

The R Tool Box

Satellite-generated climate data generally cover large areas of territory, so their file sizes are bigger than surface measurement data files, which also implies difficulty in data handling. CM-SAF has implemented a tool that facilitates its product data management called R Tool Box. CM SAF R Toolbox is a set of R-based tools for the preparation, analysis, and visualization of CM SAF NetCDF data (Pfeifroth et al., 2018). It is a simple, step-by-step interface that guides the user through obtaining results such as maps of each variable or product, time series, and even downloading the data at a selected point. The Tool Box has approximately 50 operators developed to optimize the use of satellite data (Kothe et al., 2019).

The Tool Box initialization process is relatively simple. It is a matter of calling the CM-SAF library and then calling the Run Tool Box function (Figure 6(a)). The next step is data preparation, which consists of choosing the NetCDF dataset's tar file. The function of the Prepare option of the Tool Box (Figure 6(b)) is to move from the downloaded tar file to a ready-

to-use NetCDF file, including the extraction of all tar files for each requested product, the selection of the required time range and spatial extent, and finally merging all the settings made NetCDF file which facilitates the time series analysis (Pfeifroth et al., 2018).
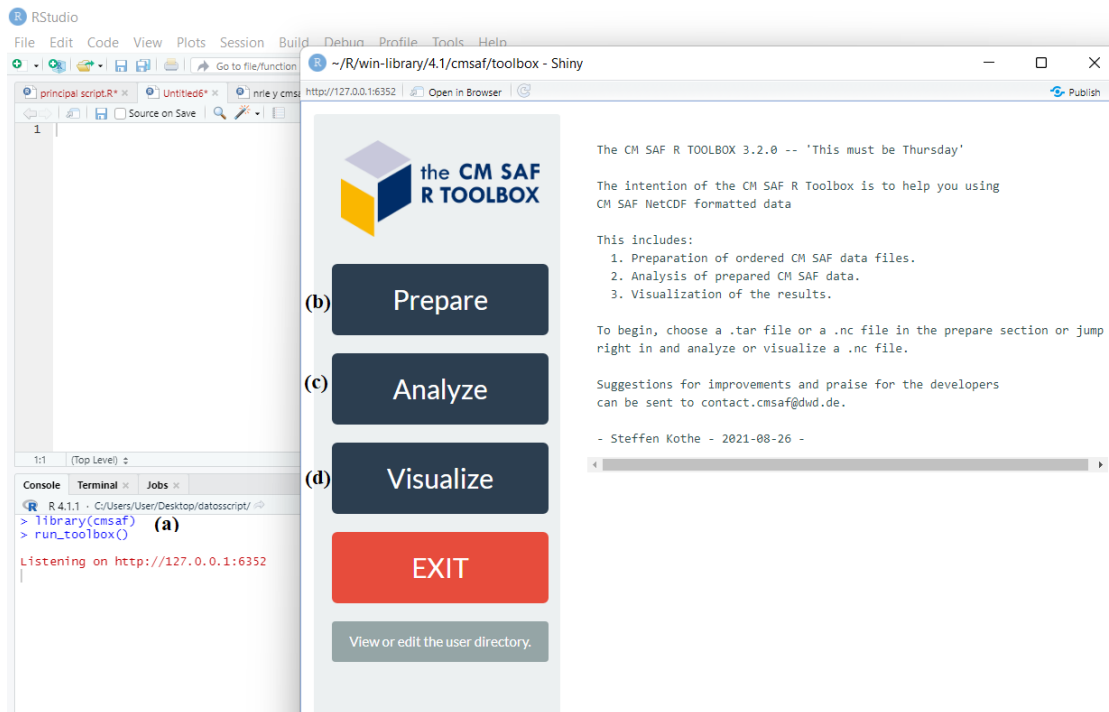
Figure 6. *CM-SAF Tool Box. a) Function of Tool Box. b) Prepare option of Tool Box. c) Analize function of Tool Box. d) Visualize function of Tool Box.*

The data analysis (Figure 6(c)) consists of choosing the NetCDF file generated in the prepare option and breaking down all the information that will be required to use a Tool Box operator, such as the name of the variable or product being analyzed, the operator to be applied, and the name of the input and output file generated (Kothe et al., 2019). As explained above, the user can choose from about 50 operators according to his requirements. The result of these configurations is generated and saved in the chosen output folder.

The Visualize option uses an application based on the R-Shiny package, which focuses on creating interactive web applications (Figure 6(d)). Thanks to this option, the user can create interactive spatial maps in two dimensions or time series in one dimension. Within this option, it is possible to make scale adjustments, color adjustments, axis names configuration. It is also a handy tool since it allows us to visualize the data in statistical graphs such as histograms, box plots, and scatter plots while viewing the metadata (Pfeifroth et al., 2018).

CLARA-A2

CLARA-A2 is an updated dataset produced by EUMETSAT derived from the Advanced Very High-Resolution Radiometer (AVHRR) sensors aboard the polar-orbiting NOAA and METOP satellites. It provides global information on cloud fraction and its properties, surface radiation, and surface albedo from 1982 to 2019 with a spatial resolution of 0.25° × 0.25° (Karlsson et al., 2017). The dataset is available for a period from January 1, 1982 to June 2019. The instantaneous AVHRR images are processed to obtain a spatio-temporally averaged data set consisting of cloud cover, surface albedo, and surface radiation products. CLARA-A2 uses vertically integrated aerosol, vapor, and ozone information, along with the surface albedo product to estimate incoming solar radiation. Daily and monthly mean operational CM SAF products are available aggregated on a 15 km sinusoidal grid (Karlsson et al., 2017).

To perform the validation of the Global Irradiation (GHI) or Surface incoming short-wave radiation (SIS), data from the period 2016 to 2019, were requested directly from the CM SAF company offering this information, since this data is not yet available on the aforementioned webpage. The data was download from the CLARA-A2 climate data record, the same data are provided as daily and monthly means. The monthly and daily SIS means from the CLARA-A2 dataset were validated in this study for the period January 2016 to December 2018 (Table 2).

The retrieval of incoming solar radiation at the surface is based on the method presented in (Mueller et al., 2009), which is based on radiative transfer modeling and allows extended information on the atmospheric state. The precise analysis of the interaction between the atmosphere, surface albedo, transmission, and upper atmospheric albedo. Surface albedo and applied aerosol information are auxiliary data used to distinguish pixels classified as cloudy and clear with Nowcasting SAF software (Trentmann, 2020). For example, if the software identifies a cloudy pixel, it is considered cloudy in the solar radiation retrieval. The temporal averaging of the instantaneous retrieval results at the pixel level is performed following the method, which considers the diurnal cycle of solar radiation. It is necessary to have at least 20 instantaneous observations in each grid cell to calculate the daily average (Trentmann, 2020).

Table 2: CM-SAF, CLARA-A2 datasets used for the validation and in the Energy Balance Surface Calculation.

CM-SAF: CLARA-A2 Products	VARIABLE	Coverage		Resolution
		Temporal	Spatial	Temporal
SIS	Surface incoming short-wave radiation	From 2016 to June of 2019	0.25∘ × 0.25∘	Monthly/Daily
SDL	Surface downward long-wave radiation	From 2016 to June of 2019	0.25∘ × 0.25∘	Monthly
SOL	Surface outgoing long-wave radiation	From 2016 to June of 2019	0.25∘ × 0.25∘	Monthly
SAL	Albedo	From 2016 to June of 2019	0.25∘ × 0.25∘	Montly

3.2.1.2. Ground-Based Data

3.2.1.2.1. Instituto de Investigación Geológico y Energético (IIGE) Solar radiation Data

In surface stations, generally only horizontal global irradiance is measured, so it is the only variable used in validation and quality control. The ex-INER implemented 26 stations to measure solar irradiance (GHI and DHI). This was done in collaboration with the Escuela Politécnica del Chimborazo (ESPOCH) and the Universidad Politécnica Salesiana de Cuenca (UPS) (Ordóñez et al., 2019). The IIGE manages these stations in the country.

INER stations registered the measurements of the CMP6 pyranometer. It performs routine global solar radiation measurements on a flat surface (180°). Its elements are covered with carbon fiber. This pyranometer does not require a power supply because it generates current with the incoming radiation (CMP6*, CMP11, and CMP21 Kipp & Zonen Solar Radiation Sensors _ Manualzz.Pdf*, n.d.)

Global horizontal irradiance (GHI) measurements from stations distributed throughout the country were used to validate the satellite-estimated data from CLARA-A2. The surface solar radiation records were provided by the IIGE and belong to the 26 INER stations located in the central region of the equator, which measure solar radiation. The data provided by the IIGE areas are daily and monthly averages. The GHI monthly and daily averages were collected in this study from January 2016 to December 2018. These stations are located near the cities Riobamba and Cuenca. Table 3 and Figure 6 show the information of the stations.

Table 3: *Name and location of the meteorological stations belonging to the IIGE.*

Station Name	Province	Code	Longitude ° E	Latitude ° S	Elevation (m)
Nulti	Azuay	INER1	-78,94	-2,87	2623
Espoch	Chimborazo	INER2	-78,68	-1,66	2754
Tixan	Azuay	INER3	-78,99	-2,83	2725
Cajas	Azuay	INER4	-79,19	-2,78	3646
Baños	Azuay	INER5	-79,09	-2,96	3062
Quimiag	Chimborazo	INER6	-78,57	-1,66	2709
Altillo	Chimborazo	INER7	-78,55	-2,19	3442
Tixan Pistilli	Chimborazo	INER8	-78,76	-2,16	3546
Urbina	Chimborazo	INER9	-78,71	-1,49	3642
Alao	Chimborazo	INER10	-78,54	-1,87	3064
Tunshi	Chimborazo	INER11	-78,63	-1,75	2840
San Juan	Chimborazo	INER12	-78,78	-1,64	3232
Cumandá	Chimborazo	INER13	-79,15	-2,21	331
Multitud	Chimborazo	INER14	-79.00	-2.13	1483
Santa Ana	Azuay	INER15	-78.93	-2.97	2651
Llacao	Azuay	INER16	-79.03	-2.85	2542
Yanuncay	Azuay	INER17	-79.02	-2.92	2561
El Vecino	Azuay	INER18	-78.99	-2.89	2556
Irquis	Azuay	INER19	-79.08	-3.08	2665
Quingeo	Azuay	INER20	-78.94	-3.03	2895
Cumbe	Azuay	INER21	-79.03	-3.11	3179
San Joaquin	Azuay	INER22	-79.07	-2.89	2764
Sayausi	Azuay	INER23	-79.06	-2.88	2727
Turi	Azuay	INER24	-79.01	-2.94	2768
Chaucha	Azuay	INER25	-79.44	-2.91	1929
Molleturo	Azuay	INER26	-79.41	-2.78	3524

3.2.1.2.2. Distrito Metropolitano de Quito (DMQ) Solar radiation Data

Five meteorological stations were selected in the city of Quito, belonging to the province of Pichincha, to obtain the data corresponding to the global solar radiation. These stations use

the CMP3 pyranometer, that consists of measuring solar irradiance. It contains a thermopile sensor that measures the solar energy received from the total solar spectrum and the entire hemisphere with a field of view of 180 degrees. The data stored by the pyranometer is expressed in watts per square meter. This instrument operates within a temperature range of -40°C to +80°C with a stability of 1% per year. The pyranometer measures global shortwave radiation in the spectral range of 300 to 2800nm and measures irradiance up to 2000 W/m² with a response time of fewer than 20 seconds. The advantage of this pyranometer is that it is easy to install and resistant to natural phenomena (*Campbell Scientific CM3 Kipp and Zonen Pyranometer User Manual*, n.d.).

Table 4: *Name and location of the meteorological stations belonging to the DMQ.*

Station Name	Code	Longitude ° E	Latitude ° S	Elevation (m)
Belisario	DMQ1	-78.49	-0.18	2835
Carapungo	DMQ2	-78.45	-0.10	2660
Cotocollao	DMQ3	-78.50	-0.11	2739
Los Chillos	DMQ4	-78.46	-0.30	2453
Tumbaco	DMQ5	-78.40	-0.21	2485

3.2.2. Net Radiation Data

3.2.2.1. Satellite Net Radiation Data

The satellite data for the calculation of the net radiation in the Zhurucay area for validation with terrestrial data belong to the CM-SAF platform, whose characteristics and specifications are specified in the previous section.

The variables used to calculate the Surface Energy Balance of the CLARA-A2 climate record are provided as monthly means. The variables are: SIS, SAL, SDL, SOL, Table 2 shows the description of each variable.

3.2.2.2. Ground Data

The data used for the validation of the net radiation belong to the study "Actual evapotranspiration in the high Andean grasslands: A comparison of measurement and

estimation methods" conducted at the Zhurucay Ecohydrological Observatory located 32 km from the city of Cuenca, in the province of Azuay (Ochoa-Sánchez et al., 2019). This study measures each component of the balance that interferes with the evapotranspiration process during one year (May 05, 2017-April 04, 2018). Net radiation data is calculated by averaging two radiometers (CNR4 KIPP & Zonen) in the Zhurucay area. This net radiation database is on a monthly scale (Annex 1).

3.3. Methodology

3.3.1. Validation of Global Solar Irradiation Satellite Data

Statistical analysis was performed in R Studio version 4.1.1 (R Core Team, 2021), to read and organize the data as time series, the zoo version 1.8-9 package (Zeileis & Grothendieck, 2005) was used. It was possible to unify the operation interface of the time series through the xts package (Ryan et al., 2020). For the implementation of metrics for the time series, the metrics package was used (Hamner & Frasco, 2018). The readxl (Wickham & Bryan, 2022) function was useful for reading files and openxlsx (Schauberger & Walker, 2021) for reading, writing, and editing Excel files. The ggplot2 package (Wickham, 2016) was used to create the graphs. The Kolmovorov-Smirnof test was performed using the ks.test function, which is included in the stats package (R Core Team, 2021). For the analysis and manipulation of satellite data, the CMSAF toolbox was used, which performs its applications through the functions of the cmsaf library (Kothe, 2021).

3.3.1.1. SIS satellite data extraction

When downloading the data set of the SIS variable from the CM-SAF portal, these data are downloaded in NetCDF format (Kothe et al., 2019), which must be transformed into time series to perform the statistical analysis. The statistical software R was used to carry out the data extraction through the R Tool Box of CM-SAF to obtain the data series.

This process was carried out following the steps of the Tool Box detailed in the dataset description section. The Tar file corresponding to the SIS variable on the hourly scale for the 2016-2018 period was chosen. Subsequently, the file was created in NetCDF format, which, when analyzed, allowed us to choose precisely the location of each point corresponding to the INER meteorological stations. The time series corresponding to each point was then created through this process, and the data were downloaded. Once the 12 time series were obtained,

they were put together in a file to continue validation. The time series are arranged in columns and sorted from 2016 to 2018.

3.3.1.2. Data Quality Control of ground datasets

The first step in using the data is to convert the raw data into time series to facilitate their handling. For this purpose, scripts written in the statistical software R were used. The objective of this first treatment is to perform a visual quality control of the time series. With the terrestrial and satellite data processed, it is essential to determine the time interval in which satellite and terrestrial data coexist in the study area to determine the statistical comparison protocol. The databases provided by INER do not present continuity in time, so it is necessary to choose a time interval containing congruent historical ground measurements at each station. For this purpose, different packages in R were used to evaluate the availability of the data. The evaluation of the ground database required the development of a script that disaggregated the time series of the 26 ground stations.

Upon visualization of the information from these 26 stations, we proceeded to choose the stations whose GHI data are complete in the years 2016, 2017, and 2018 on which the study will be developed. This step yield that out of the 26 stations only 12 have complete and reliable information that will be used as the ground measured data to proceed with the validation.

3.3.1.3. Data Optimization

When obtaining the data series from the stations, the data optimization process is fundamental to identify and correct the shortcomings in the solar data. For this, the solar data must meet a condition to be considered optimal data. According to (Ordonez et al., 2019) the condition is:

- Terrestrial irradiance data that does not exist in the satellite measurement on the same geographical location will not be considered, as well as satellite data that does not exist in the terrestrial measurement on the same geographical location, will not be considered either.

The data measured on the surface may contain outliers because it is not guaranteed that the equipment used for the measurement is in good condition all the time, so the analysis may be erroneous if these outliers are present. For this reason, by analyzing the data in boxplots, a limit will be set, and data that are not within this limit will be considered outliers and subsequently eliminated.

3.3.1.4. Obtaining series on a daily and monthly scale

The GHI or SIS data obtained must be organized so that the analysis and comparison can proceed. For this purpose, the ground data from INER and DMQ stations that were primarily on an hourly scale were aggregated on a daily scale through computing the hourly averages. Consequently, these daily data obtained were also aggregated on a monthly. The satellite data for this variable were already downloaded at daily and monthly scales, so no disaggregation process was needed.

With the two databases synchronized, we optimized the data, comparing each ground station with the satellite data. This process made possible to eliminate data that did not meet the criteria explained in the Data Optimization section.

3.3.1.5. Time series

Once the daily and monthly time series were generated for the two products at the location of each station, they were plotted in order to compare them and observe the behavior and variability of the incoming shortwave radiation or GHI of the satellite measurements concerning the real data or ground measurements over the three years of the study.

3.3.1.6. Protocol of Comparison

The GHI or SIS data measured and estimated by satellite (CM-SAF, CLARA-A2) were organized in daily and monthly time series as explained above. There were not evident outliers in the time series so that the data was used as retrieved.

Once the time series were sorted and the data classified, a statistical comparison was performed (Polo et al., 2016), analyzing some metrics to evaluate satellite-based data of solar irradiance with terrestrial measurement data. This statistical comparison was performed on a daily and monthly scale, obtaining a temporal evolution of the error that allowed analyzing the behavior of the satellite data for accuracy and stability tests, respectively. Because they have been widely used in analyzing meteorological data, and because they are suitable for analyzing historical data, dispersion and distribution similarity metrics were used for the statistical analysis. These metrics are: Pearson's correlation coefficient, root mean square error (RMSE), mean bias error (MBE) (both are indicators of dispersion between two series),

and the Kolmogorov-Smirnov test (KS test) was used to proceed with data validation to assess if the model overestimates or underestimates the phenomenon (Ordonez et al., 2019).

Pearson Correlation Coefficient: Pearson's correlation coefficient is a statistical metric that indicates the relationship between two variables measuring the same event. In other words, it is the expression that indicates the degree of relationship between two variables and the extent to which they are related linearly. This index measures the dependency between the estimate and the measured value. The value of this coefficient r, can be between -1 and 1 (Akoglu, 2018).

$$R = \frac{n(\sum_{1=1}^{n} x_{e,i} * x_{m,i}) - (\sum_{i=1}^{n} x_{e,i}) * (\sum_{i=1}^{n} x_{m,i})}{\sqrt{(n * \sum_{i=1}^{n} x^2{}_{e;i} - (\sum_{i=1}^{n} x_{e,i})^2) * (n * \sum_{i=1}^{n} x^2{}_{m;i} - (\sum_{i=1}^{n} x_{m,i})^2)}} \qquad (4)$$

Determination Coefficient or R squared: The coefficient of determination is the proportion of the variance in the dependent variable that is predictable from the independent variables (Chicco et al., 2021). This coefficient assesses the strength of the linear relationship between two variables, and is heavily used when analyzing trends.

$$R^2 = \left[\frac{n(\sum_{1=1}^{n} x_{e,i} * x_{m,i}) - (\sum_{i=1}^{n} x_{e,i}) * (\sum_{i=1}^{n} x_{m,i})}{\sqrt{(n * \sum_{i=1}^{n} x^2{}_{e;i} - (\sum_{i=1}^{n} x_{e,i})^2) * (n * \sum_{i=1}^{n} x^2{}_{m;i} - (\sum_{i=1}^{n} x_{m,i})^2)}} \right]^2 \qquad (5)$$

RMSE: The mean square error is a statistical indicator that allows to know the global error between the two groups of data, the estimated solar irradiation data from each of the information sources and the real data from the meteorological station. For the solar irradiation data to be similar to the real data, the RMSE statistical indicator must be low. The RMSE will be expressed in percentages since it facilitates the interpretation of the error obtained. The acceptable range is between 0% to 30%, while RMSE is closer to zero, it indicates that the estimated values approach or are similar to the real data (Reda & Andreas, 2004).

$$RMSE\left(\frac{W}{m^2}\right) = \sqrt{\frac{1}{n} \sum_{i=1}^{n} (x_{e,i} - x_{m,i})^2} \qquad (6)$$

$$RMSE\,(\%) = \sqrt{\dfrac{\frac{1}{n}\sum_{i=1}^{n}(x_{e,i} - x_{m,i})^2}{\frac{1}{n}\sum_{i=1}^{n}x^2_{\,m,i}}} * 100 \tag{7}$$

MBE: The mean bias error or mean bias percentage is an indicator that will show the average bias estimation, that is, it allows visualizing whether there is an average overestimation or underestimation between the estimated data and real data. This indicator is obtained by subtracting the estimated solar radiation values and the actual radiation values from the MBE. A positive result will indicate that the estimated data overestimate the real values and if it is negative, it will indicate that the estimated data underestimate the real values

$$MBE\,(\dfrac{W}{m^2}) = \dfrac{1}{n}\sum_{i=1}^{n}(x_{e,i} - x_{m,i}) \tag{8}$$

$$MBE\,(\%) = \dfrac{\frac{1}{n}\sum_{i=1}^{n}(x_{e,i} - x_{m,i})}{\frac{1}{n}\sum_{i=1}^{n}x_{m,i}} * 100 \tag{9}$$

where **n** is the number of data, $x_{m,i}$ is the i-th measured datum (GHI, ground data) and $x_{e,i}$ is the i-th estimated datum (SIS, satellite data). These acronyms used are valid for each of the equations 4 to 9.

The KS test was used to proof the goodness of fit of both data series. The test determines if two data sets differ significantly. With this test the distribution of a data set is compared to a reference distribution and differences are assessed. This is done by converting the list of data points to an unbiased estimator S(xi) of the cumulative distribution function i= 1...N, where N is the population size. In the KS, D is defined as the maximum of the absolute difference of the cumulative distribution functions of the estimated and measured data S $(x_{e,i})$ and R $(x_{m,i})$ respectively (Espinar et al., 2009).

$$D = max\left|S(x_{e,i}) - R(x_{m,i})\right| \tag{10}$$

If D characterizing the difference between one distribution and the reference distribution is lower than the threshold value Vc, the two data sets have a very similar distribution and could

statistically be the same. The critical value Vc depends on n and is calculated for a 99% level of confidence as (Massey, 1951).

$$Vc = \frac{1,63}{\sqrt{n}}, n \geq 35 \qquad (11)$$

The critical value for twelve data was used for monthly comparison (Espinar et al., 2009).

For the validation of a model to be accepted, these statistical parameters must be within a confidence range. These are: Coefficient of determination >0.7, the RMSE AND MBE <30% and the K-S Test indicator must have to be >0.05 (Raush et al., 2016).

3.3.2. Net Radiation Calculation and Validation

Satellite Variable Data Extraction

Like the SIS variable for data validation, the remaining variables (SAL, SDL, SOL) were downloaded in NC format. The same transformation process was performed with a script in the R software to obtain the time series of the four variables necessary for calculating the surface energy balance or Net Radiation Energy. These data were ordered in time series with monthly temporal resolution.

Net Radiation Validation

It is essential to have the results of the Net Radiation to continue with the validation. This radiation is quantified utilizing the Earth's Surface Energy Balance equation (3). The calculation used the previously downloaded variables. This data download belongs to the same period as the Zhurucay meteorological station data described in the data sets section. Once the net radiation for the area was calculated, the same protocol of comparison between the two data models (ground and satellite) described in the validation of the global solar irradiance was used. Since the data are on a monthly scale, the validation is also performed monthly.

Obtaining the Surface Energy Balance

The radiation balance is a parameter that controls biological and hydrological processes on the earth's surface. At the same time, at a large scale, it is a source of latent and sensitive heat origin within the atmosphere that maintains meteorological systems. At a more local scale, the balance affects daily evaporation and warming of the atmosphere's boundary layer to the ground (Núñez et al., 1994).

The direct method to obtain the net radiation by is using the equation (3). Through this equation and with all the components or variables, it is possible to calculate the net radiation, which is the index needed to know the net incidence of solar radiation and which will be an indicator of the amount of solar energy. Thanks to this index, it will be possible to estimate a project's viability or estimate periods of high or low solar incidence in the area. The downloaded satellite datais pre-filtered and treated, so that the data is considered optimal for direct use, so aspects such as cloud cover and the length of the day are not considered, since the downloaded time series contain data that can be used directly in the calculation of the balance.

In order to make it easier to compare and analyze the radiation indexes in the three provinces of study, the methodology described above was applied to calculate the surface energy balances in two locations of each province (Table 5), These balances showed indices of the different components of the surface solar balance, thus allowing a comparison between the different reference points, observing the monthly in-year variability and the gradients concerning the elevation changes.

Table 5: *Locations of each province to calculate the Surface Solar radiation Budget*

Province	Location	Latitude	Longitude	Elevation (m)
Azuay	Cajas	-2.78	-79.19	3646
	Chaucha	-2.91	-79.44	1929
Chimborazo	Alao	-1.87	-78.54	3064
	Cumanda	-2.21	-79.15	331
	San Juan	-0.18	-78.58	4280
Pichincha	Pedro Vicente Maldonado	0.06	-78.96	812

The data of each of the components of the surface energy balance extracted are presented as monthly averages within a period of four years (2016, 2017, 2018 and 2019). In total, there were 43 data points for each of the variables. Subsequently, the corresponding calculations

were carried out to obtain the monthly averages of each component for each reference station. With these data, it was possible to perform the calculations to obtain the net radiation.

Chapter 4

Results and Discussion

Solar energy as a primary energy source to meet people's basic needs is in increasing demand. The first step is to have accurate solar energy information before planning any short or long-term project that includes solar energy. Various climatic and meteorological factors condition the availability of solar radiation on the earth surface. The geographical position of Ecuador provides unique features for surface solar radiation distribution because the country poses a great variety of climates, elevation floors and because of its location on the earth surface, it maintains nearly year-round constant radiation levels. To provide alternative sources of information to the lack of solar radiation ground data it is necessary to asses the potential and drawbacks of satellite-based estimates before to exploit their application. This section explains the results obtained in the validation of satellite estimates of solar radiation and the Surface Energy Balance.

4.1.   Solar Global Radiation Validation

When performing data quality control processes, stations with data gaps were eliminated; it was found that only 12 out of the 24 stations have completed 2016-2018 GHI data in both databases on the corresponding geographic location. These stations are Baños, Altillo, Tixan Pistillí, Santa Ana, Yanuncay, El Vecino, Irquis, Quingeo, Cumbe, San Joaquín, Sayausí and Turi.

4.1.1. Outliers

When analyzing each of the databases using boxplots, it was found that only in the IIGE data were their outliers. In this database, 99% of the GHI data are in the 100 to 750 W/m2 limit, so the data not in this limit was eliminated. The boxplots for each of the stations are shown in Annex 3.

For example, at the Baños station, an outlier can be observed (Figure 7), which will be eliminated in order to proceed with the statistical analysis.
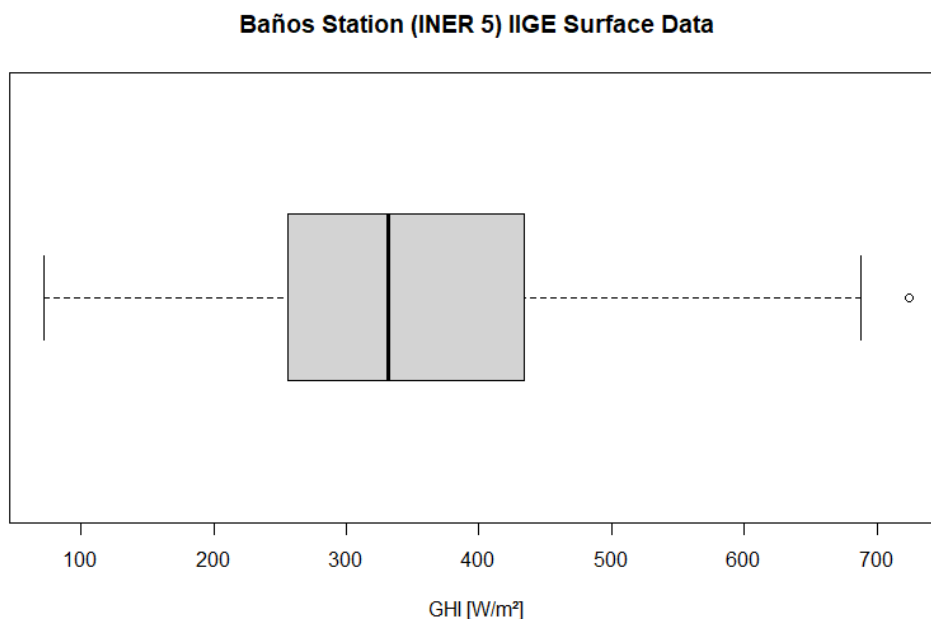
Figure 7: *Boxplot of Baños Station surface data (IIGE)*

The satellite estimates of solar radiation values were statistically analyzed and compared to the values recorded at each meteorological station during the study period. In addition, five stations in the Quito metropolitan district contained also complete data, so the validation on this dataset was performed without dropping any station.

4.1.2. Time series on daily and monthly scales of global solar irradiance (GHI)

In this section, the station Baños (Iner 5) is chosen to first depict the variability at different time scales, and then to shown statistical metrics for each year and temporal resolution of data available.

Daily Scale

Figure 8 shows ground data (blue) and satellite data (red) in Baños station, Iner 5. The graph clearly shows that the satellite data underestimate the measurements of the global solar radiation indexes at this location. Also, the chart shows that the behavior of the satellite data is similar to that of the terrestrial data. Similar variability is recorded between the two data sets. In the Annex 3 section graphs for each station are shown. The missing values between September 2017 and January 2018 are due to in the terrestrial data these data were not

registered, therefore, the satellite data was eliminated by the criteria explained in the optimization of the databases.
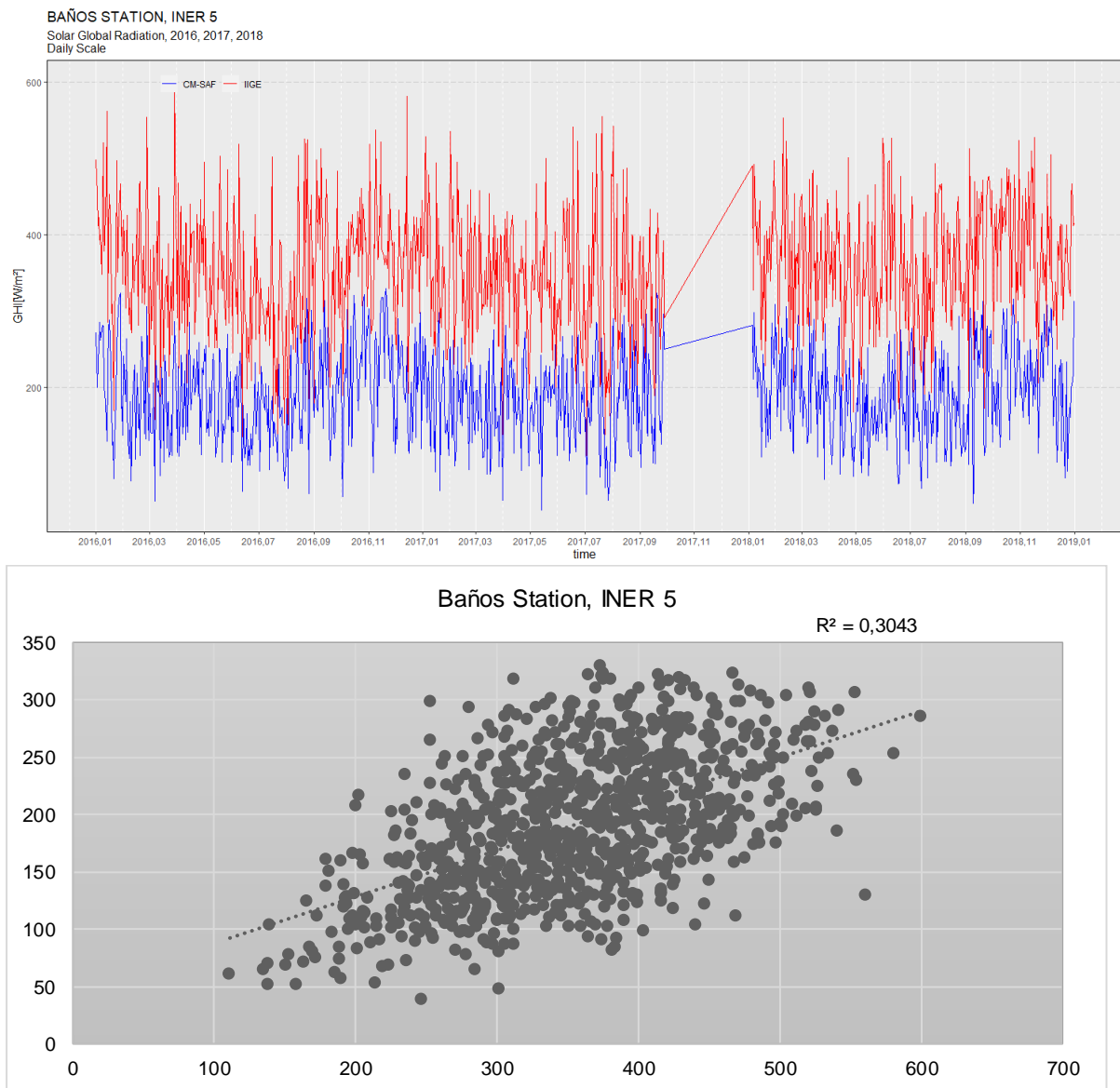
Figure 8. *Time series and dispersion plot of Baños station in daily scale.*

Monthly Scale

As in the daily time series, the main result when analyzing the annual cycles in monthly scale of this station is an underestimation of solar radiation by the satellite data model. Figure 9 shows the inter-annual variability of the Baños station, belonging to the Azuay province. The figure shows that the pattern of the global radiation in the monthly average of the terrestrial data has similar behavior to that of the satellite data. The chart shows that high and low values in solar radiation indexes of the satellite data correspond to the variability in time of the terrestrial data.
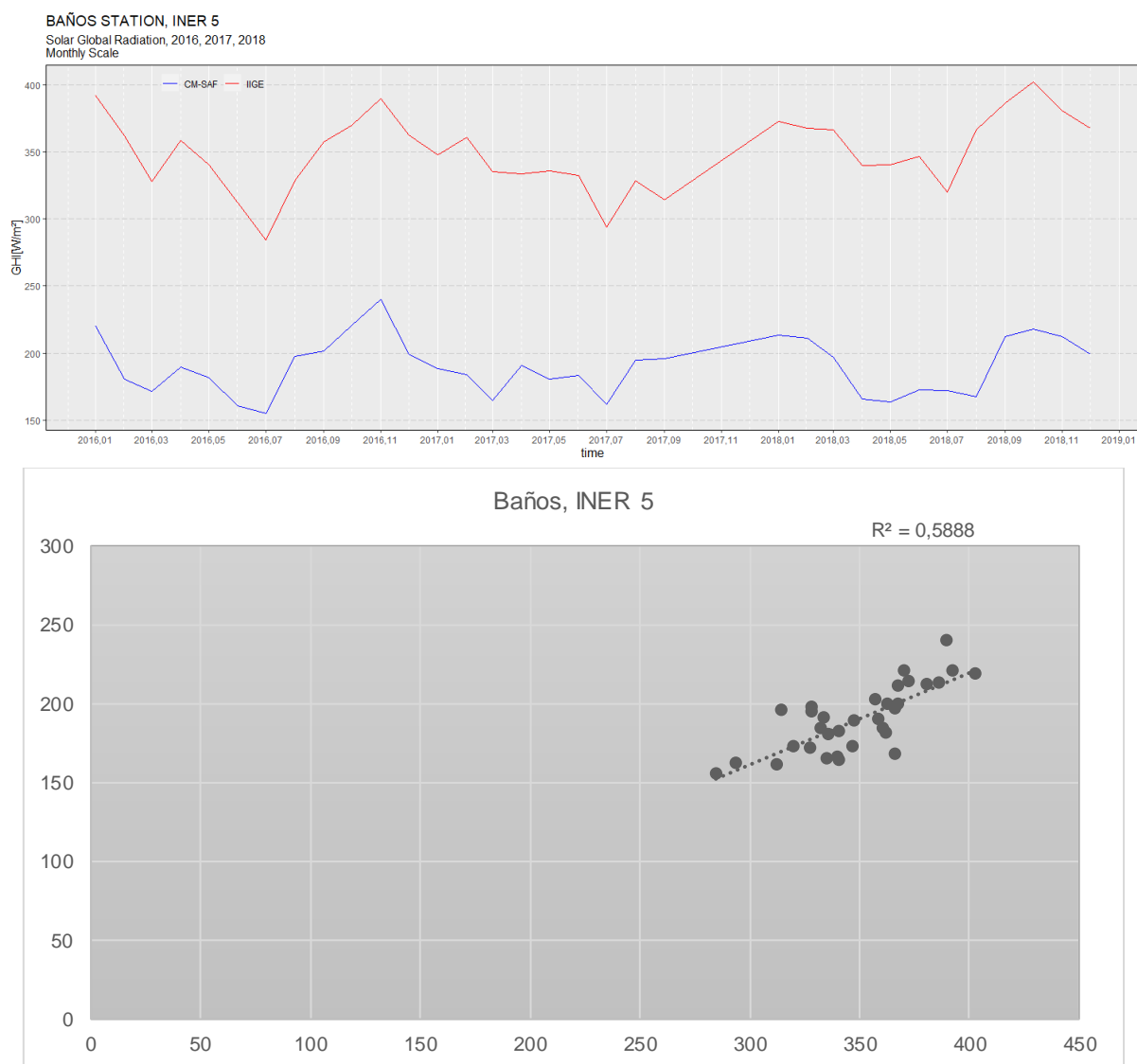
Figure 9. *Time series and dispersion plot of Baños Station in monthly scale.*

An average was made for each month to analyze the annual cycle of global solar radiation behavior. The figure 10 shows two seasons of higher irradiation, the first from March to April and the second from July to November. A season of lower irradiation is also observed, with a decrease in the months from December to March.
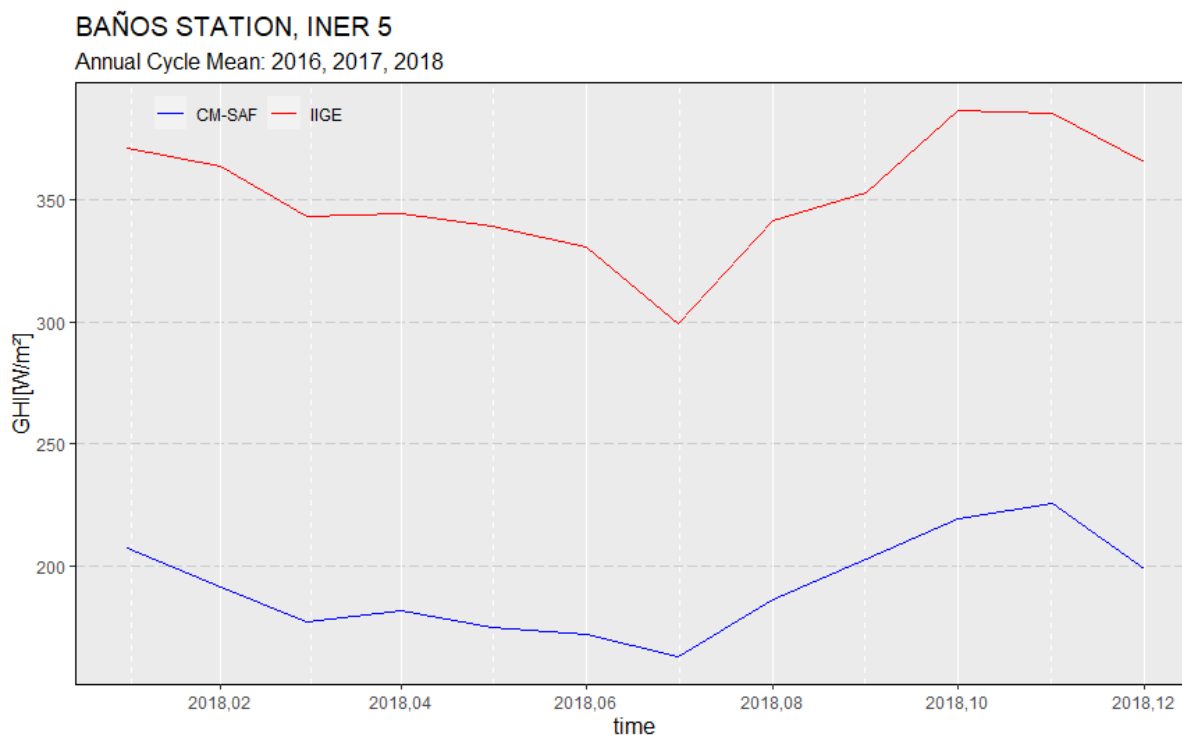
Figure 10. *Annual Cycle mean of Baños station.*

4.1.3. Yearly Statistical Comparison

The results of the statistical comparison of satellite and ground data at Baños station, Iner 5, are summarized in the Table 5. In general, the performance of the satellite data concerning the ground data at this station is good, omitting the apparent underestimation by the satellite model. The RMSE values on a daily scale are higher than those on a monthly scale. The satellite data model presents an RMSE greater than 100W/m^2 at both scales and in the three years study period. There is a significant bias between the data.

Table 6: *Summary of the daily (D) and monthly (M) comparison results of the Baños meteorological station, Iner 5, for each year of study.*

Station	Year	D/M	RMSE	RMSE%	MBE	MBE%	R	R2	KS indicator
BAÑOS	2016	D	171.826	48.952	-157.497	-44.870	0.567	0.321	0.354
		M	156.267	44.799	-157.497	-44.870	0.879	0.773	0.536
	2017	D	170.032	50.531	-154.097	-45.796	0.521	0.271	0.388
		M	149.786	45.205	-154.097	-45.796	0.323	0.104	0.126
	2018	D	184.847	50.797	-172.491	-47.401	0.557	0.310	0.514
		M	171.568	47.250	-172.491	-47.401	0.826	0.682	0.869

For this reason, the MBE% oscillates between (-47.40% and -44.87%). The negative sign of the mean bias error represents the underestimation by the satellite data. The Pearson correlation coefficient is higher for the monthly scale data because, when aggregated monthly, these data present a similar behavior to the terrestrial data and reproduce the monthly anomalies of the global solar radiation optimally. The monthly averaging acts as noisy filter improving linear correlation metrics. The K-S indicator shows that, at this station, the data are normalized except on the daily scale of 2016, where it is observed that the test result is less than 0.05 concerning ground measurements. Although the monthly data pass statistical indicators such as coefficient of determination and KS test, both daily and monthly satellite data could not replace the ground measurements data at this station because, in statistical analysis such as RMSE and MBE, the indices are within the allowed range. The statistical results for each station in the study are shown in Annex 5.

The following section discusses the results obtained in the statistical analyses applied to the 12 stations within the entire period 2016-2018.

4.1.4. Long-term comparison of satellite estimates and stations operated by IIGE

This section shows the averages of the most critical comparative dispersion and similarity statistics applied to the comparison of global solar radiation data from meteorological stations operated by IIGE (INER stations) and satellite estimates in order to perform a multi-criteria assessment. The daily and monthly results obtained annually are detailed in Annex 6.

4.1.4.1. Determination Coefficient: R squared

The calculation of the coefficients was performed in daily and monthly scale, considering data from 2016, 2017, and 2018, mainly to verify that there is a level of association between the two databases of global horizontal solar radiation.
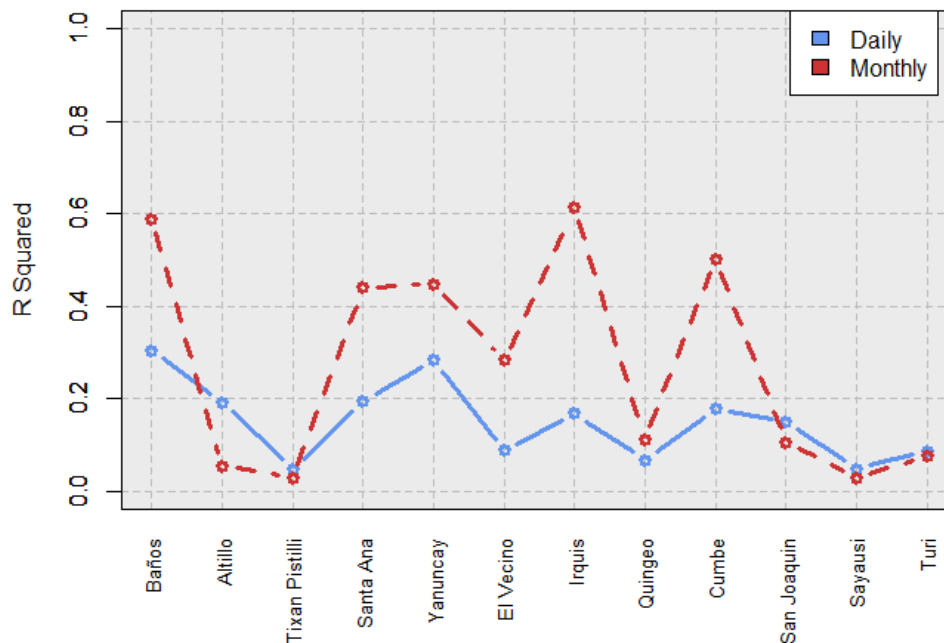
Figure 11. *Averaged R squared results of the INER stations.*

The following results were obtained by performing the application of this statistical indicator between satellite and surface data (Figure 11). As it can be seen, on daily scale, the coefficients of determination are in the range of (0.0 to 0.4), which means a low confidence on the satellite model compared with the ground data. The data from the Baños and Irquis station show the highest correlation, while the data from the Turi, Tixan Pistilli and Altillo station show the lowest correlation. On the monthly scale, the coefficients are in a range of (0.0 to 0.6), which indicates that in some stations, the correlation is low, as in Turi, Tixan Pistilli and Altillo. In this scale, the data from the Baños and Irquis stations show a higher correlation. With these results, it can be said that the satellite data show the anomalies, and the confidence of the satellite data is moderate in both on monthly and daily scales, the satellite does not optimally reproduce the global solar radiation anomalies.

4.1.4.2. Root Mean Square Error (RMSE)

Figure 12 shows a chart of the twelve chosen stations evaluated at daily and monthly scales, summarizing the RMSE by year from 2016 to 2018. The RMSE varies depending on whether the data grouping is daily or monthly. The RMSE varies between 50% and 56% on a monthly scale and is lower than on a daily scale, which varies between 45% and 54%. In none of the cases, the RMSE can be considered acceptable. This error was higher than 30% in all cases.

Despite this, the RMSE analysis revealed lower monthly measurement rates than daily ones. The root mean error calculation was calculated for the 12 stations in the different years of the study (2016, 2017, and 2018), and an average of the three study years was performed to obtain an annual value.
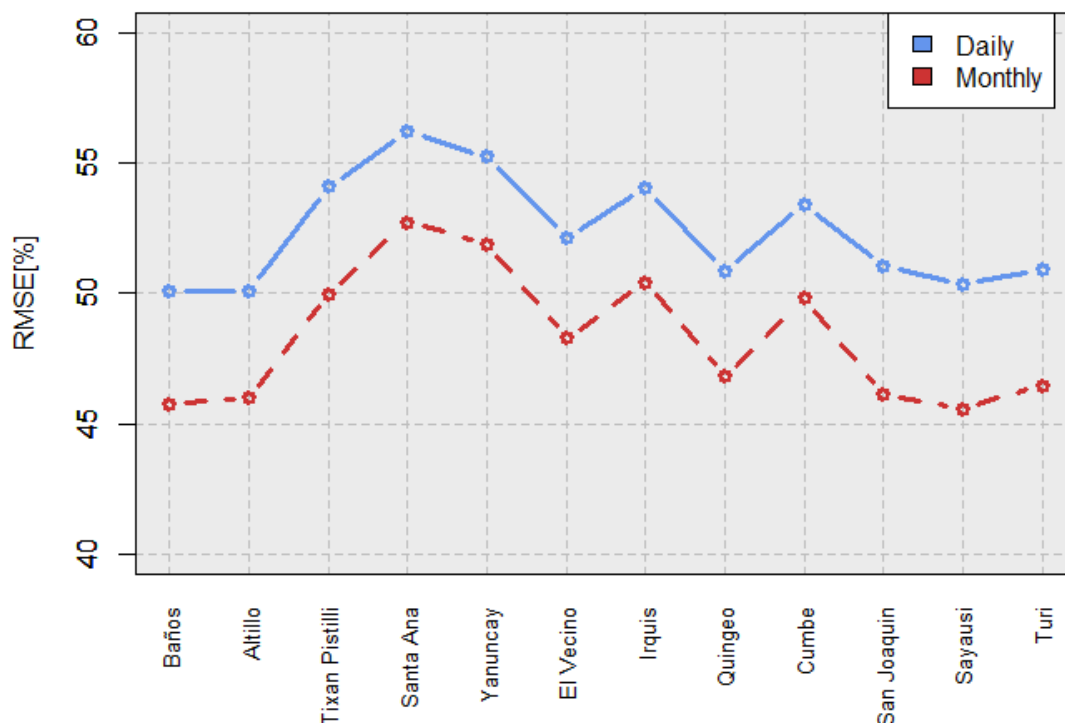
Figure 12. *Averaged RMSE results for INER stations.*

4.1.4.3. Mean Bias Error

As in the previous statistics, the Figure 13 shows the annual Mean Bias Error results for each station analyzed in the study. The results of the MBE indicator show that the CMSAF satellite data model underestimates the global solar radiation values at the locations where the stations are operated by INER. The MBE varies between -50 to 0 on average for the 12 stations. In none of the cases, the percentage of MBE is within the accepted range, so the satellite model of global solar radiation heavily underestimates ground measurements.
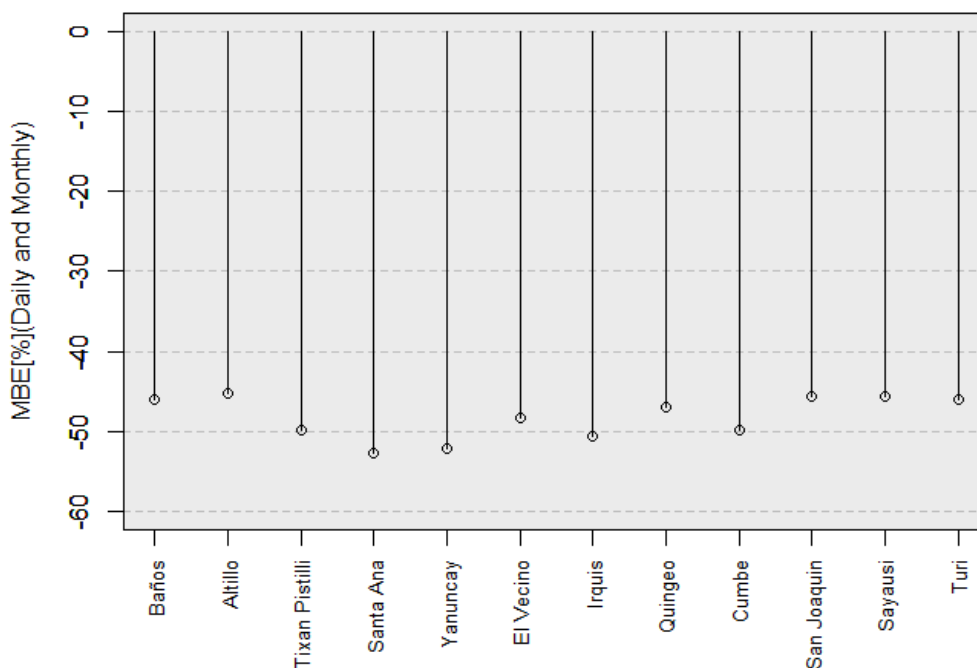
Figure 13. Averaged MBE results for INER stations

4.1.4.4. Kolmogrov Smirnov Test

The test for this set of stations shows that only 33% of the data are related to each other on a daily scale. On the other hand, the data from the 12 stations passed the test on a monthly scale (Figure 14).
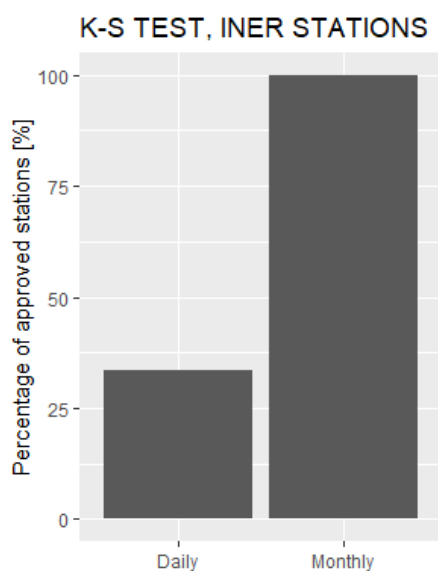
Figure 14. *Percentage of approved INER stations and daily and monthly scale*

4.1.5. Long-term comparison of satellite estimates and stations operated by Secretaría del Distrito Metropolitano de Quito

The average of each of the statistical indicators is necessary for the analysis. This section shows the results of the statistical indicators performed between satellite and ground data from the stations located on the northern Andes, DMQ group.

4.1.5.1. Determination Coefficient: R squared

As in the case of the INER stations, the coefficient of determination is one of the statistical metrics used to determine whether the satellite data are reliable. This calculation shows that the daily scale data have a moderate linear relationship of 0.4 to 0.6 between satellite and ground data. Carapungo station registered the worst correlation. In contrast, the monthly scale data have a higher association between 0.6 to 0.8, Tumbaco station has the best R squared index.
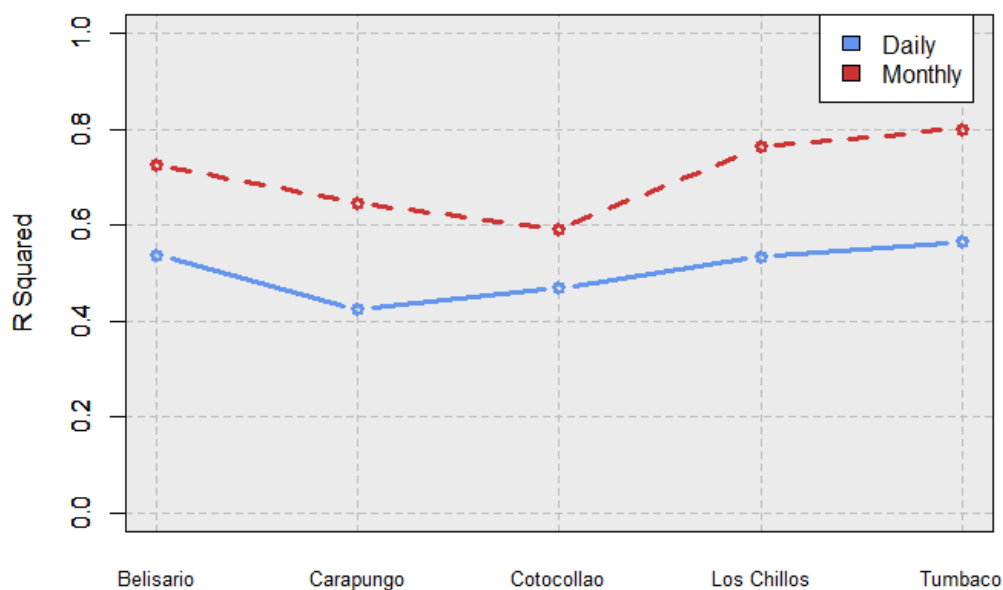
Figure 15. Averaged R squared results of the DMQ stations.

4.1.5.2.   Root Mean Square Error (RMSE%)

The root mean square error test is presented in the figure and shows an error between 46 to 54 % on a daily scale and a range of (34 to 52%) on a monthly scale. The RMSE varies as in the INER stations depending on whether the data are on a monthly or daily scale. In both scales, Belisario station present the lowest RMSE of all stations.
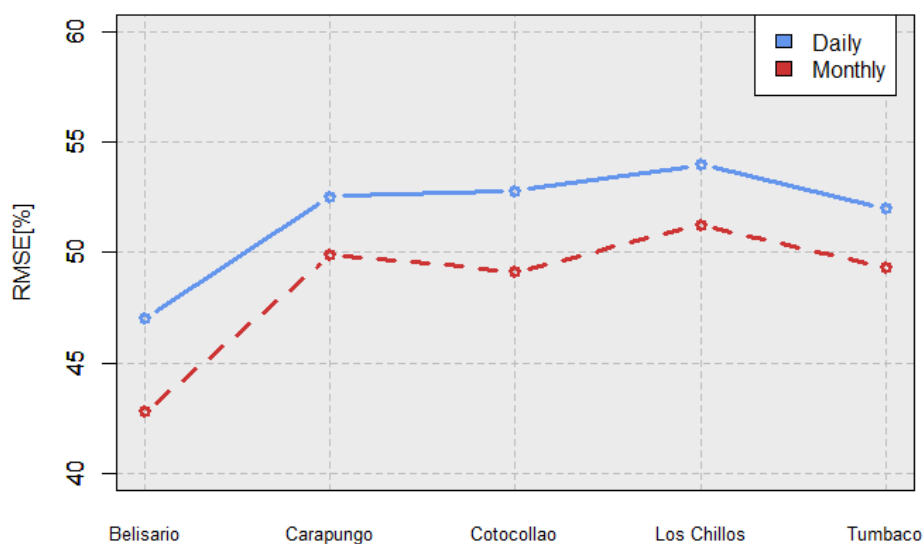
Figure 16. *Averaged RMSE results for DMQ stations.*

4.1.5.3.   Mean Bias Error (MBE%)

The MBE shows that the satellite model of global solar radiation shows underestimation since it varies from 41 to 51%. As the RMSE, Belisario station shows the lowest value in MBE.
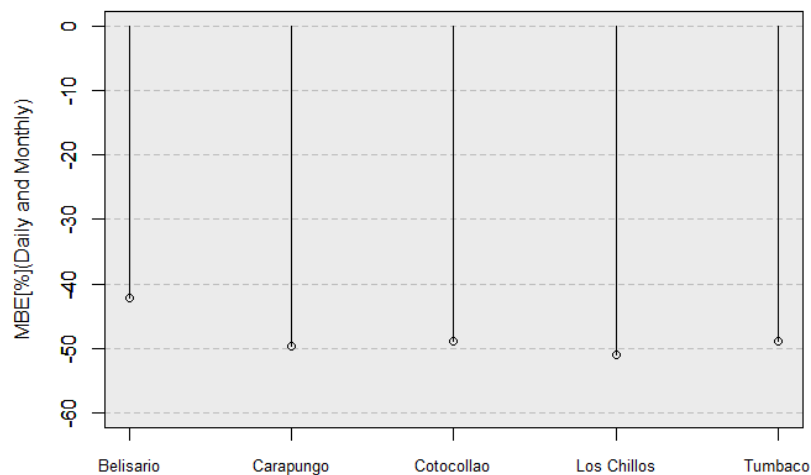
Figure 17. *Averaged MBE results for DMQ stations.*

4.1.5.4. Kolmogrov Smirnov Test

The Kolmogorov Smirnov test shows that 100% of the monthly data are related, and the distribution of the daily data estimates is not related to reference ground dataset.
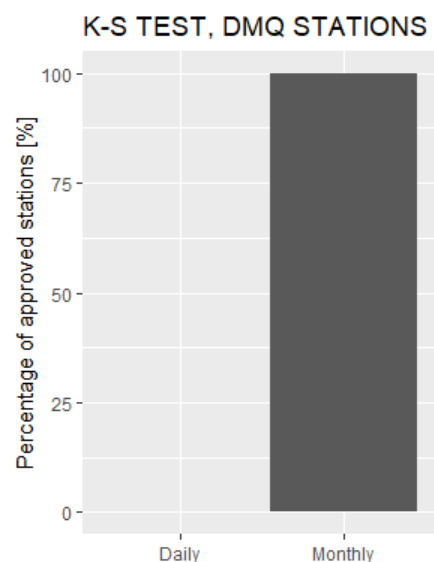
Figure 18. *Percentage of approved DMQ stations and daily and monthly scale.*

As a result of applying the statistical indicators in each set of meteorological stations, it was found that the satellite data of global solar radiation on a daily and monthly scale can be used to evaluate the temporal variation in different places or territories. These satellite values have a significant bias concerning the terrestrial data of the two data sets, so to be used promptly in projects involving the exact amount of solar radiation, a bias correction must be performed.

4.1.5.5. Proposed equations for calculating GHI in the studied provinces

After analyzing the data corresponding to the solar radiation of both models, an equation can be defined. The calculation of GHI can be carried out only with the information from the satellite data and the MBE%. This equation is recommended in cases where the MBE% indicator has already been calculated. The equation is as follows:

Azuay:

$$GHI = \frac{SIS}{48,3\%} \tag{12}$$

Chimborazo:

$$GHI = \frac{SIS}{47,5\%} \tag{13}$$

Pichincha:

$$GHI = \frac{SIS}{48,1\%} \tag{14}$$

Where,

GHI: Global Horizontal Irradiation

SIS: Surface Incoming Shortwave radiation (satellite data)

MBE%: Mean Bias error between the two datasets

4.2. Spatial distribution of Solar Global Irradiation (Solar Map 2019)

The spatial and temporal distribution of the solar resource is of utmost importance for the country's energy sector. Identifying strategic regions for the utilization of solar energy is the first step in solving the energy needs of the communities (Benedek et al., 2018). To our knowledge, the most recent assessment of Solar Global Irradiation was conducted by Vaca-Revelo et al., (2019) to validate satellite data belonging to National Renewable Energy

Laboratory (NREL). In such study, the Solar Map of Ecuador 2019 was published in an annual and monthly scale (Figure 19). It presents the yearly average global irradiation for Ecuador expressed in KWh/m^2 per day. The map reflects that at least 75% of the territory in Ecuador has annual global solar irradiance levels greater than 3.8 kWh/day (158.33W/m^2) (Cevallos-Sierra & Ramos-Martin, 2018). Provinces such as Pichincha, Galapagos, Loja, and Imbabura are the provinces with the highest solar potential, reaching up to 6 kWh/m^{2}day (~250 W/m^2). Due to the location of the Galapagos Islands, this province has the highest levels of global solar irradiation, exceeding 6.4 kWh/m^{2}day (266.66 W/m^2). The territories with the lowest global solar irradiation are those located in the coastal region. Global solar irradiation in the Amazon region ranges between 4.5 and 4.8 kWh/m^2 per day (187,49-199.99 W/m^2).
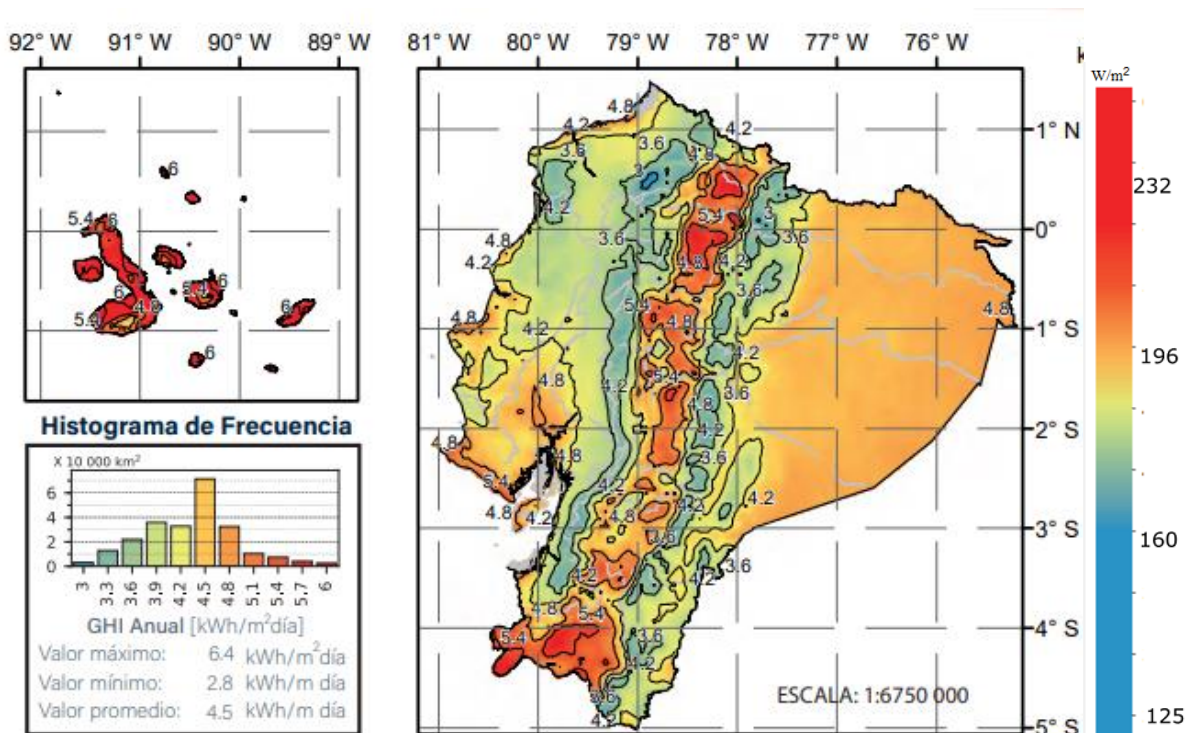
Figure 19. *Solar global radiation map with NRLE data.*

Source: (Vaca et al., 2019)

During seasons with a vertical position of the sun, more energy is received at the surface because the path through the atmosphere is shorter and less energy is absorbed by particles (aerosols) or gases. The same is valid for elevated sites, where the way through the atmosphere is reduced because more energy is received in the mountain ranges. Therefore, solar radiation generally increases with altitude (positive gradient). Another important factor is the exposure and slope of the terrain because hills facing the sun receive more energy. However, solar radiation depends on cloud cover as well. Much of the solar radiation is

absorbed and reflected by clouds in cloudy locations, reducing the energy received at the surface. Because of this, more solar energy reaches the surface during dry periods than during rainy periods if the sun's position is equivalent.

The map generated with the CM-SAF satellite data (Figure 20) clearly shows a similar spatial pattern of the global solar radiation as the Solar Map of Ecuador. A higher global solar radiation index is registered in the provinces of Galapagos, Loja, Pichincha, and Imbabura, reaching levels of 230W/m^2. In continental Ecuador, the region of Loja reports the highest levels of global solar irradiation with indexes of approximately 230W/m^2. The results of the solar radiation indexes in the province of Loja are because this province has the lowest cloud cover in the country. Therefore, solar radiation is higher since clouds do not reflect it. On the other hand, areas such as Pichincha are located at a high elevation, explaining the increased solar radiation indexes. The map generated by the CM-SAF Tool-Box reflects the exact behavior of the global solar radiation variability in the Ecuadorian territory. Still, these satellite data only represent the behavior of the annual solar resource. As mentioned, the satellite does manage to cover the areas with higher radiation, such as Loja and Galapagos. Still, it presents difficulties when calculating solar irradiance in places such as the country's coastal zone. Annex 4 shows the maps generated by the CM-SAF for each month of Ecuador.
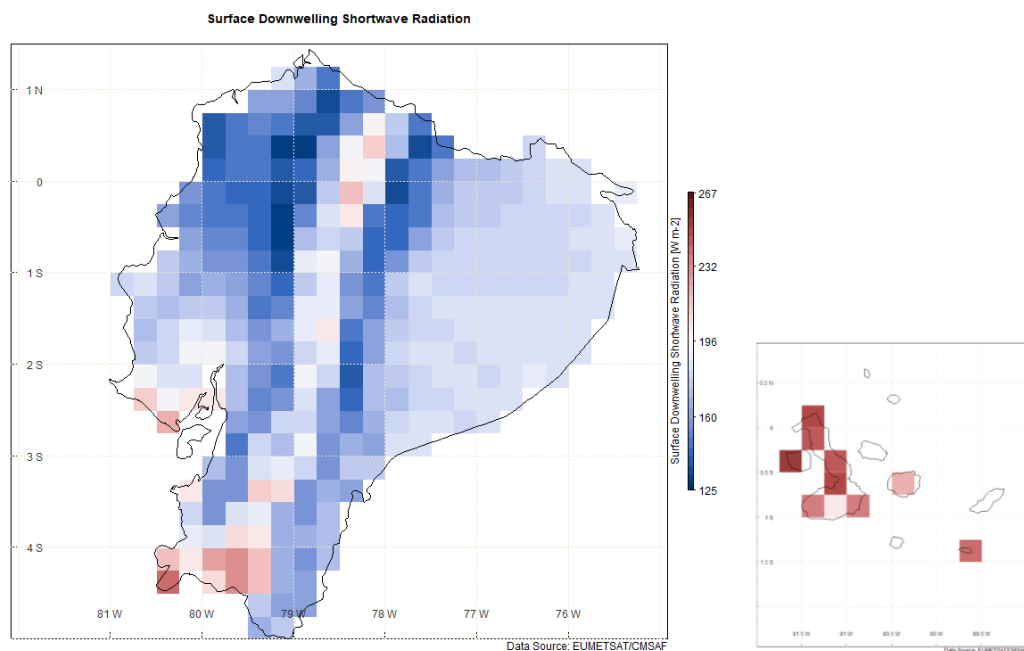
Figure 20. *Solar global radiation map with CM-SAF data*

4.3. Net Radiation Validation

The validation of the net radiation was performed on a monthly scale because the two data sets used are only available on this scale.

4.3.1. Monthly Net Radiation

In Figure 21, the graph shows Net Radiation time series on a monthly scale of the Zhurucay ground data and the satellite estimation used for this validation. The plot shows that the satellite model meets the variability over time of the net radiation.

The coefficient of determination shows that the satellite net radiation data is reliable concerning the ground-based data.
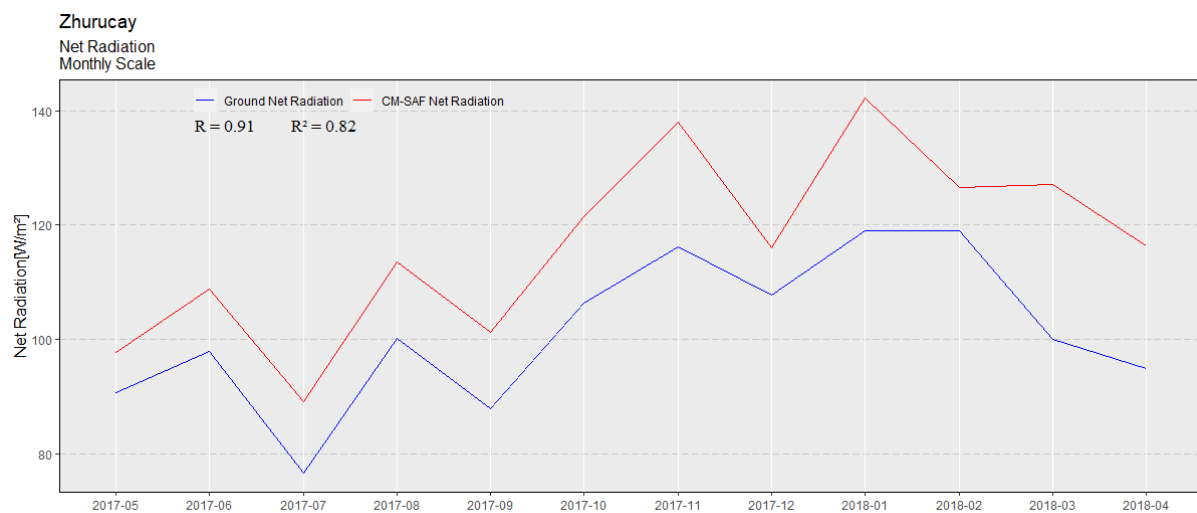
Figure 21. *Time series of the net radiation data, satellite and ground data.*

4.3.2. Root Mean Square Error (RMSE)

Figure 22 represent the statistical comparison results between the CM-SAF net radiation and ground-based measurements in the Zhurucay area of for the annual cycle (March 2017 - April 2018). The satellite data, in general, have a good representation throughout the study period with RMSE% in the range of 5-17%, except March and April, which exceed 17%.
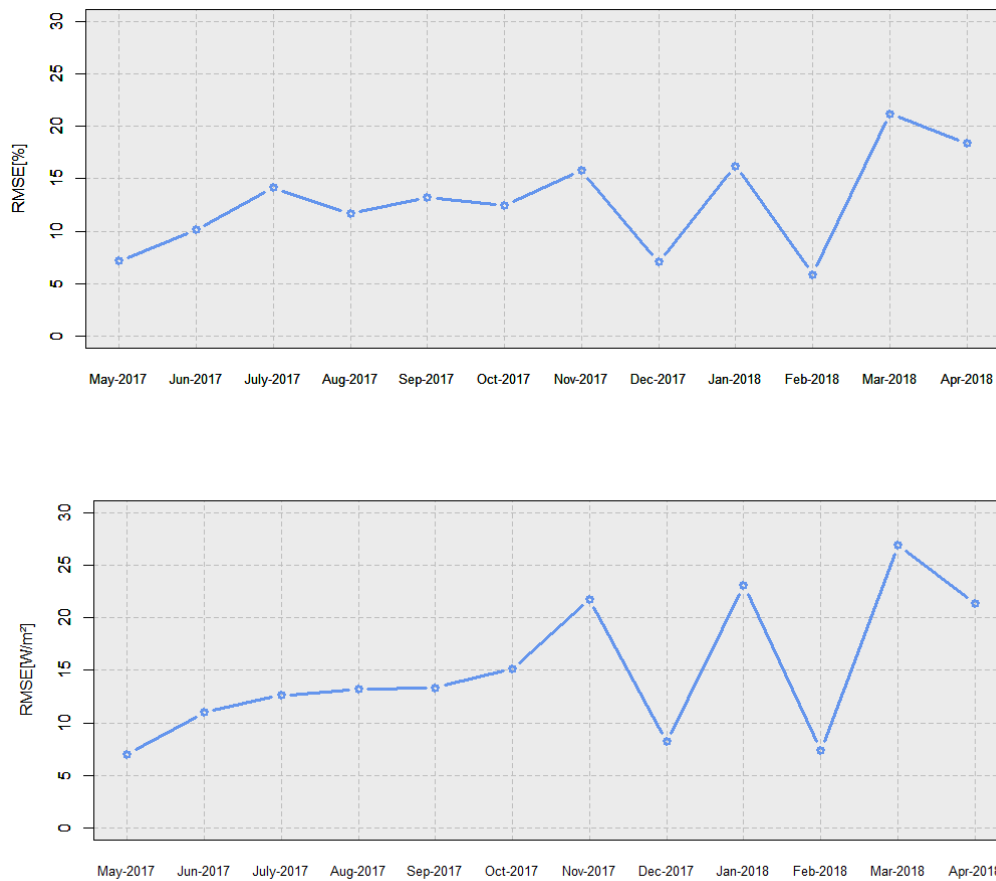
Figure 22. *RMSE % and RMSE results of each month of the net radiation calculation.*

4.3.3. Mean Bias Error (MBE)

The figures show the statistical comparison of MBE developed between satellite and ground measurement data of net radiation in the Zhurucay area. These results show that there is an overestimation of the net radiation values. Throughout the study period, it is observed that the overestimation varies between a range of 5 to 20%, except for March and April 2018, when the MBE exceeds 20%. The overestimates may occur since cloudiness increases in months such as March and April, producing an increase in precipitation, thus inducing errors in the calculations made by the satellite.
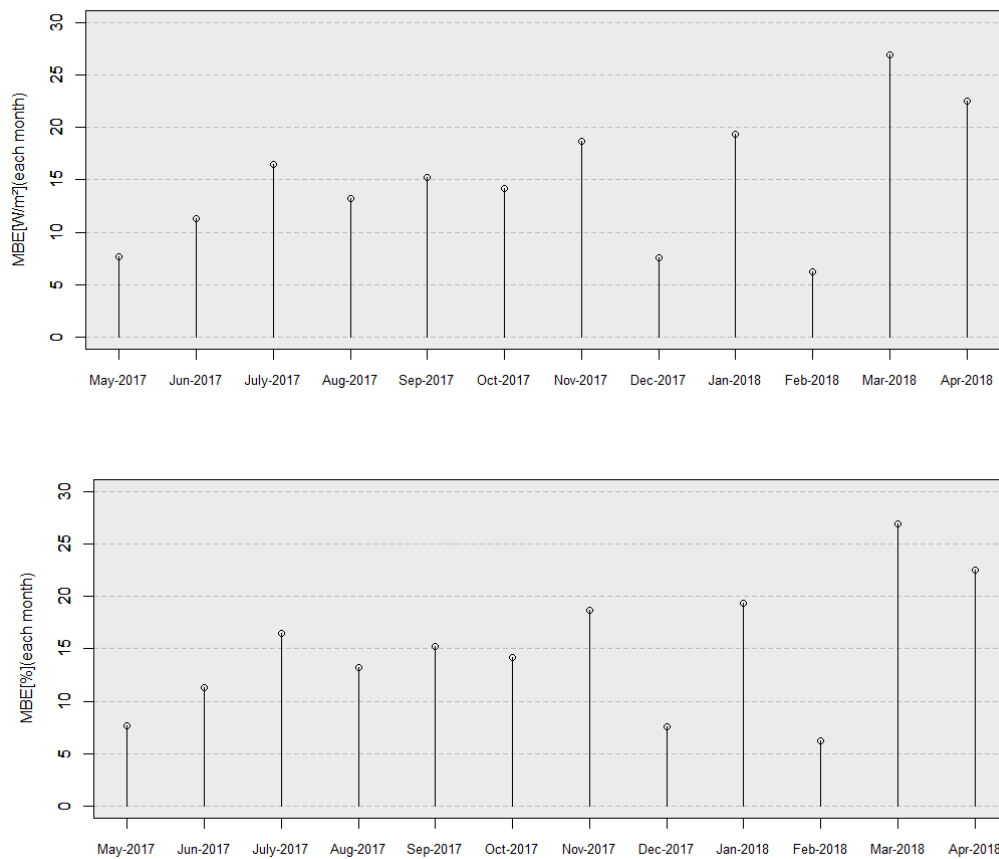
Figure 23: *MBE % and MBE results of each month of the net radiation calculation.*

With the results of the statistical comparison made between terrestrial and satellite data on Net Radiation on a monthly scale, it can be said that it is acceptable to use satellite data to perform the calculation of net radiation. The ranges of the calculated errors of RMSE and MBE are low. They are within the acceptable values of the statistical indicators, and the value of the coefficient of determination is high. Consequently, the net radiation obtained from the satellite data is correctly adjusted to the real values of the net radiation.

We proceeded to calculate the Energy Balances or Net Radiation in the following section.

4.4. Surface Solar Energy Balance Results

The methodology described in Section 3.3.2.3 to calculate surface energy balances was applied in two locations in the province of Azuay, the same ones that correspond to Nulti and Cajas locations. On the other hand, in the province of Chimborazo, the balance calculation was carried out in two locations too, corresponding to Alao and Cumanda locations. And finally, in Pichincha province, the energy balances were calculated in the locations of San

Juan and Pedro Vicente Maldonado parishes. These balances showed indices of the different components of the surface solar balance, thus allowing a comparison between the different reference points, observing changes during the different months of the year and the variations related to elevation.

The data of each of the components of the surface energy balance extracted are presented as monthly averages within a period of four years (2016, 2017, 2018, and 2019). In total, there were 43 data points for each of the variables. Subsequently, the corresponding calculations were carried out to obtain the monthly averages of net radiation for each reference station, as shown in Table 6. With these data, it was possible to perform the calculations to obtain the net radiation.

The surface energy balance between incoming and outgoing shortwave and incoming and outgoing longwave waves corresponds to the Net Radiation. This radiation is a key component in calculating the Energy Balance at the Earth's surface because it represents the primary energy source for the physical and chemical processes occurring at the earth surface and in the atmosphere, such as photosynthesis and evapotranspiration in hydrological balances. Consequently, net radiation plays a significant role in determining the Earth's thermal conditions in studying earth-surface processes and climate change. Obtaining net radiation is the foremost step to developing research in meteorology, hydrology, global climate change, and agriculture.

The satellite data made available by CM-SAF validated and accepted to calculate the net radiation are used to calculate the net radiation balance in different points of Azuay, Chimborazo and Pichincha provinces.

The incoming short-wave radiation (SWin) or global radiation on the surface is composed of direct and diffuse solar radiation. Diffuse radiation is the result of a series of processes on direct radiation: selective absorption and molecular diffusion caused by gases and water vapor; and by diffusion and absorption due to aerosols or turbidity (Whiteman et al., 1988).

The incoming long-wave radiation (LWin) is the result of the process of re-emission of radiation from the Atmosphere to the Earth. The transfer of long-wave radiation flux depends on the amount of cloud cover, the height of the clouds, the temperature of the base and top of the clouds, the efficiency with which the clouds absorb the radiation, and the absorbing gas temperature and absorption efficiency at each wavelength (Kiehl & Trenberth, 1997). The incoming long-wave radiation flux is strongly dependent on the presence of clouds. Much of the radiation emitted by clouds is produced at the base of low clouds and therefore difficult to calculate from satellite observations. Due to the high dependence of this parameter on the

height of the cloud base and the amount of low clouds, it is considered highly uncertain and undoubtedly explains a large part of the variation in the global balance (Kiehl & Trenberth, 1997).

Outgoing short-wave radiation (SWout) is the result of reflection processes by the earth's surface and scattering by clouds, atmospheric gases and aerosols. Its magnitude depends on: the time of year, the latitude, the percentage of cloud cover, the nature of the surface and the number of aerosols present in the Atmosphere. Some of these effects are very difficult to assess (Kiehl & Trenberth, 1997).

The outgoing long-wave radiation (LWout) is the result of the emission by the earth's surface of long-wave energy and the emission of the atmosphere (especially from the cloud cover) into space, which is function of the absorption capacity of water vapor, oxygen, ozone and cloud cover (Kiehl & Trenberth, 1997).

4.4.1. Net Radiation in Azuay Province

Nulti and Cajas zones were the reference points for calculating surface energy balances or net radiation in Azuay province, Table 7 shows the average values corresponding to the study period of net radiation of Nulti, with an elevation of 2623m and Cajas, with a height of 3246m. Figure 24a and 24b show the representative Solar Radiation Budget of the two locations. The solar balance in Nulti shows that in November, the highest net radiation is reached on the surface (143.66 W/m^2) and, on the other hand, in July, the solar incidence is the lowest (87.54 W/m^2). During the December-April period, a high and constant net radiation is maintained at the surface. In the May-July period, net radiation suffers a notable decrease, this period being the one with the lowest net radiation index on the surface. The albedo at these two locations varies by minimal amounts (Table 6), so the indices of each of the balance components vary by minimal amounts as well. An increase in radiation incidence has been observed from August onwards, causing the net radiation to rise considerably until reaching the highest rate in November. Low values of net radiation with high global radiation must then correspond to a high long-wave radiative balance. When receiving intense global radiation, the earth's surface raises its temperature and emits high long-wave radiation. We can see that the outgoing long-wave radiation values at these stations are, of course, increased.
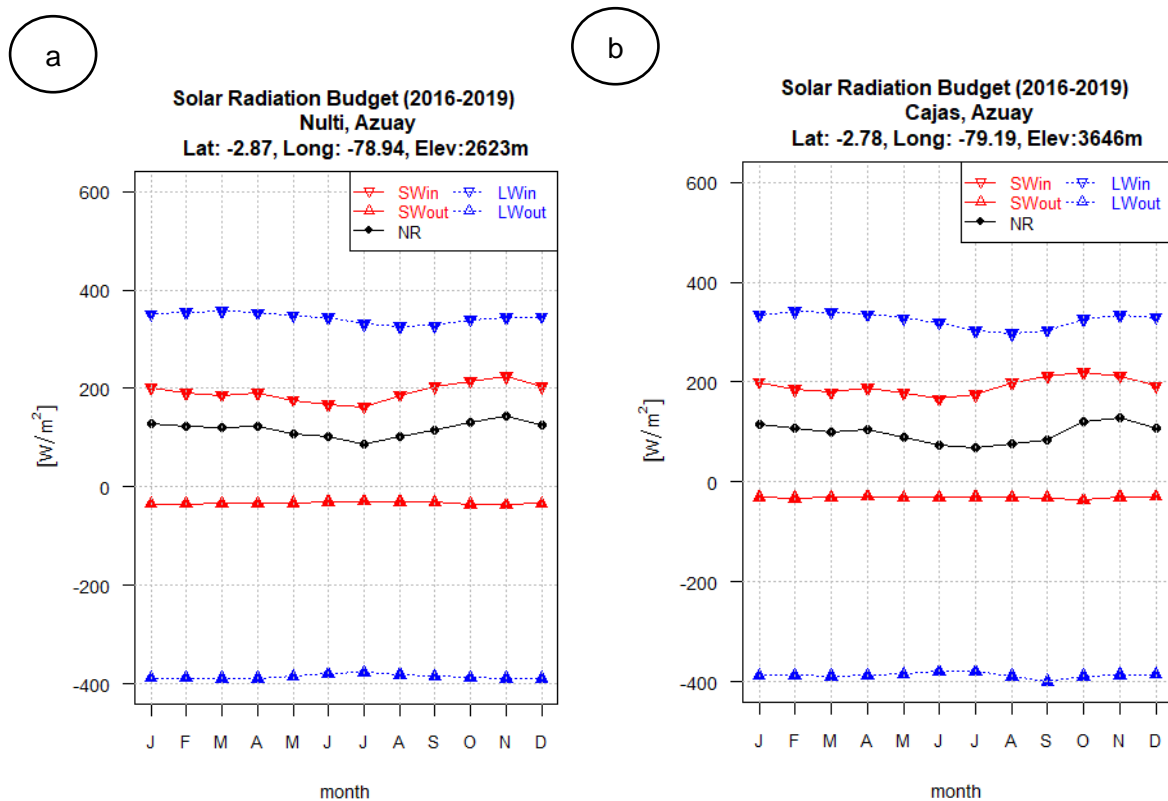
Figure 24: *Solar Radiation Budget in Azuay province. a) Nulti, b) Cajas*

Regarding Cajas zone, the balance of this location shows that the solar radiation has similar comportment as in Nulti. During the December-April period, a high and constant net radiation is maintained at the surface. In the May-July period, net radiation suffers a notable decrease, this period being the one with the lowest net radiation index on the surface (62.72 W/m^2) (Table 6). An increase in radiation incidence has been observed from August onwards, causing the net radiation to rise considerably until reaching the highest rate in November (140.24 W/m^2).

Table 7: *Monthly Net radiation and albedo of Azuay Province*

	Nulti 4280m		Cajas 812m	
month	Net Radiation [W/m2]	Albedo	Net Radiation [W/m2]	Albedo
Jan	129.41	0.15	119.24	0.16
Feb	122.00	0.18	114.69	0.17
Mar	119.48	0.17	109.83	0.16

Apr	121.92	0.16	110.00	0.15
May	106.27	0.15	96.99	0.15
Jun	101.27	0.16	80.70	0.15
Jul	87.54	0.16	62.72	0.14
Aug	101.44	0.14	82.11	0.12
Sep	114.52	0.12	95.86	0.11
Oct	131.97	0.15	126.65	0.14
Nov	143.66	0.14	140.24	0.12
Dec	126.40	0.15	116.56	0.14
Prom	117.15	0.15	104.63	0.14
Max	143.66	0.18	140.24	0.17
Min	87.54	0.12	62.72	0.11

In this province, the values of global solar radiation (SWin) are moderately high. The incoming flux of short-wave radiation presents a seasonal behavior with a maximum in November and a minimum in July (Figure 24a) in Nulti. The incoming short-wave radiation in Cajas presents the minimum value in the month of July and in the month of November its maximum value (Figure 24b). The variation during the year may be due to the influence of the solar declination, which would generate different climatic seasons and would produce a decrease in the length of the day in winter in the middle latitudes. Also, due to the influence of the Intertropical Convergence Zone (ITCZ) which is located in the Southern Hemisphere (~ 5°S), during October to December, brings masses of hot and humid air that cumulus increasing cloudiness levels (Rossel & Cadier, 2009). Conversely, when the ITCZ is located in the opposite hemisphere from July to August, cold and dry air masses and more stable atmosphere predominate in the territory. There is also a synoptic-scale influence of the Pacific Anticyclone that would cause a cloudy period in the winter months (October-May) whose influence might change due to the notorious difference in latitudes in the region. These factors show the reason for the maximums and minimums recorded in terms of global radiation. The difference in the annual average global solar radiation between these two stations is ~15 W/m^2.

The incoming long-wave radiation flux (LWin) exhibits a seasonal variation of lesser magnitude than the incoming short-wave radiation flux (global radiation). The minimum average value of these two stations is observed in August, respectively (Figure 24a and 24b). The maximum average value corresponds to January to March in both studied points. The intensity of this radiation flux is greater than that of the incoming short-wave radiation flux. It represents a large part of the energy portion that enters the Earth-atmosphere system in the study area.

4.4.2. Net Radiation of Chimborazo Province

The first location analyzed in this province was Alao located at 3,064m, it presents nearly-constant net radiation during the winter months (December-May) (Figure 25a). In July, its minimum value is registered with 67.74 W/m^2. The following months show a significant rise until reaching the month of November, where its maximum value is recorded 129.06 W/m^2.
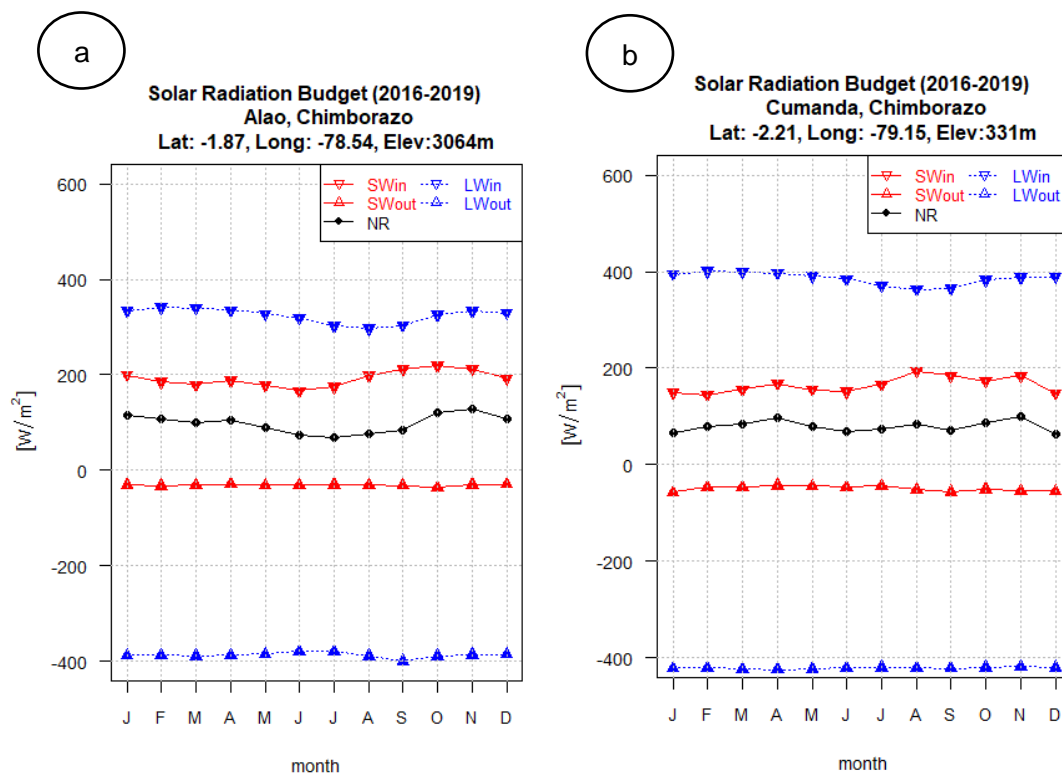
Figure 25: *Solar Radiation budget in Chimborazo Province, a) Alao, b) Cumanda*

The Cumanda station, which is located at the lowest elevation of all the stations, according to its energy balance in Figure 25b, shows the lowest net radiation averages. Its monthly average is 79.35 W/m^2. In this station, the lowest net radiation value is recorded in December (Figure 25b). The maximum value corresponds to November (Table 8). The incoming longwave radiation has a seasonal variation, in this province, June registered the low solar global radiation and, the maximum value is registered in October and August respectively.

The net radiation of this station represents the lowest percentage of the Global Radiation. Cumanda located at 331m, has the lowest value. In this station, the albedo (Table 8) has a higher index than the Alao zone, so the outgoing long-wave radiation flux increases, causing the net radiation at the surface to be the lowest. We can observe that net radiation, as in the

province of Azuay, represents ~ 50% of the global radiation that enters the atmosphere (global radiation), a consequence of reduced atmospheric radiation and high terrestrial radiation, as shown in the description of the energy balance variables. The values of Net Radiation are constant in the stations having an elevation between 2000 and 4000m.

Table 8: *Monthly net radiation and albedo of Chimborazo province.*

	Alao 3064m		Cumanda 331m	
month	Net Radiation [W/m2]	Albedo	Net Radiation [W/m2]	Albedo
Jan	115.11	0.17	64.86	0.37
Feb	106.39	0.18	77.84	0.32
Mar	99.50	0.18	85.19	0.30
Apr	106.23	0.16	97.59	0.25
May	89.52	0.18	79.25	0.28
Jun	74.17	0.21	68.26	0.30
Jul	67.74	0.20	73.55	0.26
Aug	75.88	0.16	84.03	0.26
Sep	83.45	0.17	72.34	0.29
Oct	120.54	0.17	86.36	0.29
Nov	129.06	0.16	100.19	0.30
Dec	107.03	0.18	62.80	0.36
Prom	97.88	0.18	79.35	0.30
Max	129.06	0.21	100.19	0.37
Min	67.74	0.16	62.80	0.25

The incoming solar shortwave radiation (SWin) in Alao has a constant behavior from January to June when the lowest value is observed. From July, there is an increase until October when the maximum is observed (Figures 25a and 25b). The variations in the values are due to the reasons already explained in the province of Azuay. In Cumanda, the flux of this radiation is lower due to the influence of cloudiness.

The outgoing shortwave radiation (SWout) in these two zones is constant in all months of the year, with an evident increase in the Cumanda station (Figures 25a and 25b) since this component of the solar radiation balance depends on cloud cover.

As for the incoming and outgoing longwave radiation fluxes (LWin and LWout) (Figures 25a and 25b), in Alao, the incoming flux registers a constant incidence throughout the year, except July through September when this index decreases. On the other hand, in Cumanda, this flux is higher than in Alao, and this is clearly due to the cloudiness indexes; since Cumanda is at a lower elevation, this index is lower. The long wave outgoing flux in Alao is lower than in Cumanda, and this is due to the fact that in Cumanda, the albedo recorded is higher than in Alao, which causes a greater reflection of radiation, registering that the outgoing flux of longwave radiation is more elevated in Cumanda.

4.4.3. Net Radiation of Pichincha Province

As in the previous provinces, two locations were chosen to calculate the energy balance in the province of Pichincha. The first location is in San Juan, with an elevation of 4280m. Secondly, the balance was calculated to obtain the net radiation in Pedro Vicente Maldonado with an elevation of 812m (Figures 26a and 26b). Table 9 shows the mean values of net radiation at both study sites.

As already known, different variables are involved in calculating net radiation (equation 3). In this province, more precisely in the San Juan area, the net radiation has a constant behavior with a monthly average of 139.22 W/m^2. From January to July, the net radiation index is remarkably constant until May, when it reaches its lowest value (128.48W/m^2) (Figures 26a and 26b). This constant radiation is maintained until July. The net radiation indexes increase from August onwards until October when it reaches the highest value (163.96W/m^2).

Net radiation in the Pedro Vicente Maldonado area is lower than in San Juan, registering a monthly average of 94.69W/m^2. The behavior of net radiation in this zone is also constant from January to August, registering minimum increases and decreases. In July, it reached the minimum value (67.43W/m^2). From September to November, the net radiation increases, the maximum value of net radiation is registered in November (108.42W/m^2), and after this month, a decrease is registered. In this area, the albedo is higher than in San Juan (Table 9), so there is an increase in the outgoing longwave radiation fluxes, and this explains the decrease in the net radiation indexes.

Table 9: *Monthly net radiation and albedo of Pichincha Province*

month	San Juan 4280m Net Radiation [W/m2]	Albedo	Pedro Vicente Maldonado 812m Net Radiation [W/m2]	Albedo
Jan	133.55	0.16	89.60	0.29
Feb	130.86	0.17	100.52	0.25
Mar	132.63	0.15	104.13	0.24
Apr	135.84	0.15	102.63	0.24
May	128.37	0.14	106.23	0.19
Jun	129.77	0.14	88.34	0.25
Jul	128.48	0.13	94.76	0.21
Aug	136.53	0.12	91.43	0.27
Sep	141.16	0.14	76.13	0.33
Oct	163.12	0.12	106.66	0.25
Nov	163.96	0.14	108.42	0.22
Dec	146.37	0.15	67.43	0.37
Prom	139.22	0.14	94.69	0.26
Max	163.96	0.17	108.42	0.37
Min	128.37	0.12	67.43	0.19

As mentioned in section 4.2, the province of Pichincha is one of the provinces of Ecuador with the highest global solar radiation. It can be seen in the solar radiation Budget the SWin indices are moderately high. Figure 26a shows that the incoming shortwave radiation flux in San Juan presents a seasonal behavior with the minimum value in May and the maximum in September. Likewise, in the Pedro Vicente Maldonado area, incoming shortwave radiation remains constant from December, where it reaches its lowest value, to August, where the lowest is recorded. These variations are explained, as in the province of Azuay, by the influence of the solar declination that generates the climatic seasons and the influence of the intertropical convergence zone that increases cloud levels.

The incoming longwave radiation (LWin) depends on the cloudiness indexes present in the study zones; for this reason, in the San Juan zone, the incoming longwave radiation is lower than in Pedro Vicente Maldonado (Figures 26a and 26 b), in the second study zone, there is a higher percentage of cloudiness, and this is explained because it is located in a zone of lower elevation.
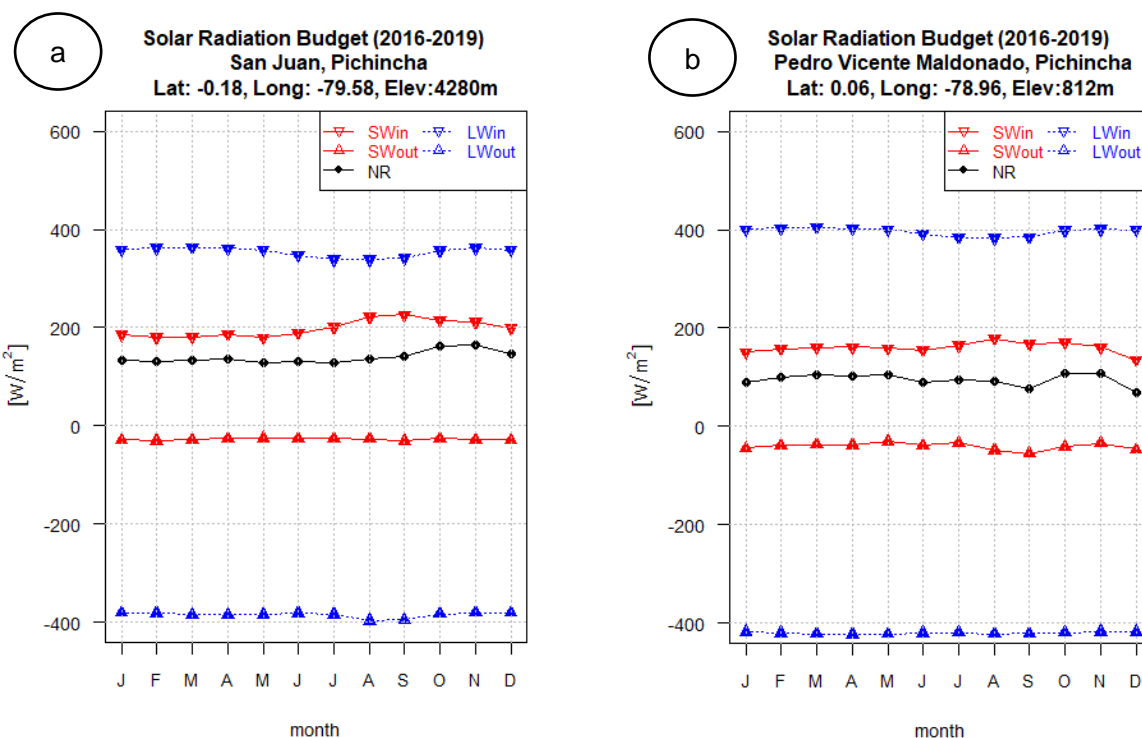
Figure 26: *Solar Radiation Budget in Pichincha Province, a) San Juan, b) Pedro Vicente Maldonado*

The outgoing shortwave radiation flux (SWout) is constant in San Juan and depends on cloud cover and atmospheric gases. In Pedro Vicente Maldonado, this flux has more variation during July, August, September, and October since this area are at a lower elevation and cloudiness indexes increase.

The outgoing longwave radiation flux (LWout) represents a large part of the energy entering the Earth. In San Juan, the LWout is lower than in Pedro Vicente Maldonado; this is explained by the increase of albedo in the second zone. This flux is only slightly higher than the absorbed shortwave radiation received in these two locations.

4.4.4. Annual Net Radiation

Figure 27 shows the map with the annual net radiation in the locations of each province. The annual net radiation is different depending on the zone where it is measured. Net radiation rates vary with altitude. Net radiation is a fraction of global solar radiation. In Azuay Province, net radiation is constant in the two zones studied.

On the other hand, there is a notable difference in the annual net radiation in the province of Chimborazo. Cumanda has low net radiation due to the altitude at which this station is located.

The region of Pichincha has higher rates of solar radiation incidence that is why the results of net annual radiation are higher in this province. As in Chimborazo, when calculating the net radiation in a lower altitude area, the net radiation decreases, as in the station of Pedro Vicente Maldonado, where the net annual radiation is lower than in San Juan. The results of net radiation are linked to the characteristics of each of the components involved in the surface solar energy balance, for example, in provinces with a higher incidence of global solar radiation, net radiation will be higher. In areas with higher albedo, the net radiation will be lower. Cloud cover also plays a role in calculating net radiation; in areas with more cloud cover, net radiation will decrease.
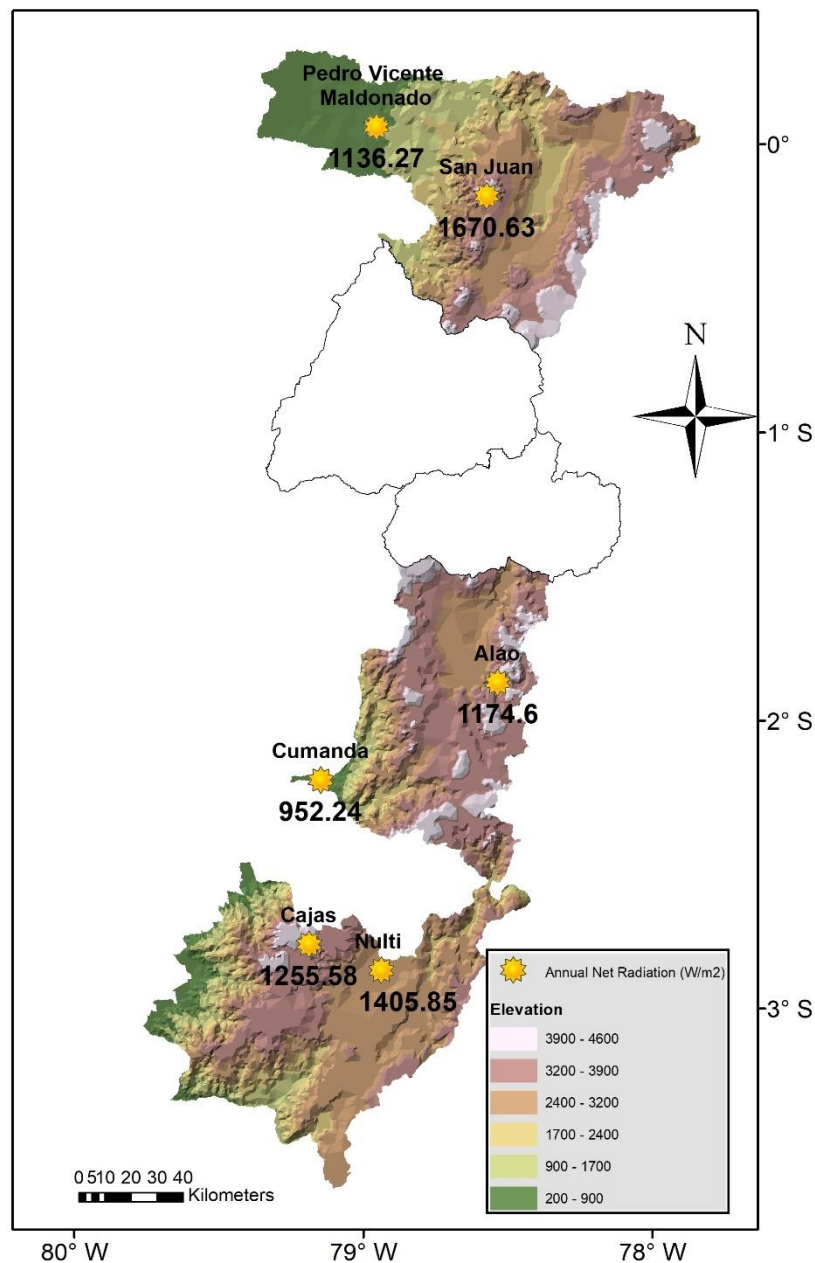
Figure 27: Annual Net Radiation in the locations of each province.

Chapter 5

Conclusions

One of the objectives of this work was to develop a methodology to validate CM-SAF satellite solar radiation data using ground measurements in the highlands of Ecuador. The methodology was described and applied to statistically compare satellite and ground data using time series and metrics of distribution similarity of the meteorological stations selected in the study.

It was necessary to perform a debugging of the terrestrial measurement databases because sometimes, not all radiation measurements are recorded, and this can cause problems when transforming the series from hourly to daily and monthly scale.

The RMSE calculated for the pairs of ground and satellite data showed that the solar global radiation satellite data are not yet reliable for direct use in solar radiation applications since these indices show values larger than 40% when the accepted range is up to 30%.

The MBE for the pairs of compared meteorological data show indices of around -40% thus an underestimation of data was found.

The KS test performed on the INER stations comparison shows that 33.3% of the meteorological stations studied on a daily scale exhibit normality of data, while 100% of the monthly measurements are normal.

The KS test performed on the DMQ stations comparison shows that data in daily scale are not related, while 100% of the monthly measurements are normal. The satellite global solar radiation data, on a monthly scale performs better than on the daily data concerning the surface data. According to the statistical analysis, although the monthly data passed tests such as the KS-test and the coefficient of determination, the other statistical tests such as RMSE and MBE were not passed.

In order to use the CM-SAF satellite data in monthly scale, it is necessary to perform a bias adjustment based on statistical indicators. By performing this bias adjustment, a complete database in monthly scale is made available, which provides us with GHI data.

Despite the satellite data limitations described above it was found that the product represents the major spatial pattern of global solar radiation and also its temporal variability because the satellite reflects the positive or negative anomalies in a daily, monthly or annual analysis.

The monthly net radiation data in the Zhurucay area were statistically validated since the calculated RMSE and MBE are within the accepted ranges, making it reliable to calculate net radiation with the monthly satellite data from CM-SAF.

This study has made possible to determine the particular characteristics of the radiative balance in the Ecuadorian highlands. Intense global solar radiation (due to the latitude and altitude of the area) corresponds to a constant high net radiation. In areas with an elevation equal or higher than 2000m, a relatively high net radiation is recorded, while in areas of lower altitude, the net radiation is low as seen on the areas of Cumanda and Pedro Vicente Maldonado.

The annual variation of incoming short-wave radiation in the analyzed points would influence solar declination and cloudiness. The incoming long-wave radiation flux presents a seasonal variation of lesser magnitude. The intensity of this radiation flux is greater than that of the incoming short-wave radiation flux and would represent a large part of the energetic portion that enters the Earth-Atmosphere system in the study area. The outgoing short-wave radiation shows less seasonal variation than the other variables. The albedo indices were very important in explaining the variation of the outgoing short-wave radiation flux. The outgoing long-wave radiation has a higher monthly mean intensity with seasonal variation. Cloud cover fraction and aerosol data are important tools in analyzing the contributions of the different parameters.

Radiative conditions in these provinces are very favorable for agriculture. High global radiation favors intense photosynthesis and important plant production and, in addition, low net radiation induces low water requirements for crops. These results are important for the development of agricultural production; the evidence of a low evapotranspiration might call for rethinking of irrigation strategies. However, the results are only based on measurements over 4 years (2016-2019).

Recommendations

It is recommended to use the monthly satellite global solar radiation data from CM-SAF after a bias correction.

It is recommended to conduct a more focused study to collect firstly net radiation data in different provinces of the country and subsequently to perform the validation of net radiation at various points. This would allow to asses the suitability of the evaluation criterion used in this study.

It is recommended to carry out a study focused only on cloud conditions throughout the country since they represent an essential part of the study of solar radiation.

REFERENCES

Achim Zeileis and Gabor Grothendieck (2005). zoo: S3 Infrastructure for Regular and Irregular Time Series. Journal of Statistical Software, 14(6), 1-27. doi:10.18637/jss.v014.i06

Akoglu, H. (2018). User's guide to correlation coefficients. Turkish Journal of Emergency Medicine, 18(3), 91–93. https://doi.org/10.1016/j.tjem.2018.08.001

Allen, P. . . (2009). *Earth Surface Processes* (J. W. & Sons. (Ed.)).

An, N., Hemmati, S., & Cui, Y. (2017). Engineering Assessment of the methods for determining net radiation at different time-scales of meteorological variables. *Journal of Rock Mechanics and Geotechnical Engineering*, *9*, 239–246. https://doi.org/10.1016/j.jrmge.2016.10.004

ARCONEL. (2020, March). *Balance Nacional de Energía Eléctrica*. https://www.regulacionelectrica.gob.ec/balance-nacional/

Augustine, J. A., DeLuisi, J. J., & Long, C. N. (2000). SURFRAD - A national surface radiation budget network for atmospheric research. *Bulletin of the American Meteorological Society*, *81*(10), 2341–2357. https://doi.org/10.1175/1520-0477(2000)081<2341:SANSRB>2.3.CO;2

Baigorria, G. A., Villegas, E. B., Trebejo, I., Carlos, J. F., & Quiroz, R. (2004). *ATMOSPHERIC TRANSMISSIVITY : DISTRIBUTION AND EMPIRICAL ESTIMATION AROUND THE CENTRAL ANDES*. *1136*, 1121–1136. https://doi.org/10.1002/joc.1060

Battan, L. J. (1979). Fundamentals of meteorology. In *Fundamentals of meteorology*. https://doi.org/10.1007/978-3-030-52655-9

Ben Hamner and Michael Frasco (2018). Metrics: Evaluation Metrics for Machine Learning.

R package version 0.1.4. https://CRAN.R-project.org/package=Metrics

Benavides, H., Simbaqueva, O., & Zapata, H. (2017). *Atlas de Radiacion Solar, Ultravioleta y Ozono de Colombia*.

Benedek, J., Sebestyén, T. T., & Bartók, B. (2018). Evaluation of renewable energy sources in peripheral areas and renewable energy-based rural development. *Renewable and Sustainable Energy Reviews*, *90*, 516–535. https://doi.org/10.1016/J.RSER.2018.03.020

Byrne, J., Taminiau, J., Kurdgelashvili, L., & Kim, K. N. (2015). A review of the solar city concept and methods to assess rooftop solar electric potential, with an illustrative application to the city of Seoul. *Renewable and Sustainable Energy Reviews*, *41*, 830–844. https://doi.org/10.1016/j.rser.2014.08.023

Caldwell, M. M., Teramura, A. H., & Tevini, M. (1989). The changing solar ultraviolet climate and the ecological consequences for higher plants. *Trends in Ecology and Evolution*, *4*(12), 363–367. https://doi.org/10.1016/0169-5347(89)90100-6

Campbell Scientific CM3 Kipp and Zonen Pyranometer User Manual. (n.d.). Retrieved March 19, 2022, from https://manualmachine.com/campbellscientific/cm3kippandzonenpyranometer/1396953 -user-manual/

Carl, C. (2014). Calculating Solar Photovoltaic Potential on Residential Rooftops in Kailua Kona, Hawaii. *Geographic Information Science and Technology*, *MASTER OF*(May), 1–83.

Cevallos-Sierra, J., & Ramos-Martin, J. (2018). Spatial assessment of the potential of renewable energy: The case of Ecuador. *Renewable and Sustainable Energy Reviews*, *81*(July 2016), 1154–1165. https://doi.org/10.1016/j.rser.2017.08.015

Chamorro, M. V., Ortíz, E. V., & Viana, L. A. (2015). Cuantificación y caracterización de la

radiación solar en el departamento de La Guajira-Colombia mediante el cálculo de transmisibilidad atmosférica. *Prospectiva*, *13*(2), 54–63.

Chicco, D., Warrens, M. J., & Jurman, G. (2021). The coefficient of determination R-squared is more informative than SMAPE, MAE, MAPE, MSE and RMSE in regression analysis evaluation. *PeerJ Computer Science*, *7*, 1–24. https://doi.org/10.7717/PEERJ-CS.623/SUPP-1

CMP6, CMP11, and CMP21 Kipp & Zonen Solar Radiation Sensors _ Manualzz.pdf. (n.d.).

CONELEC. (2008). Atlas solar del ecuador. *Conelec*, 1–51. http://www.conelec.gob.ec/archivos_articulo/Atlas.pdf

Dincer, I. (1998). Energy and environmental impacts: Present and future perspectives. *Energy Sources*, *20*(4–5), 427–453. https://doi.org/10.1080/00908319808970070

Dudley, B. (2018). BP Statistical Review of World Energy. *BP Statistical Review of World Energy*, *67*, 1–56.

Echegaray-Aveiga, R., Masabanda, M., Rodríguez, F., Toulkeridis, T., & Mato, F. (2018). *Solar Energy Potential in Ecuador*. 46–51. https://www-computer-org.bibliotecavirtual.udla.edu.ec/csdl/proceedings/icedeg/2018/2521/00/08372318.pdf

Emck, P. (2007). *A Climatology of South Ecuador*. 1–159.

Espinar, B., Ramírez, L., Drews, A., Beyer, H. G., Zarzalejo, L. F., Polo, J., & Martín, L. (2009). Analysis of different comparison parameters applied to solar radiation data from satellite and German radiometric stations. *Solar Energy*, *83*(1), 118–125. https://doi.org/10.1016/j.solener.2008.07.009

Figueira, G., & Angel, H. J. (2015). Climatologia: Radiación, Balance energético. Temperatura. *Books Abroad*, *19*(3), 8. http://www.jstor.org/stable/10.2307/40085784?origin=crossref

Garg, H. ., & Prakash, J. (2000). *Solar Energy: Fundamentals and applications.* (T. M.-H. Education (Ed.)).

Geraldo-Ferreira, A., Soria-Olivas, E., Gómez-Sanchis, J., Serrano-López, A. J., Velázquez-Blazquez, A., & López-Baeza, E. (2011). Modelling net radiation at surface using "in situ" netpyrradiometer measurements with artificial neural networks. *Expert Systems with Applications*, *38*(11), 14190–14195. https://doi.org/10.1016/j.eswa.2011.04.231

Gueymard, C. A., & Myers, D. R. (2008). *Solar Radiation Measurement: Progress in Radiometry for Improved Modeling BT - Modeling Solar Radiation at the Earth's Surface: Recent Advances*. 1–27. https://doi.org/10.1007/978-3-540-77455-6_1

Hadley Wickham and Jennifer Bryan (2022). readxl: Read Excel Files. R package version 1.4.0. https://CRAN.R-project.org/package=readxl

Jeffrey A. Ryan and Joshua M. Ulrich (2020). xts: eXtensible Time Series. R package version 0.12.1. https://CRAN.R-project.org/package=xts

Karlsson, K. G., Anttila, K., Trentmann, J., Stengel, M., Fokke Meirink, J., Devasthale, A., Hanschmann, T., Kothe, S., Jaäskelaïnen, E., Sedlar, J., Benas, N., Van Zadelhoff, G. J., Schlundt, C., Stein, Di., Finkensieper, S., Häkansson, N., & Hollmann, R. (2017). CLARA-A2: The second edition of the CM SAF cloud and radiation data record from 34 years of global AVHRR data. *Atmospheric Chemistry and Physics*, *17*(9), 5809–5828. https://doi.org/10.5194/acp-17-5809-2017

Kiehl, J. T., & Trenberth, K. E. (1997). Earth ' s Annual Global Energy Budget. *Bulletin of the American Meteorological Society*, *78*(2), 197–208.

Kothe, S., Hollmann, R., Pfeifroth, U., Träger-Chatterjee, C., & Trentmann, J. (2019). The CM SAF R Toolbox—a tool for the easy usage of satellite-based climate data in NetCDF format. In *ISPRS International Journal of Geo-Information* (Vol. 8, Issue 3). https://doi.org/10.3390/ijgi8030109

Laine, V., Venäläinen, A., Heikinheimo, M., & Hyvärinen, O. (1999). Estimation of surface solar global radiation from NOAA AVHRR data in high latitudes. *Journal of Applied Meteorology*, *38*(12), 1706–1719. https://doi.org/10.1175/1520-0450(1999)038<1706:EOSSGR>2.0.CO;2

Liang, S. (2004). Quantitative remote sensing of land surfaces. In J. W. & Sons (Ed.), *The Photogrammetric Record* (Vol. 19, Issue 108). https://doi.org/10.1111/j.0031-868x.2004.295_1.x

Liou, K. N. (2002). *An Introduction to atmospheric radiation.* (Elsevier (Ed.)).

Liu, B. Y. H., & Jordan, R. C. (1960). The interrelationship and characteristic distribution of direct, diffuse and total solar radiation. *Solar Energy*, *4*(3), 1–19. https://doi.org/10.1016/0038-092X(60)90062-1

Massey, F. J. (1951). The Kolmogorov-Smirnov Test for Goodness of Fit. *Journal of the American Statistical Association*, *46*(253), 68. https://doi.org/10.2307/2280095

McGregor, G. R., & Nieuwolt, S. (1998). *Tropical climatology: an introduction to the climates of the low latitudes* (J. W. & S. Ltd. (Ed.); 2nd ed.).

Meza, F., & Varas, E. (2000). *Estimation of mean monthly solar global radiation as a function of temperature. 100*, 231–241.

Meza, F., & Yebra, M. (2016). Estimation of daily global solar radiation as a function of routine meteorological data in Mediterranean areas. *Theoretical and Applied Climatology*, *125*(3–4), 479–488. https://doi.org/10.1007/s00704-015-1519-6

Mueller, R. W., Matsoukas, C., Gratzki, A., Behr, H. D., & Hollmann, R. (2009). The CM-SAF operational scheme for the satellite based retrieval of solar surface irradiance - A LUT based eigenvector hybrid approach. *Remote Sensing of Environment*, *113*(5), 1012–1024. https://doi.org/10.1016/j.rse.2009.01.012

Munkhammar, J. (2019). *Solar Radiation Theory* (Issue April). https://doi.org/10.33063/diva-381852

Nicol, N., & Concepci, E. Z. (2019). *Evaluación empírica de modelos de transposición de radiación solar difusa Tesis para optar al grado de Magíster en Ciencias de la Ingeniería con*.

Nikolov, T., & Petrov, N. (2014). Main factors influencing climate change: A review. *Comptes Rendus de L'Academie Bulgare Des Sciences*, *67*(11), 1455–1476.

Núñez, M., Valiente, J. A., Fortea, J. C., Baeza, E. L., & Moreno, J. (1994). *Estimación del balance de radiación en superficie mediante datos de satélite*. 3–6.

Ochoa-Sánchez, A., Crespo, P., Carrillo-Rojas, G., Sucozhañay, A., & Célleri, R. (2019). Actual evapotranspiration in the high andean grasslands: A comparison of measurement and estimation methods. *Frontiers in Earth Science*, *7*(March), 1–16. https://doi.org/10.3389/feart.2019.00055

Olcoz Larrayoz, A., Solano Goñi, M., & Barrio, I. P. (2014). *Implementación de método Heliosat para la estimación de la radiación solar a partir de imágenes de satélite*. 92. http://academica-e.unavarra.es/handle/2454/11784

Olmo, F. J., Vida, J., Foyo, I., Castro-Diez, Y., & Alados-Arboledas, L. (1999). Prediction of global irradiance on inclined surfaces from horizontal global irradiance. *Energy*, *24*(8), 689–704. https://doi.org/10.1016/S0360-5442(99)00025-0

Ordonez, F., Vaca-Revelo, D., & Lopez-Villada, J. (2019). Assessment of the Solar Resource in Andean Regions by Comparison between Satellite Estimation and Ground Measurements: Study Case of Ecuador. *Journal of Sustainable Development*, *12*(4), 62. https://doi.org/10.5539/jsd.v12n4p62

Paulescu, M., Paulescu, E., Gravila, P., & Badescu, V. (2013). Weather Modeling and Forecasting of PV Systems Operation. *Green Energy and Technology*, *103*.

https://doi.org/10.1007/978-1-4471-4649-0

Perez, R., Ineichen, P., Seals, R., Michalsky, J., & Stewart, R. (1990). Modeling daylight Availability and Irradiance Components from Direct and Global Irradiance.pdf. *Solar Energy*, *44*(5), 271–289.

Pfeifroth, U., TrentmMüller, R., & Kothe, S. (2018). *Product User Manual Meteosat Solar Surface Irradiance and effective Cloud Albedo Climate Data records The SARAH climate data records*. 1–33. https://doi.org/10.5676/EUM

Philipp Schauberger and Alexander Walker (2021). openxlsx: Read, Write and Edit xlsx Files. R package version 4.2.5. https://CRAN.R-project.org/package=openxlsx

Polo, J. (2010). *Optimización de modelos de estimación de la radiación solar a partir de imágenes de satélite*.

Polo, J., Wilbert, S., Ruiz-Arias, J. A., Meyer, R., Gueymard, C., Súri, M., Martín, L., Mieslinger, T., Blanc, P., Grant, I., Boland, J., Ineichen, P., Remund, J., Escobar, R., Troccoli, A., Sengupta, M., Nielsen, K. P., Renne, D., Geuder, N., & Cebecauer, T. (2016). Preliminary survey on site-adaptation techniques for satellite-derived and reanalysis solar radiation datasets. *Solar Energy*, *132*, 25–37. https://doi.org/10.1016/j.solener.2016.03.001

R Core Team (2021). R: A language and environment for statistical computing. R Foundation for Statistical Computing, Vienna, Austria. URL https://www.R-project.org/.

Raush, J. R., Chambers, T. L., Russo, B., & Crump, K. (2016). Assessment of local solar resource measurement and predictions in south Louisiana. *Energy, Sustainability and Society*, *6*(1). https://doi.org/10.1186/s13705-016-0083-y

Reda, I., & Andreas, A. (2004). Solar position algorithm for solar radiation applications. *Solar Energy*, *76*(5), 577–589. https://doi.org/10.1016/j.solener.2003.12.003

Rossel, F., & Cadier, E. (2009). Advanced Bash-Scripting Guide An in-depth exploration of the art of shell scripting Table of Contents. *Hyrdrological Process*, *2274*(November 2008), 2267–2274. https://doi.org/10.1002/hyp

Rubio, A. A., Ciobotaru, C. K., & Peinado, P. L. (2015). *Innovación conocimiento.*

Saffaripour, M. ., & Mehrabian, M. . (2009). Numerical methods applied to global solar radiation modeling – comparison with measured data. *International Journal of Numerical Methods for Heat & Fluid.* https://doi.org/10.1108/09615530910973002

Salcedo, A. B., Hollmann, R., Stuhlmann, R., & Baeza, L. (2001). *El balance de radiación de onda corta en superficie a partir de medidas de satélite.* 437–444.

Sanchez-Lorenzo, A., Wild, M., & Trentmann, J. (2013). Validation and stability assessment of the monthly mean CM SAF surface solar radiation dataset over Europe against a homogenized surface dataset (1983-2005). *Remote Sensing of Environment*, *134*, 355–366. https://doi.org/10.1016/j.rse.2013.03.012

Sengupta, M., Habte, A., Wilbert, S., Gueymard, C., & Remund, J. (2021). *Best Practices Handbook for the Collection and Use of Solar Resource Data for Solar Energy Applications: Third Edition. June*, 1–348.

Suarez, R. A. (2017). *Estimación del recurso solar en Uruguay mediante imágenes satelitales.*

Steffen Kothe (2021). cmsaf: A Toolbox for CM SAF NetCDF Data. R package version 3.2.0. https://CRAN.R-project.org/package=cmsaf

Trentmann, J. (2020). *EUMETSAT Satellite Application Facility on Climate Monitoring Product User Manual CM SAF Cloud , Albedo , Radiation data record , Cloud Products. 2*, 1–22. https://doi.org/10.5676/EUM

Trentmann, J., Pfeifroth, U., Cremer, R., & Stengel, M. (2020). *Global validation of satellite-*

based and reanalysis surface solar radiation data sets. 5194.

Urraca, R., Gracia-Amillo, A. M., Huld, T., Martinez-de-Pison, F. J., Trentmann, J., Lindfors, A. V., Riihelä, A., & Sanz-Garcia, A. (2017). Quality control of global solar radiation data with satellite-based products. *Solar Energy*, *158*(September), 49–62. https://doi.org/10.1016/j.solener.2017.09.032

Vaca, D., Ordóñez, F., & Villada López, J. (2019). Mapa Solar del Ecuador 2019. *Scinergy*, 12–26. https://www.ingenieriaverde.org/wp-content/uploads/2020/01/Mapa_Solar_del_Ecuador_2019.pdf

Van den Broeke, M., Fettweis, X., & Mölg, T. (2011). Surface energy balance. *Encyclopedia of Earth Sciences Series*, *Part 3*, 1112–1123. https://doi.org/10.1007/978-90-481-2642-2_132

Vignola, F., Michalsky, J., & Stoffel, T. (2019). *Solar and Infrared Radiation Measurements.* CRC press.

Volpe, P. (2014). A Theoretical Overview of Bioresponse to Magnetic Fields on the Earth's Surface. *International Journal of Geosciences*, *05*(10), 1149–1162. https://doi.org/10.4236/IJG.2014.510097

Wald, L. (2018). Basics in Solar Radiation At Earth Surface. *Hal*, *January*, 57. https://doi.org/10.13140/RG.2.2.36149.93920

Wang, Y., Trentmann, J., Yuan, W., & Wild, M. (2018). Validation of CM SAF CLARA-A2 and SARAH-E surface solar radiation datasets over China. *Remote Sensing*, *10*(12), 1–18. https://doi.org/10.3390/rs10121977

Whiteman, C. D., Allwine, J., Fritschen, L., Orgill, M., & Simpson, J. (1988). Deep Valley Radiation and Surface Energy Budget Microclimates. *Journal of Applied Meteorology*, *Radiation*.

Woick, H., Dewitte, S., Feijt, A., Gratzki, A., Hechler, P., Hollmann, R., Karlsson, K. G., Laine, V., Löwe, P., Nitsche, H., Werscheck, M., & Wollenweber, G. (2002). The satellite application facility on climate monitoring. *Advances in Space Research*, *30*(11), 2405–2410. https://doi.org/10.1016/S0273-1177(02)80290-3

World Metereological Organization. (2008). *Guide to meteorological instruments and methods of observation.* (7th ed., Issue 8).

Zaror, C. A. (2002). *" INTRODUCCION A LA INGENIERIA AMBIENTAL PARA LA INDUSTRIA DE PROCESOS "* (U. de Concepción (Ed.)).

Zuñiga, I., & Crespo del Arco, E. (2021). *Meteorología y climatología.* (E. UNED. (Ed.)).

ANNEXES

Annex 1.

Table A 1. *Net Radiation data of Zhurucay Zone*

date	Net Radiation [W/m^2]
2017-04	90.74
2017-05	97.829
2017-06	76.56
2017-07	100.24
2017-08	87.9
2017-09	106.33
2017-10	116.26
2017-11	107.75
2017-12	119.09
2018-01	119.09
2018-02	100.1
2018-03	94.99

Net Radiation of Zhurucay zone.
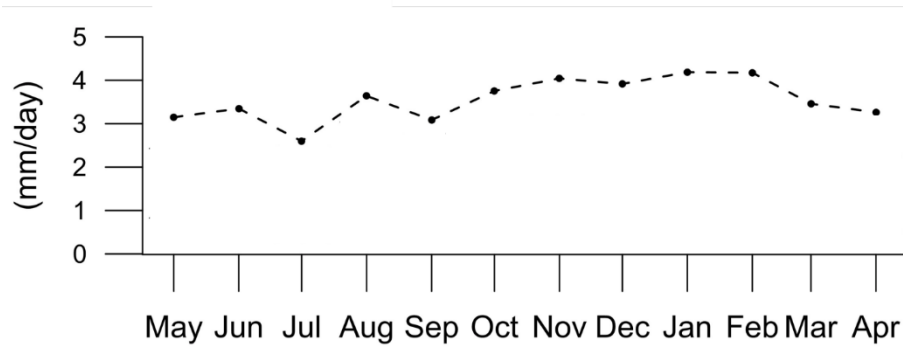
Annex 2.

BoxPlots to identify outliers of IIGE stations

Baños Station (INER 5) IIGE Surface Data

GHI [W/m²]
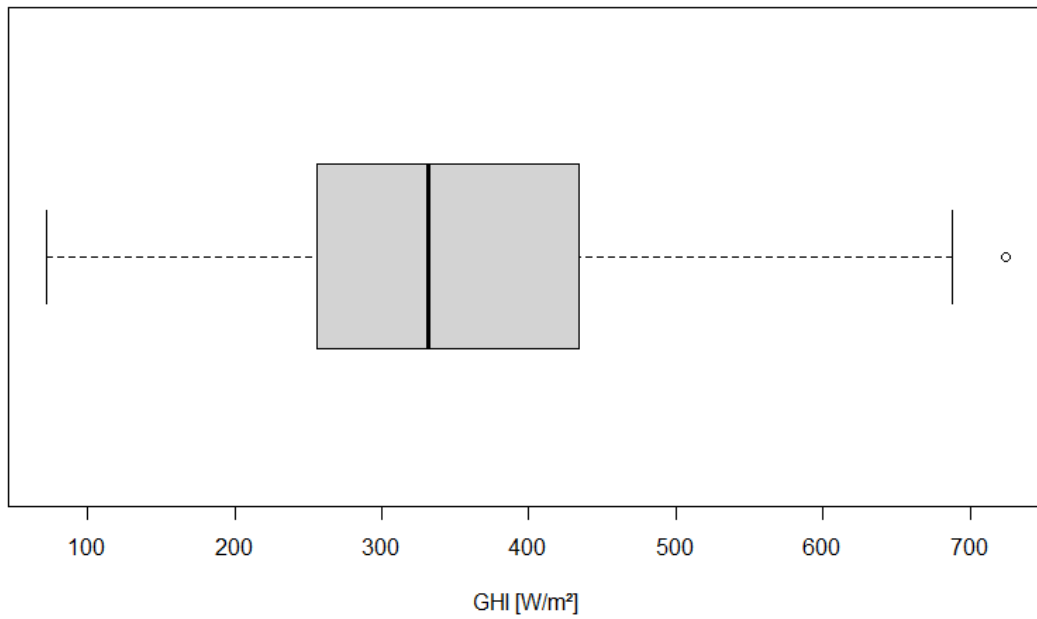
Altillo Station (INER 7) IIGE Surface Data

GHI [W/m²]
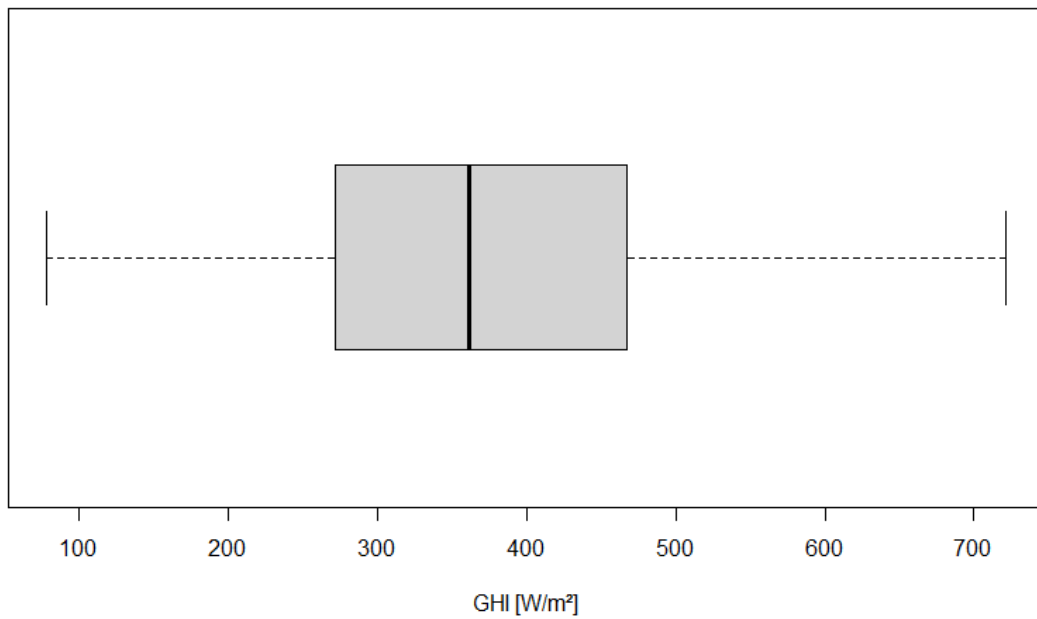
Tixan Pistilli Station (INER 8) IIGE Surface Data

GHI [W/m²]
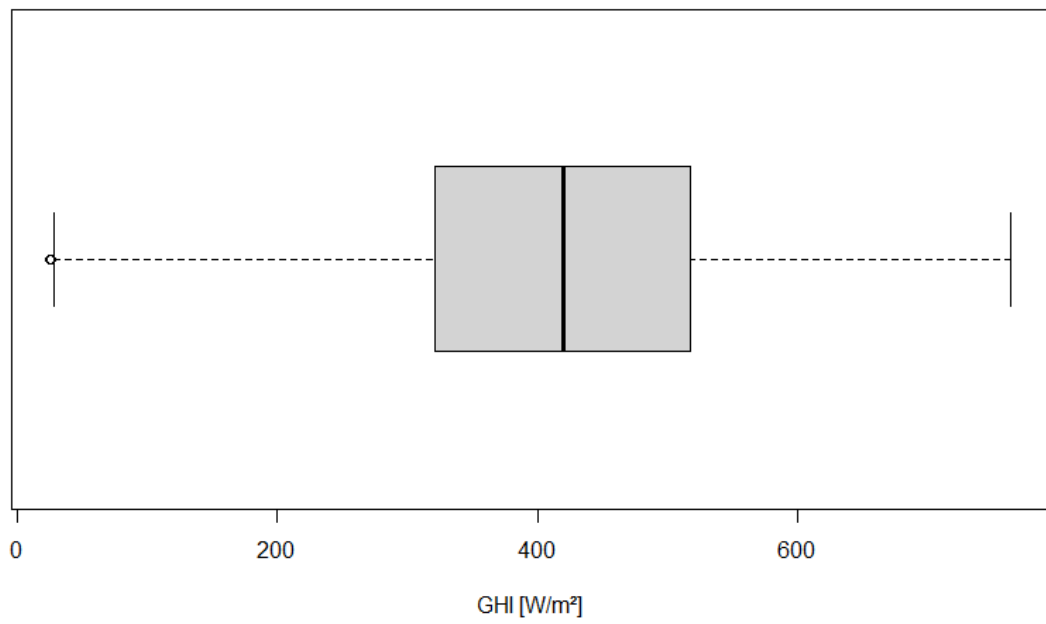
Santa Ana Station (INER 15) IIGE Surface Data

GHI [W/m²]
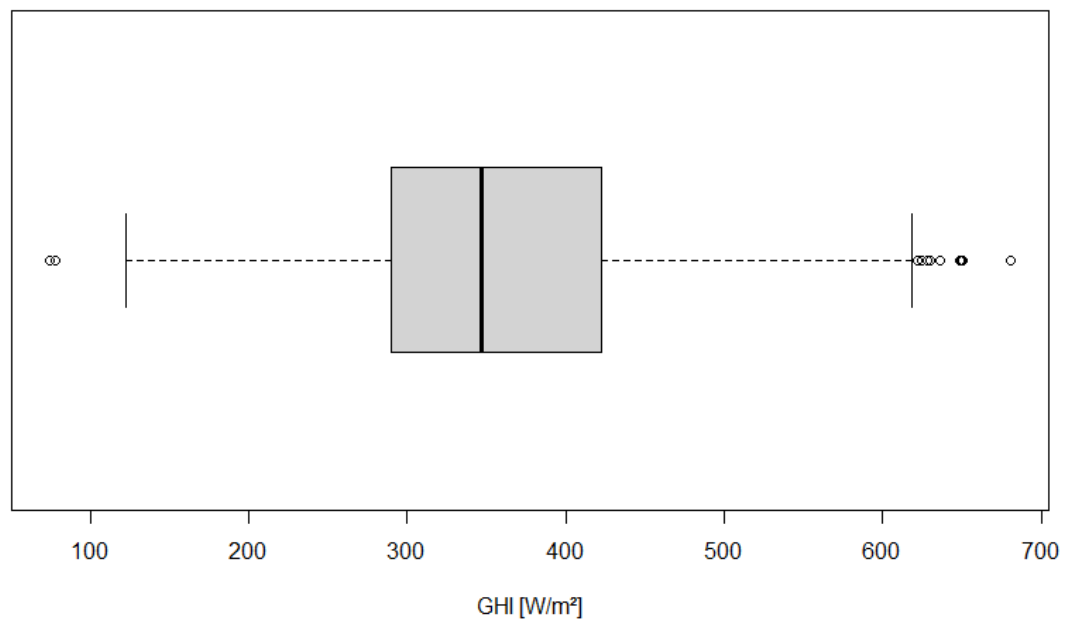
Yanuncay Station (INER 17) IIGE Surface Data

GHI [W/m²]
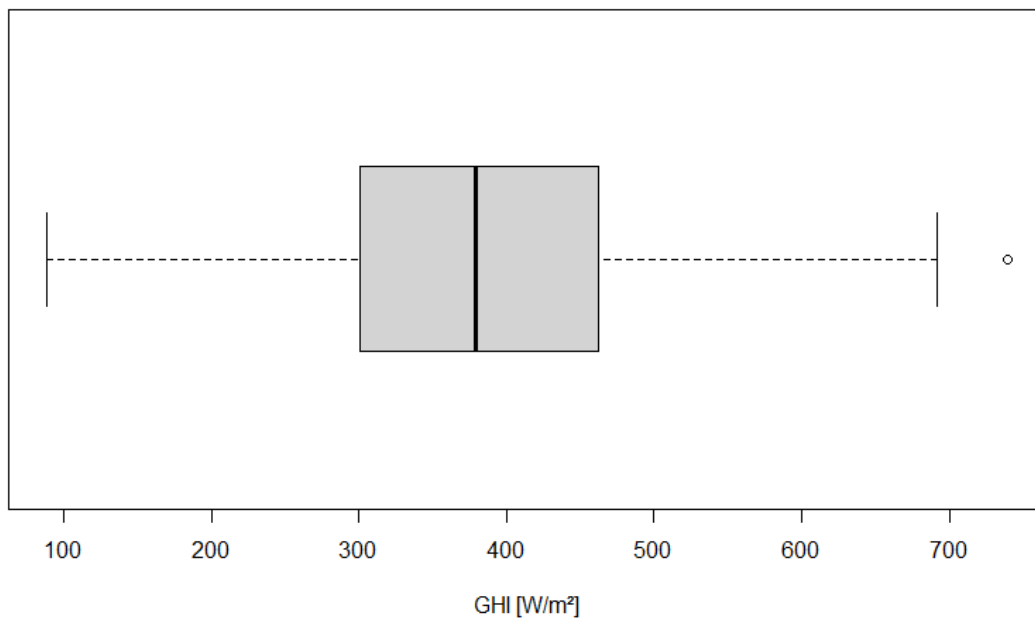
El Vecino Station (INER 18) IIGE Surface Data

GHI [W/m²]
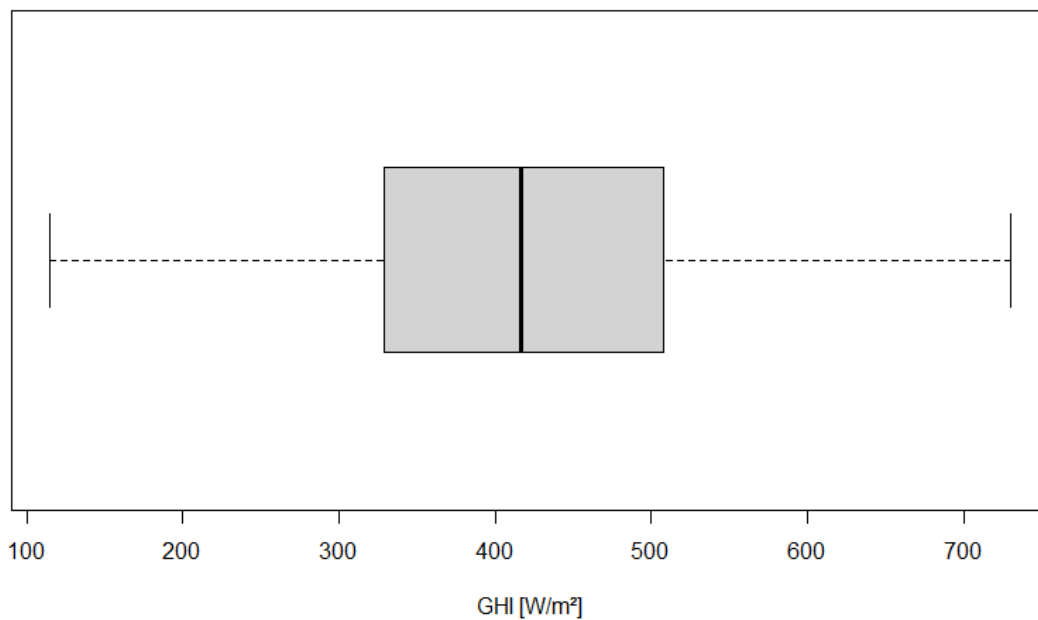
Irquis Station (INER 19) IIGE Surface Data

GHI [W/m²]
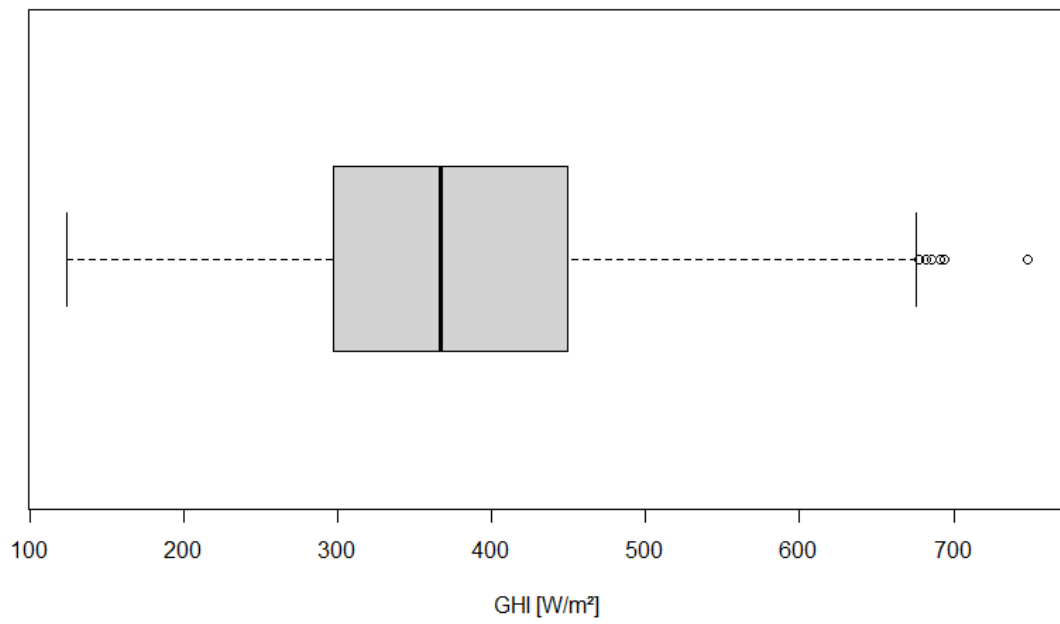
Quingeo Station (INER 20) IIGE Surface Data

GHI [W/m²]
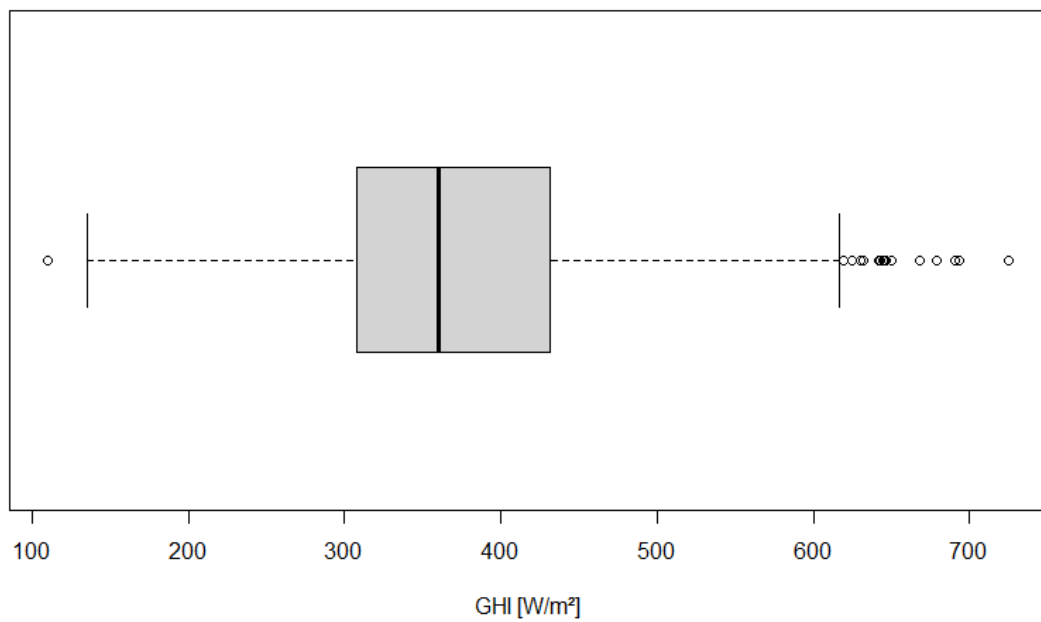
Cumbe Station (INER 21) IIGE Surface Data

GHI [W/m²]
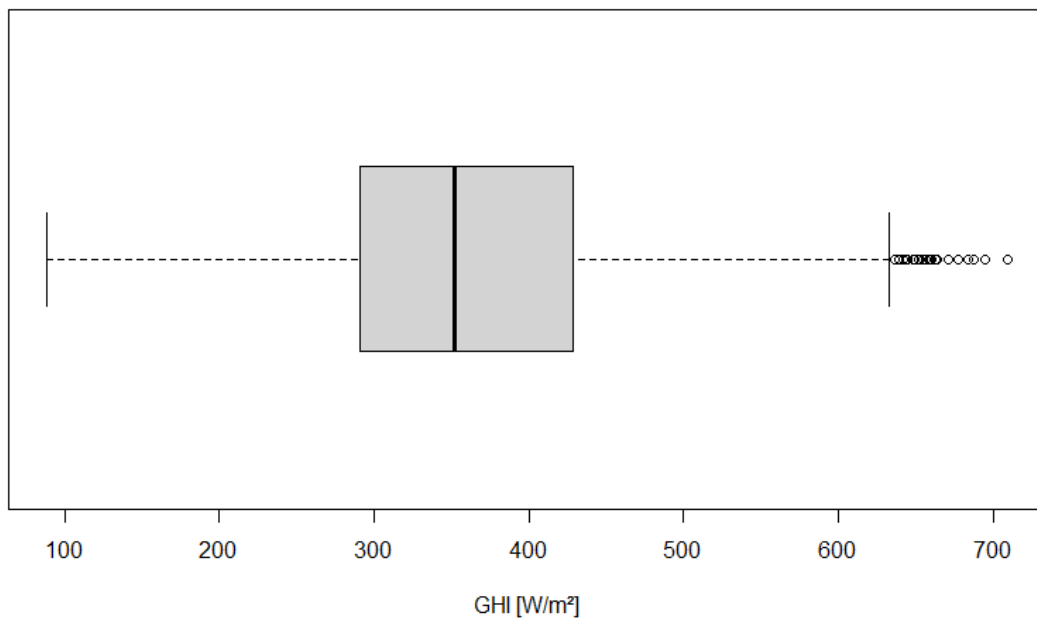
San Joaquin Station (INER 22) IIGE Surface Data

GHI [W/m²]
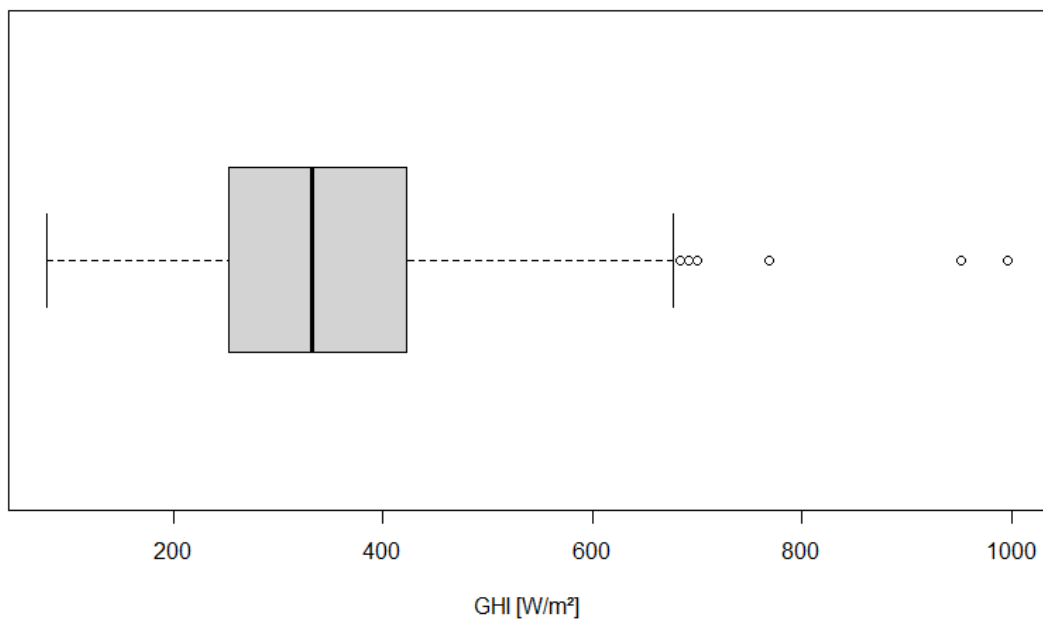
Sayausi Station (INER 23) IIGE Surface Data

GHI [W/m²]
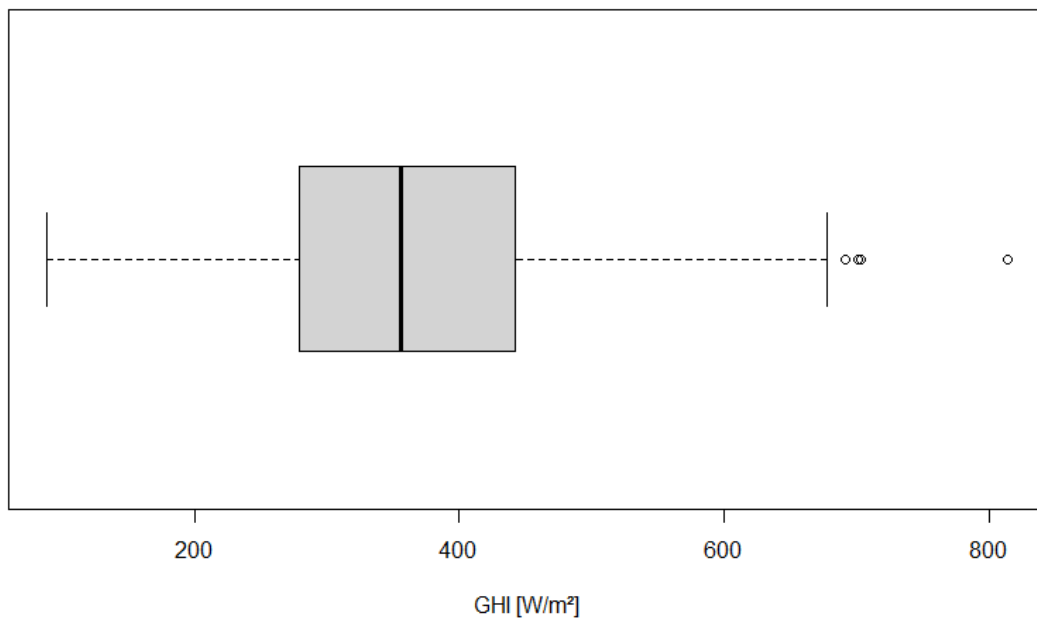
Turi Station (INER 24) IIGE Surface Data

GHI [W/m²]
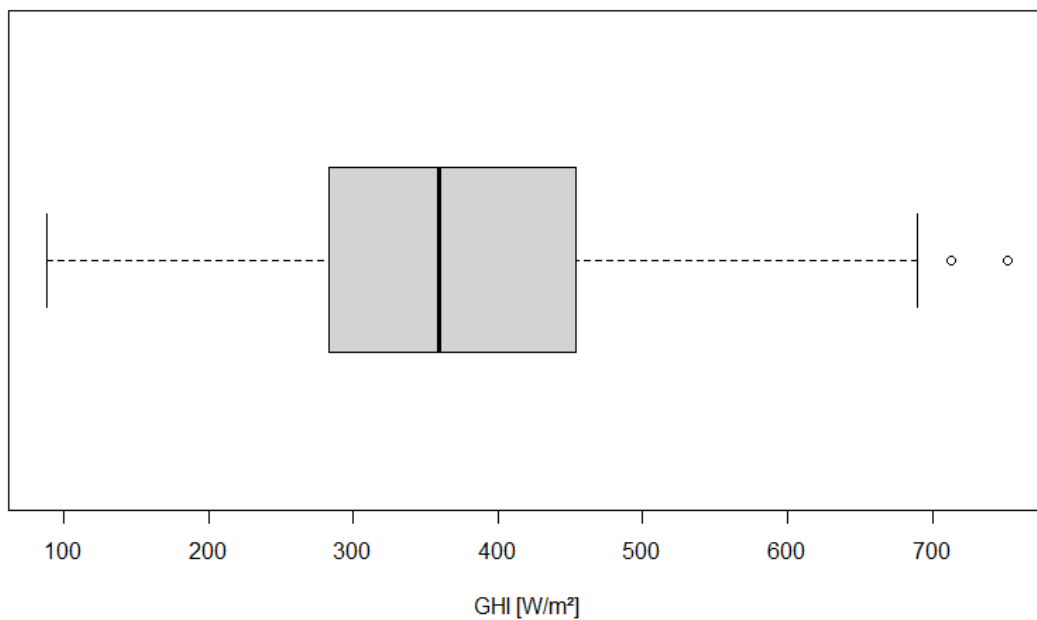
Annex 3.

Time series in monthly and daily scale of INER and DMQ stations and satellite data and the annual cycle average of 2016, 2017 and 2018.

Altillo Station

ALTILLO STATION, INER 7
Solar Global Radiation, 2016, 2017, 2018
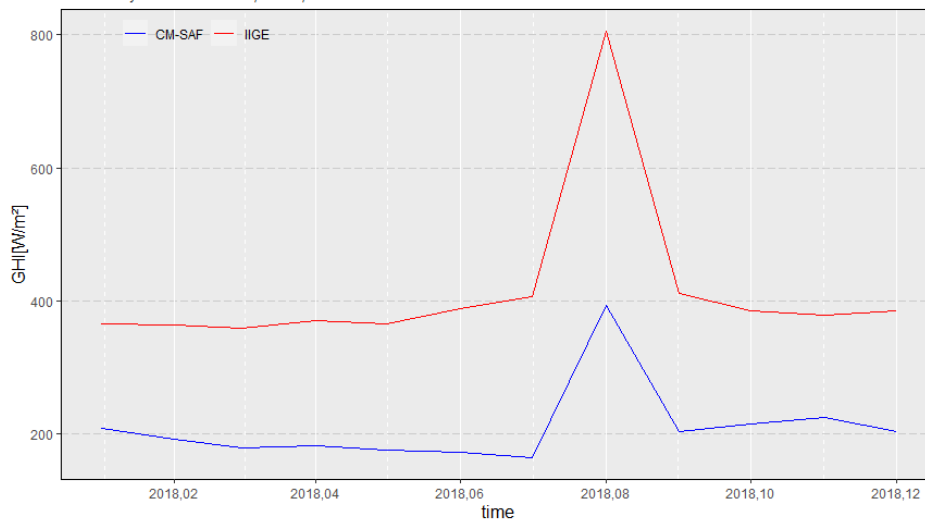Daily Scale

Altillo Station, INER 7   R² = 0,1928
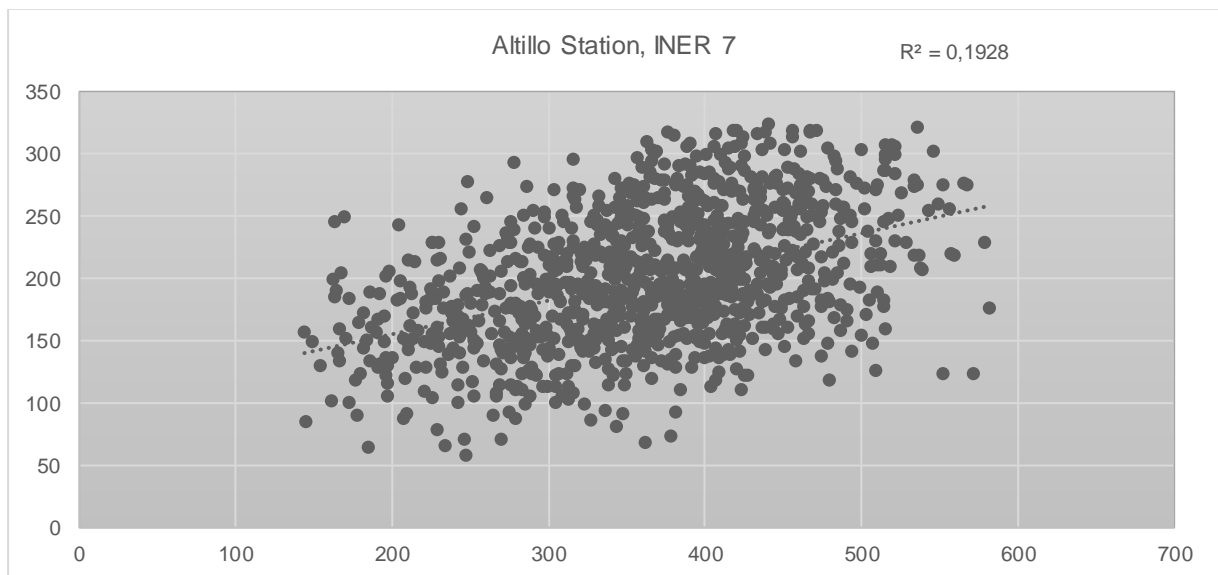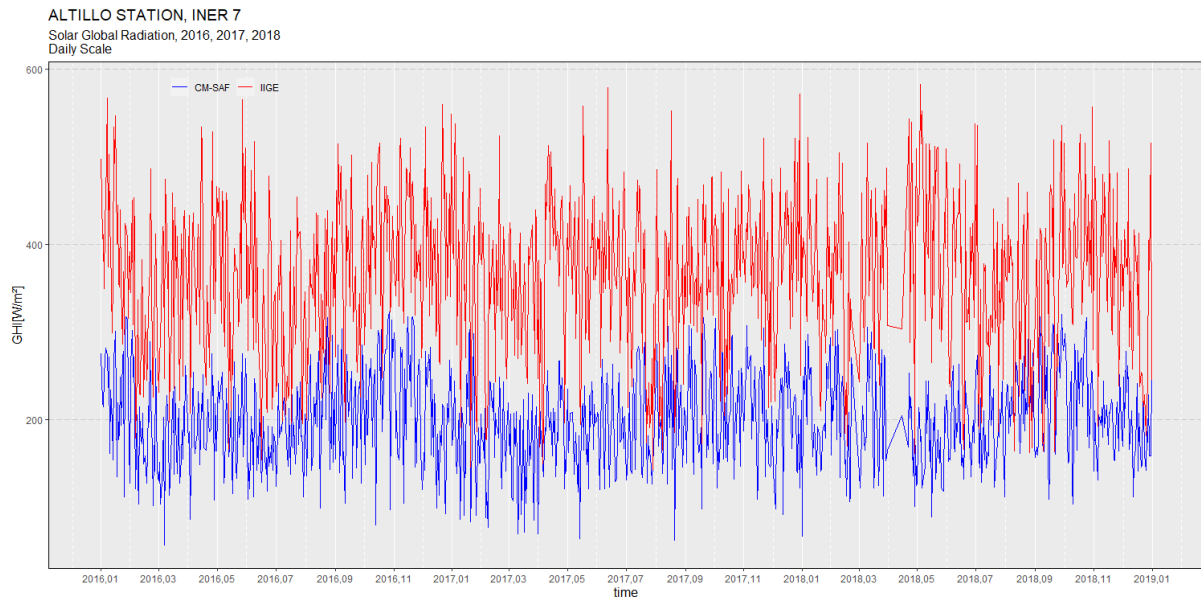
ALTILLO STATION, INER 7
Solar Global Radiation, 2016, 2017, 2018
Monthly Scale

Altillo, INER 7

R² = 0,0545
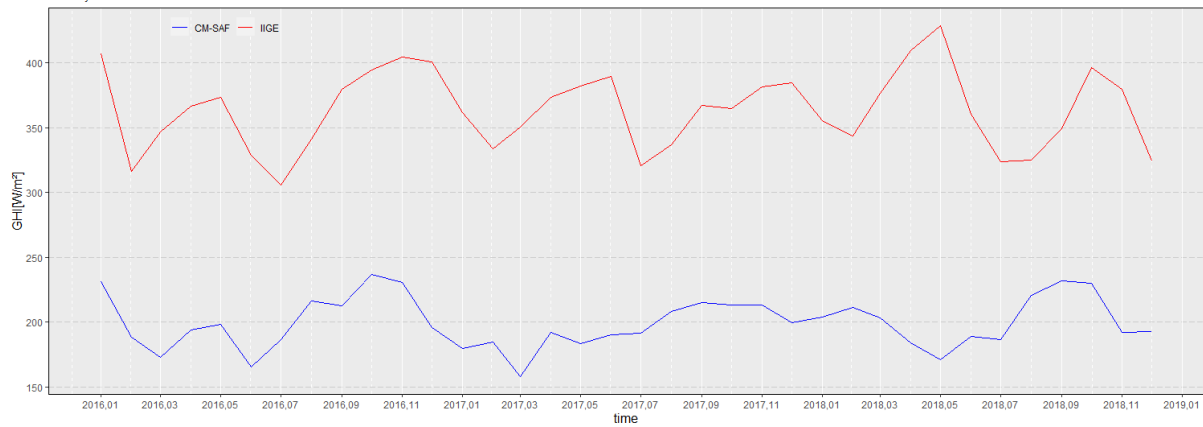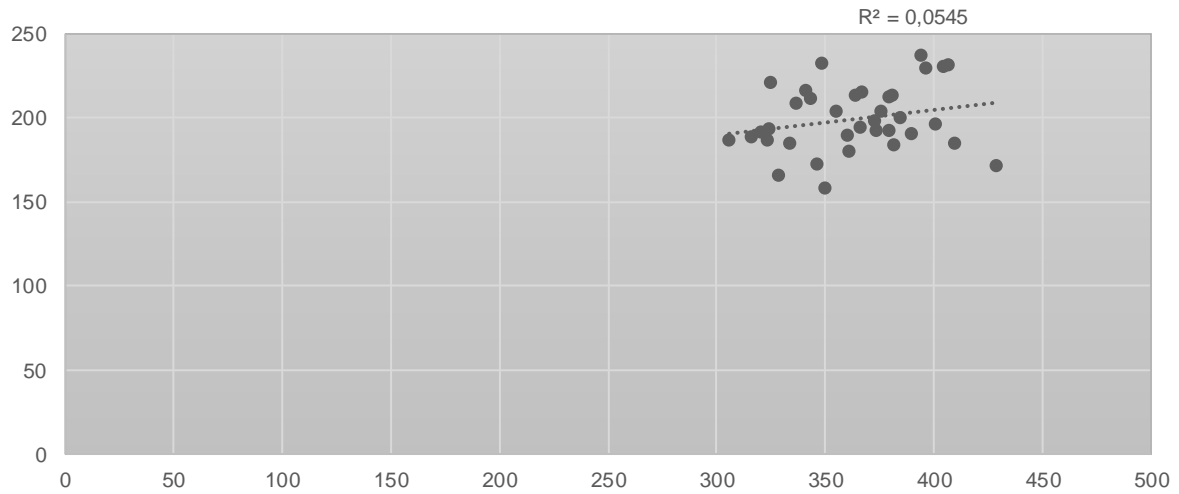
ALTILLO STATION, INER 7
Annual Cycle Mean: 2016, 2017, 2018
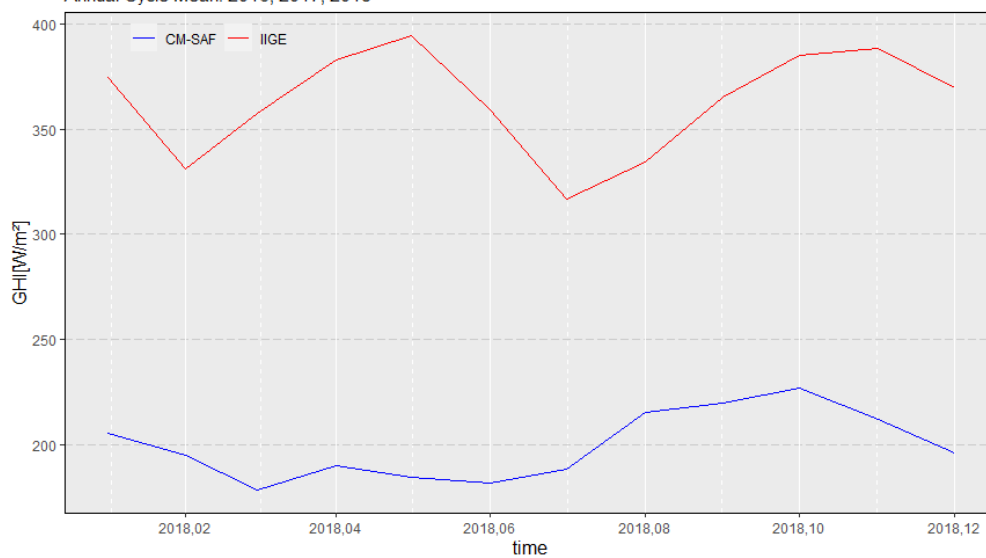
Tixan Pistilli station

TIXAN PISTILLI STATION, INER 8
Solar Global Radiation, 2016, 2017, 2018
Daily Scale
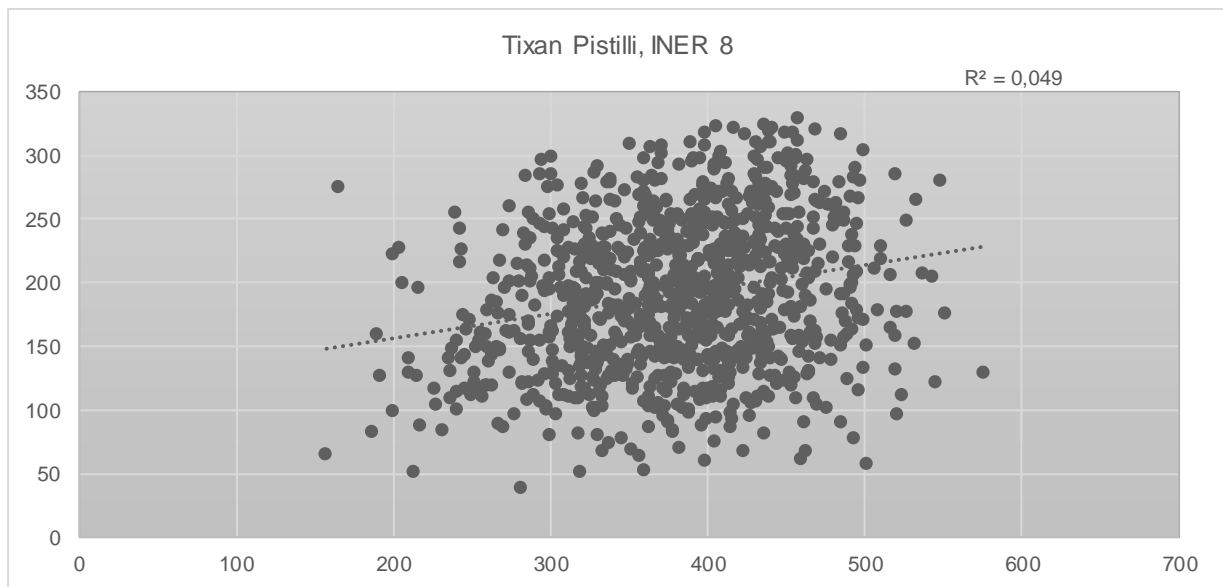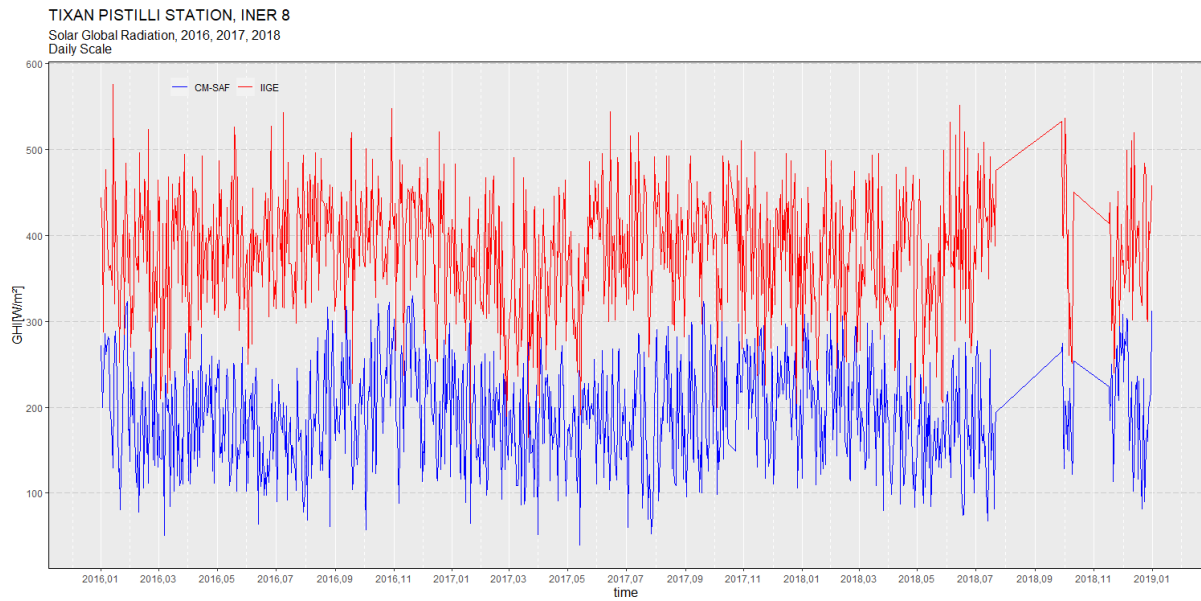
TIXAN PISTILLI STATION, INER 8
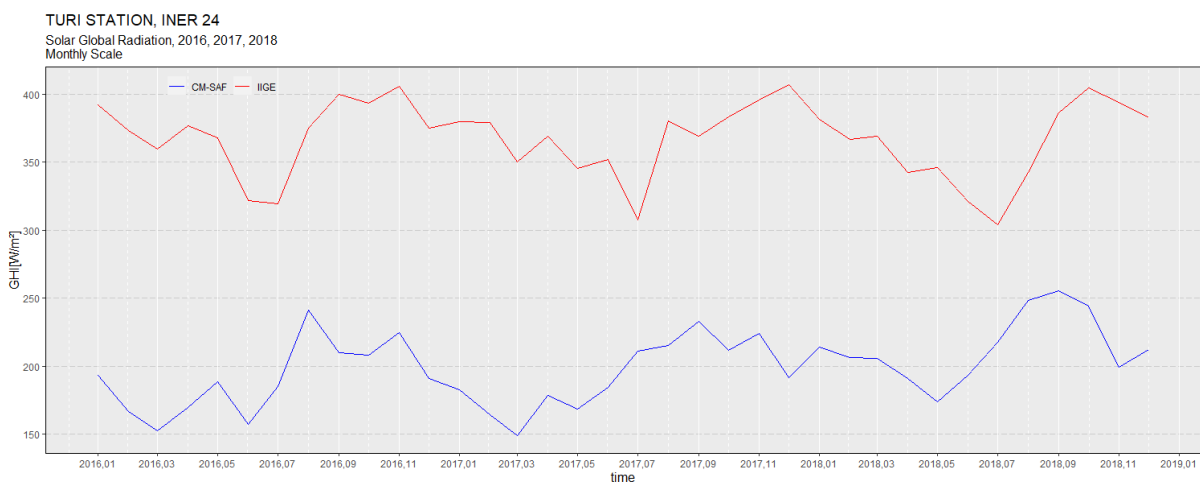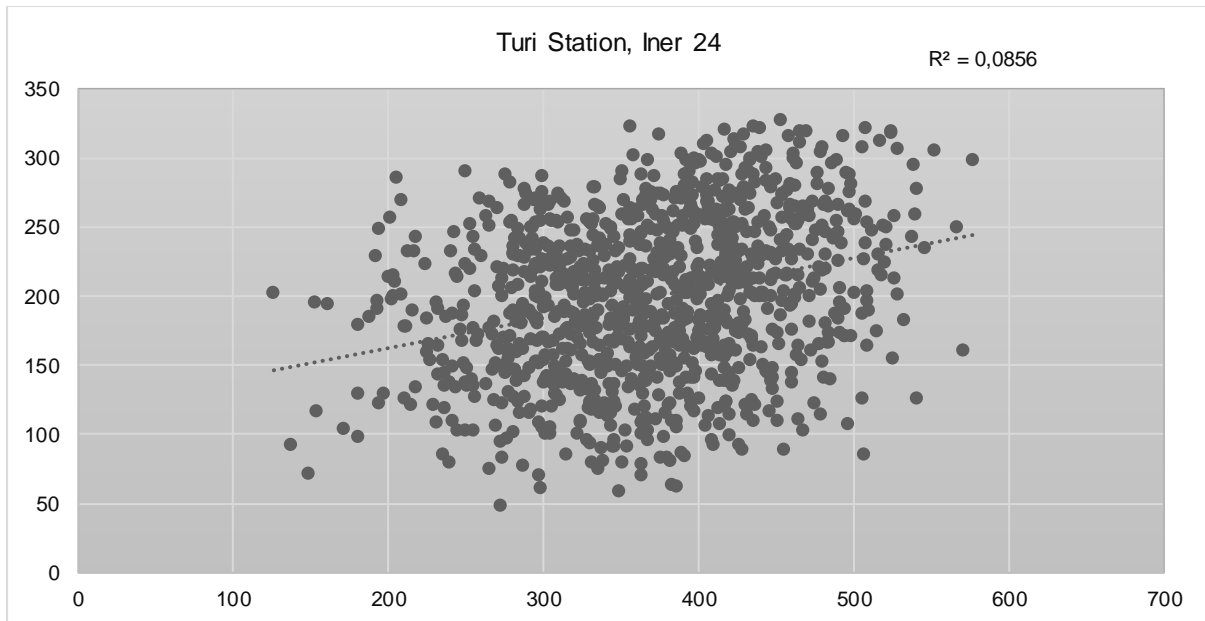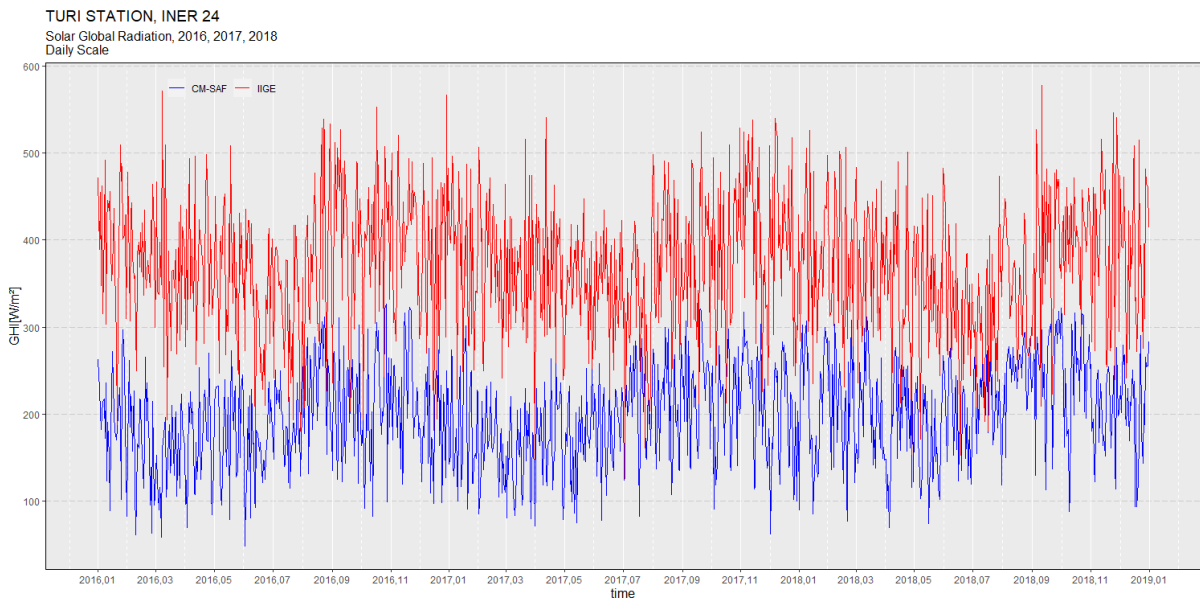Solar Global Radiation, 2016, 2017, 2018
Monthly Scale
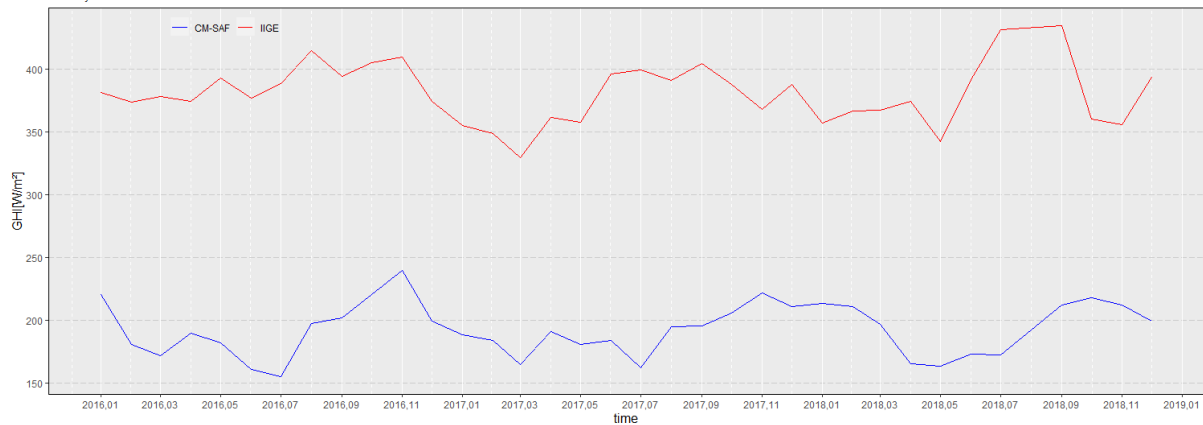
Tixan Pistilli, INER 8

R² = 0,0296
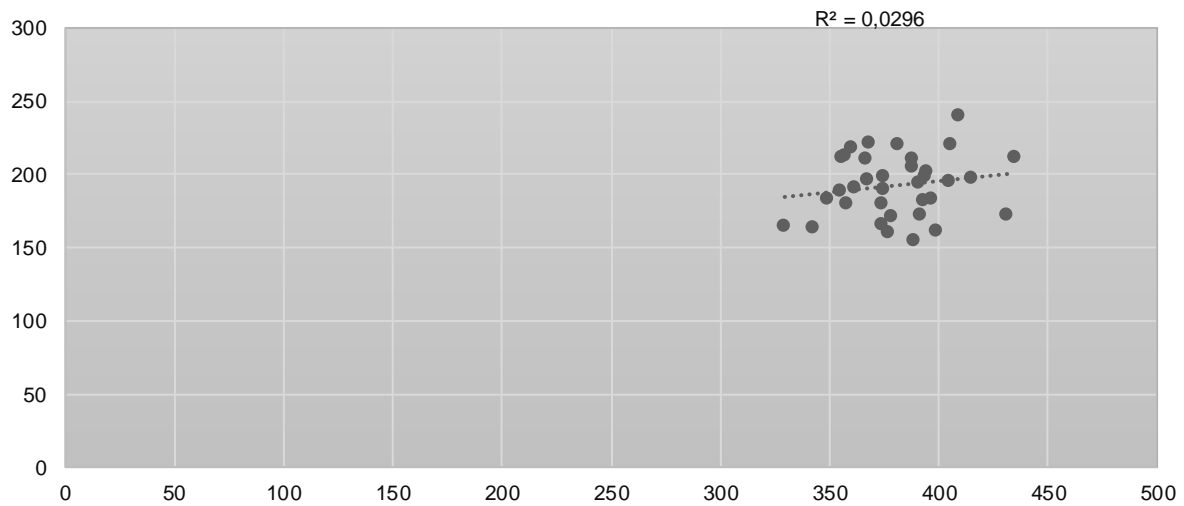
TIXAN PISTILLI STATION, INER 8
Annual Cycle Mean: 2016, 2017, 2018
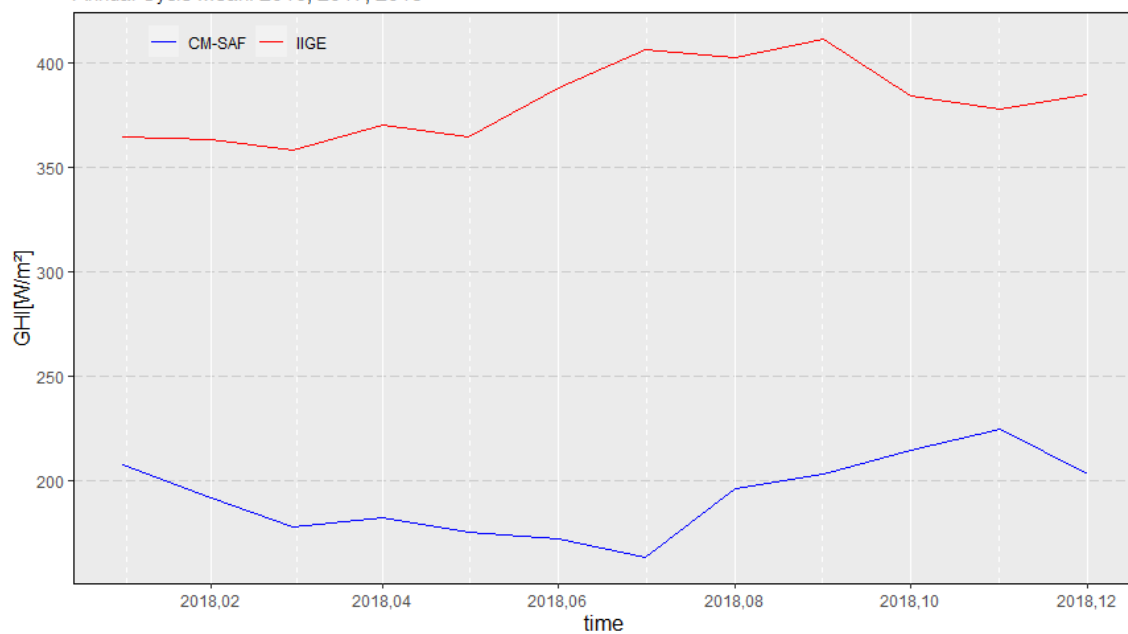
Santa Ana Station

SANTA ANA STATION, INER 15
Solar Global Radiation, 2016, 2017, 2018
Daily Scale

Santa Ana, INER 15

$R^2 = 0{,}195$
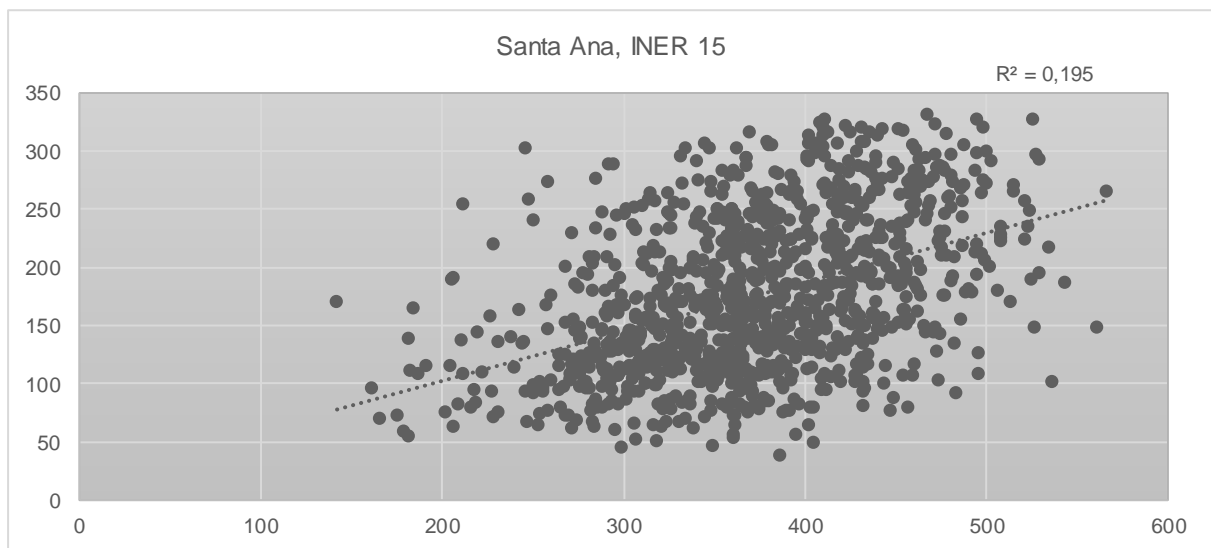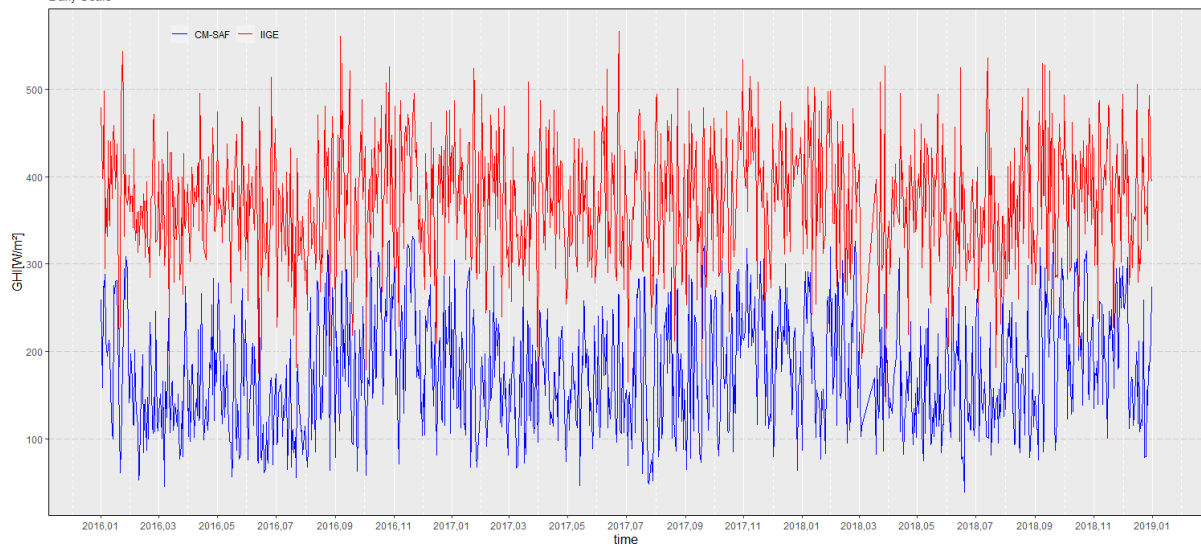
SANTA ANA STATION, INER 15
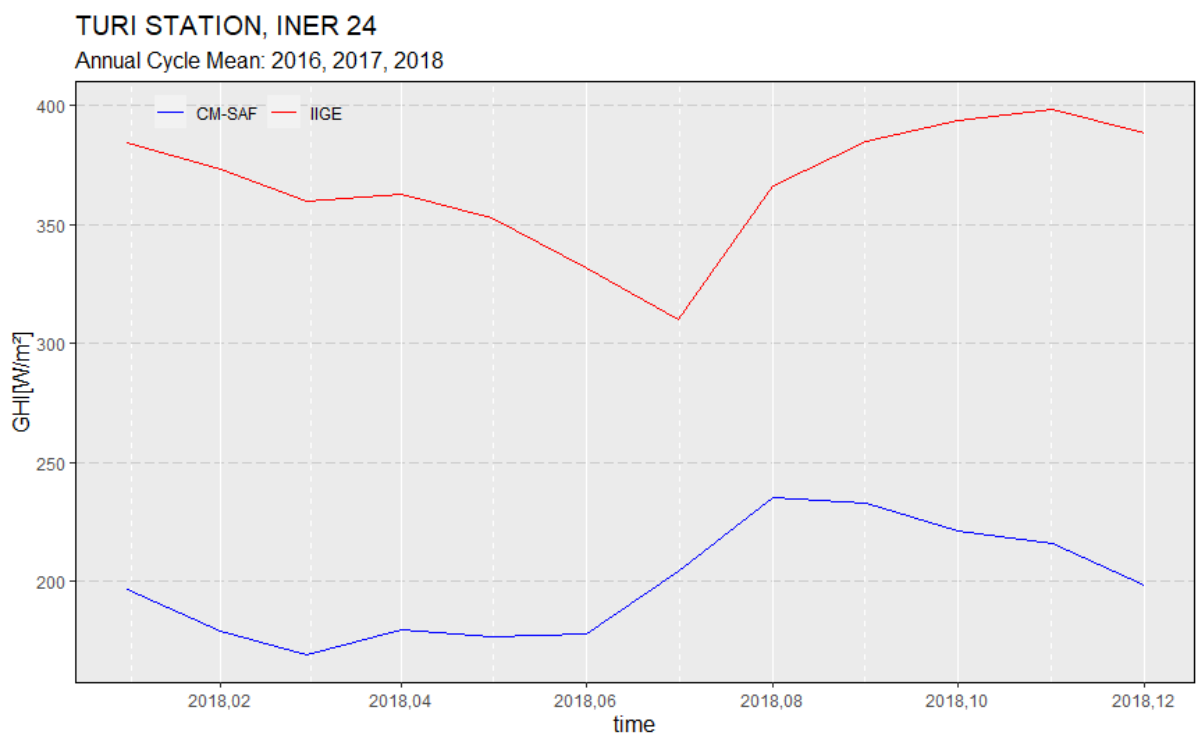Solar Global Radiation, 2016, 2017, 2018
Monthly Scale

Santa Ana, INER 15

R² = 0,4395
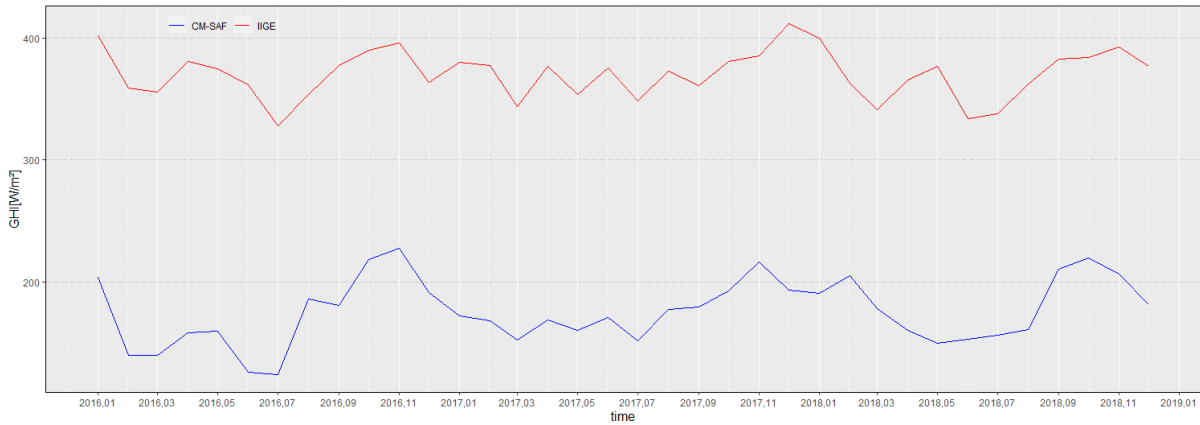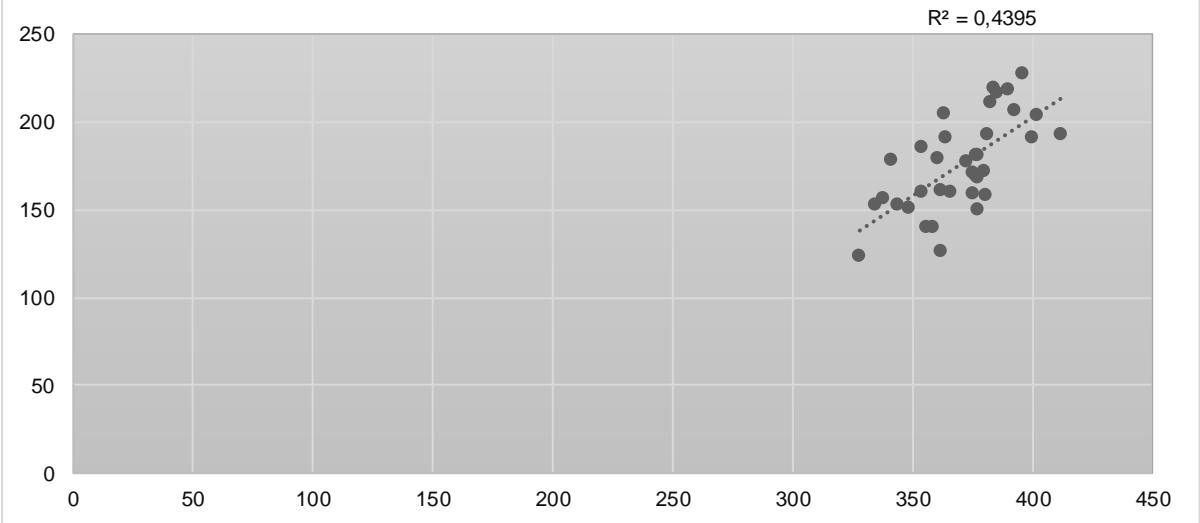
SANTA ANA STATION, INER 15
Annual Cycle Mean: 2016, 2017, 2018
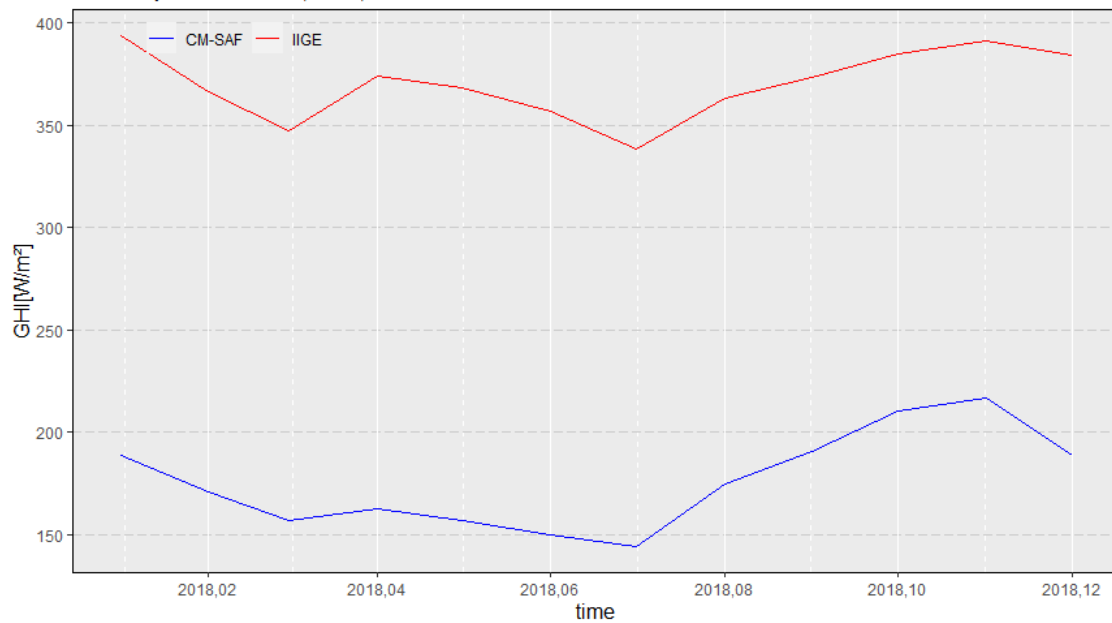
Yanuncay Station

YANUNCAY STATION, INER 17
Solar Global Radiation, 2016, 2017, 2018
Daily Scale
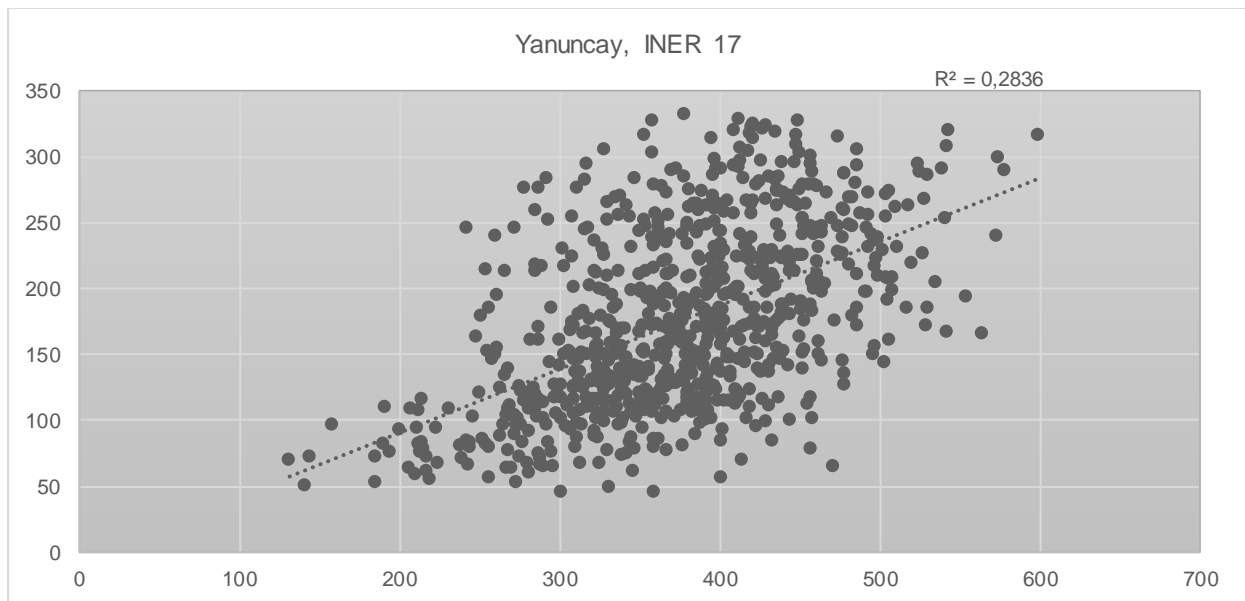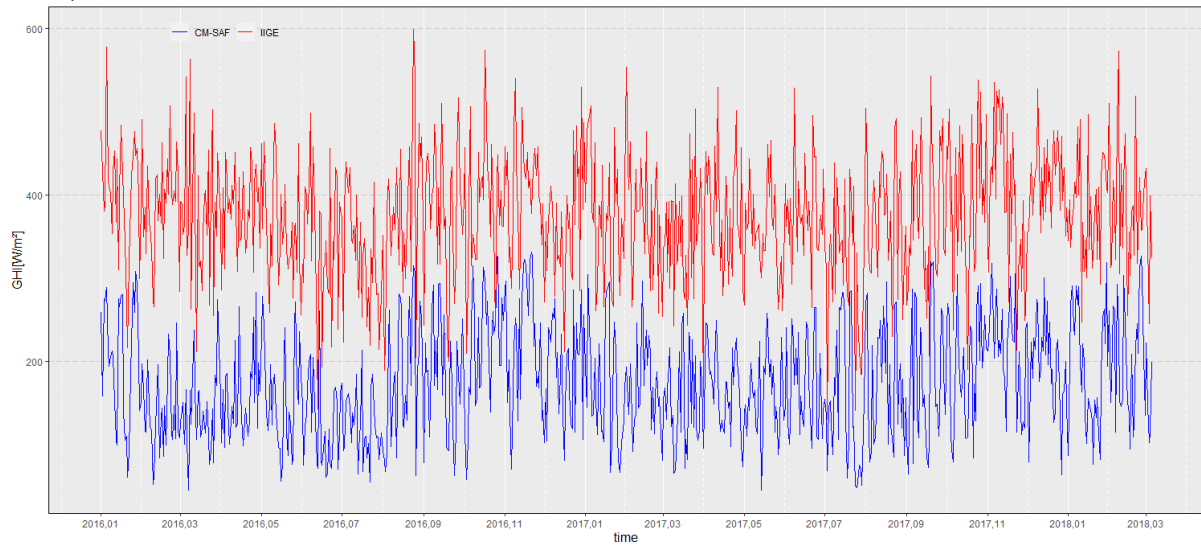
YANUNCAY STATION, INER 17
Solar Global Radiation, 2016, 2017, 2018
Monthly Scale

Yanuncay, INER 17

R² = 0,4489
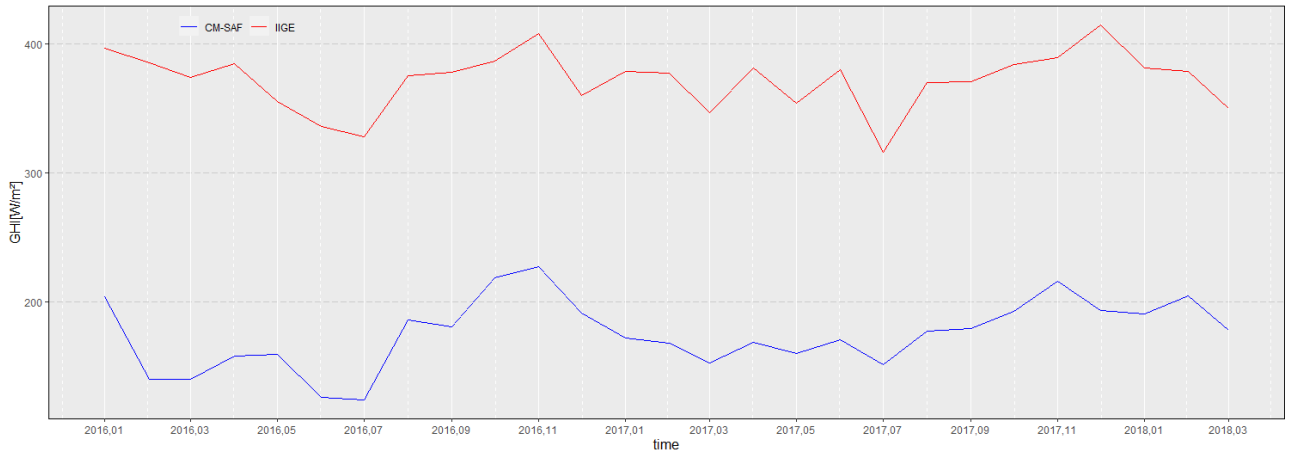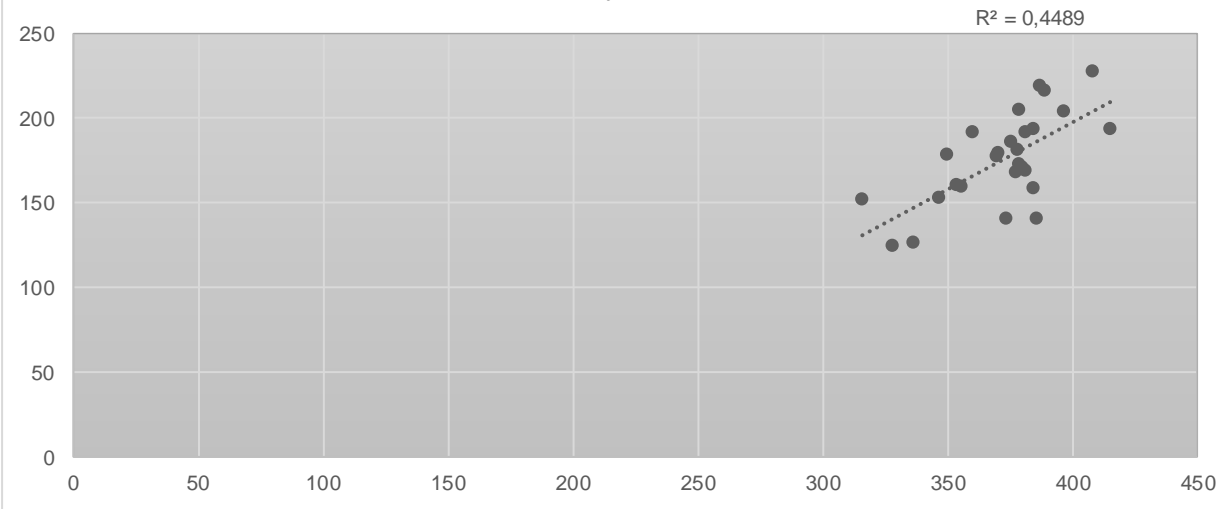
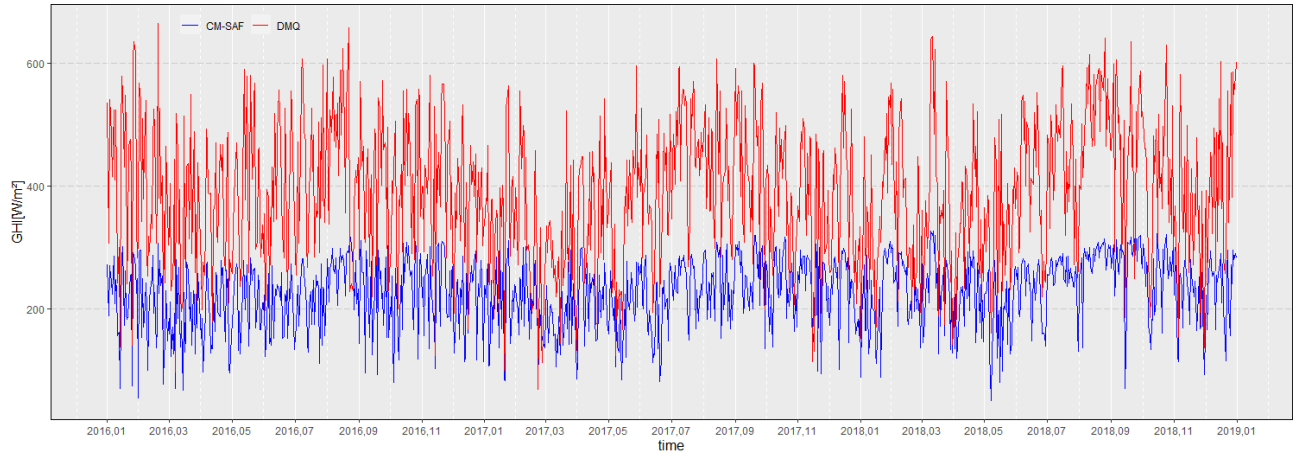YANUNCAY STATION, INER 17
Annual Cycle Mean: 2016, 2017, 2018
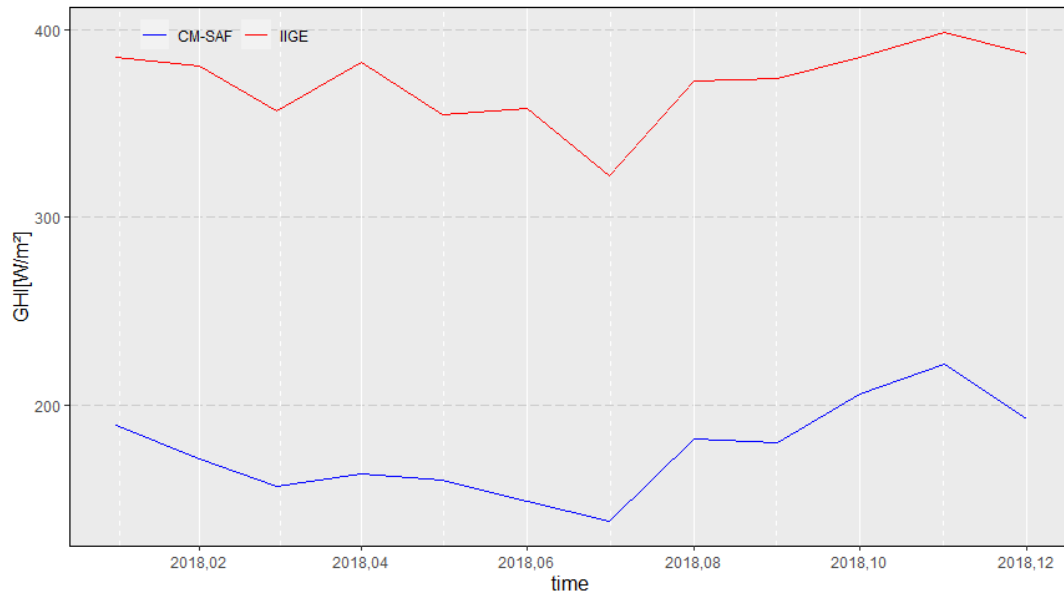
El Vecino Station

EL VECINO STATION, INER 18
Solar Global Radiation, 2016, 2017, 2018
Daily Scale

El Vecino, INER 18

R² = 0,0881
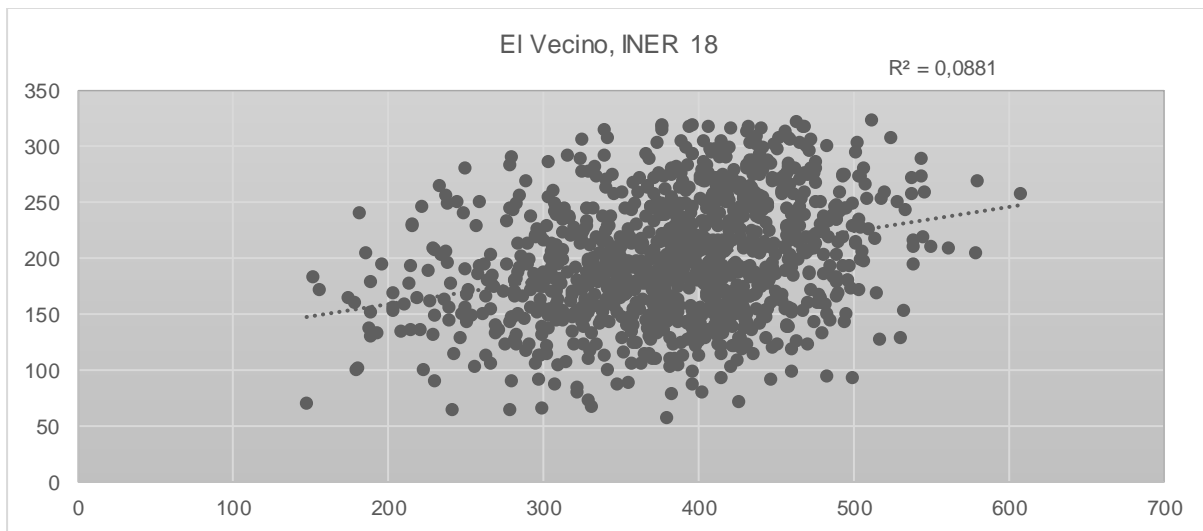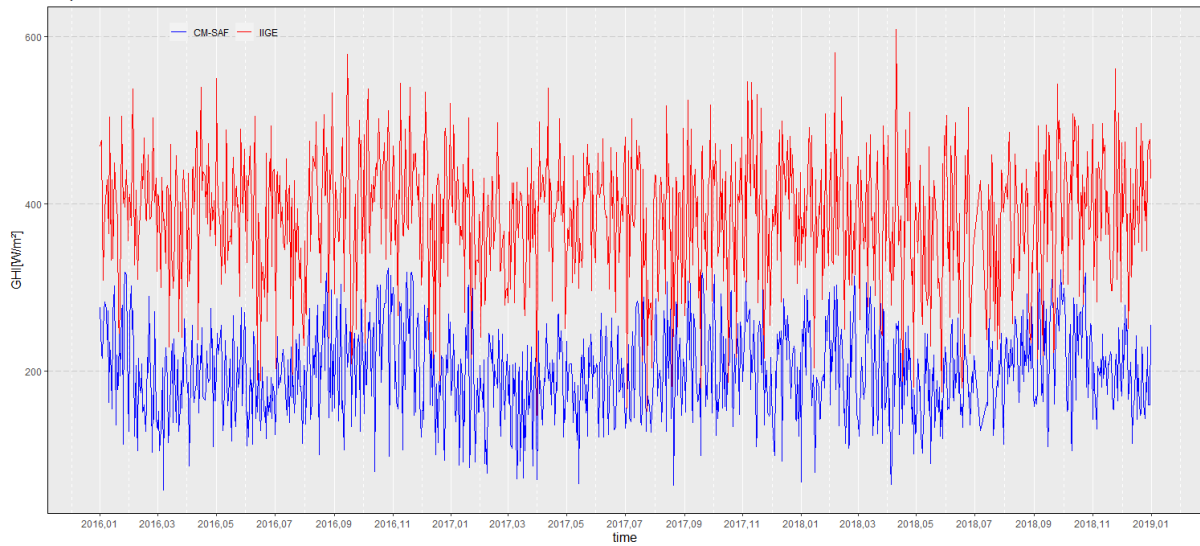
EL VECINO STATION, INER 18
Solar Global Radiation, 2016, 2017, 2018
Monthly Scale

El Vecino, INER 18

R² = 0,2833
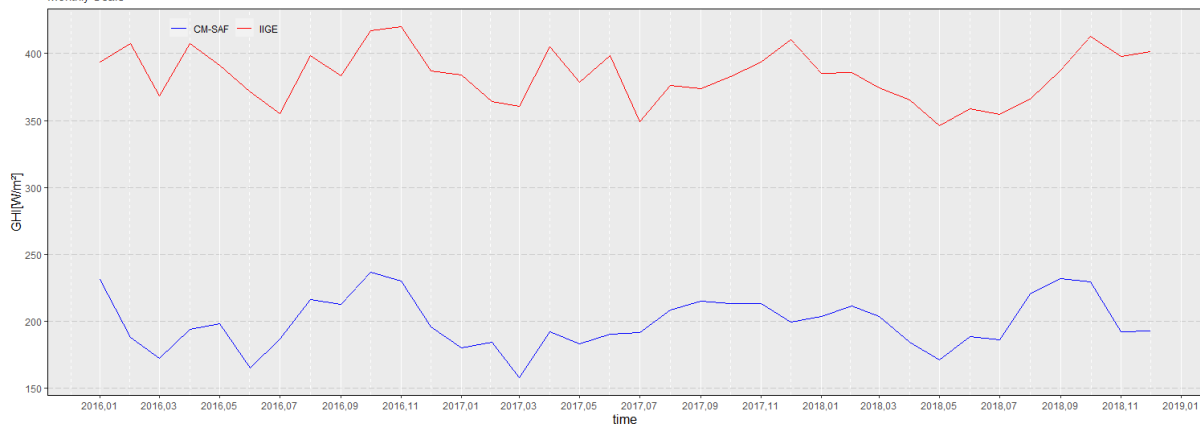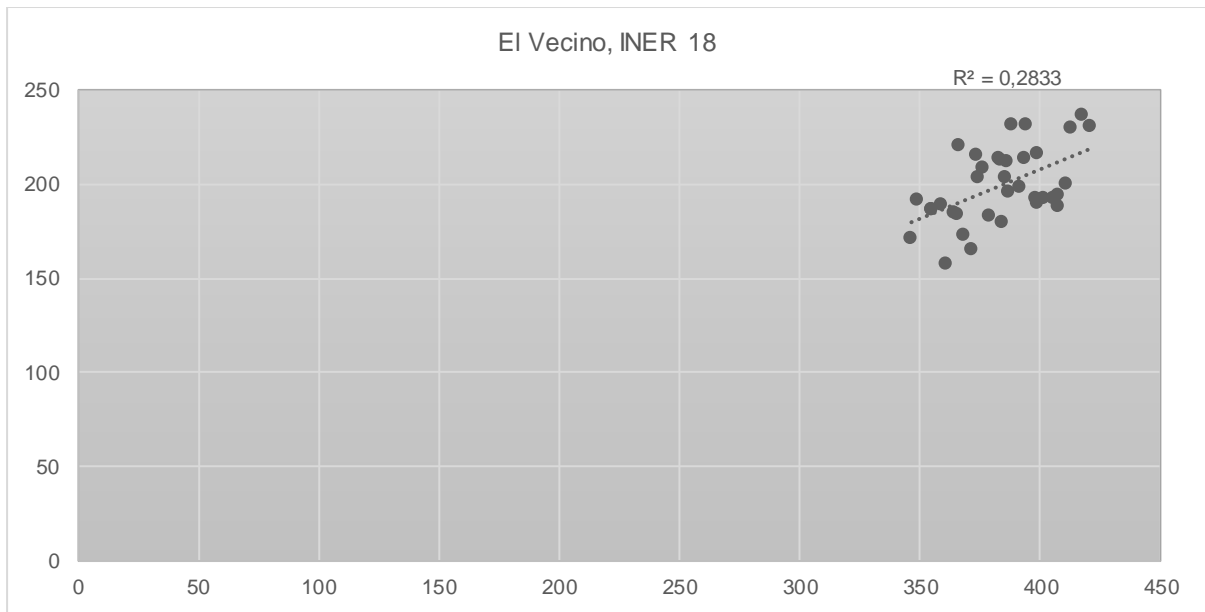
EL VECINO STATION, INER 18
Annual Cycle Mean: 2016, 2017, 2018

Irquis Station

IRQUIS STATION, INER 19
Solar Global Radiation, 2016, 2017, 2018
Daily Scale

Irquis, INER 19

R² = 0,1682

EL VECINO STATION, INER 18
Solar Global Radiation, 2016, 2017, 2018
Monthly Scale

School of Earth Sciences, Energy and Environment   Yachay Tech University

Irquis, INER 19

R² = 0,6149

IRQUIS STATION, INER 19
Annual Cycle Mean: 2016, 2017, 2018
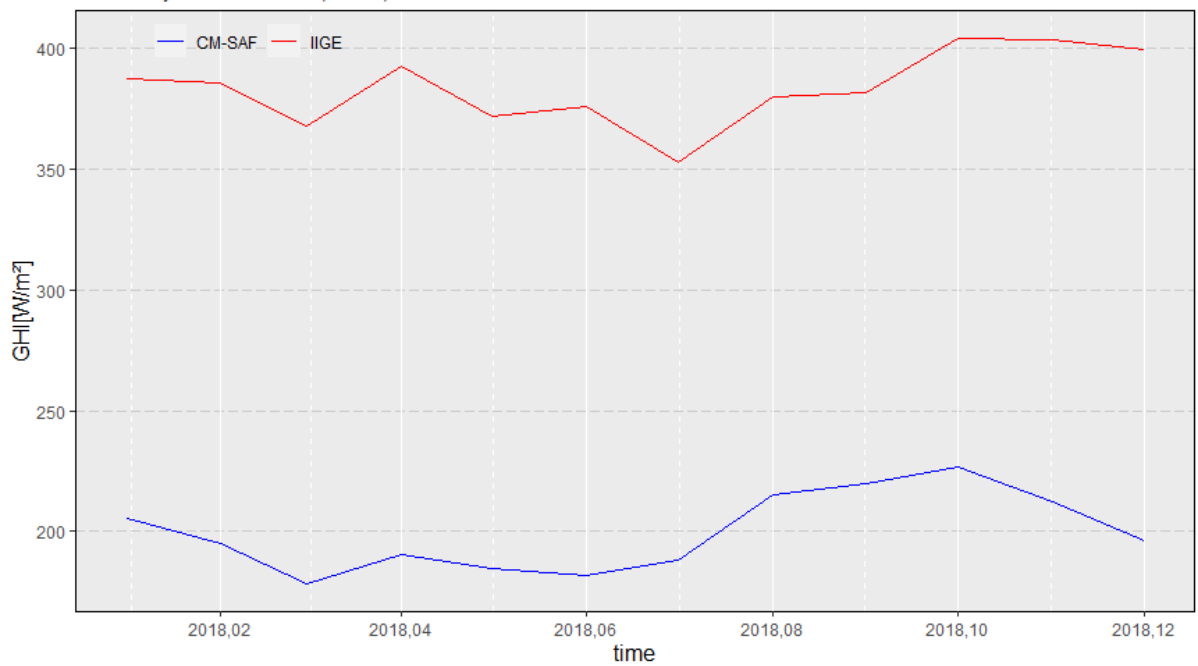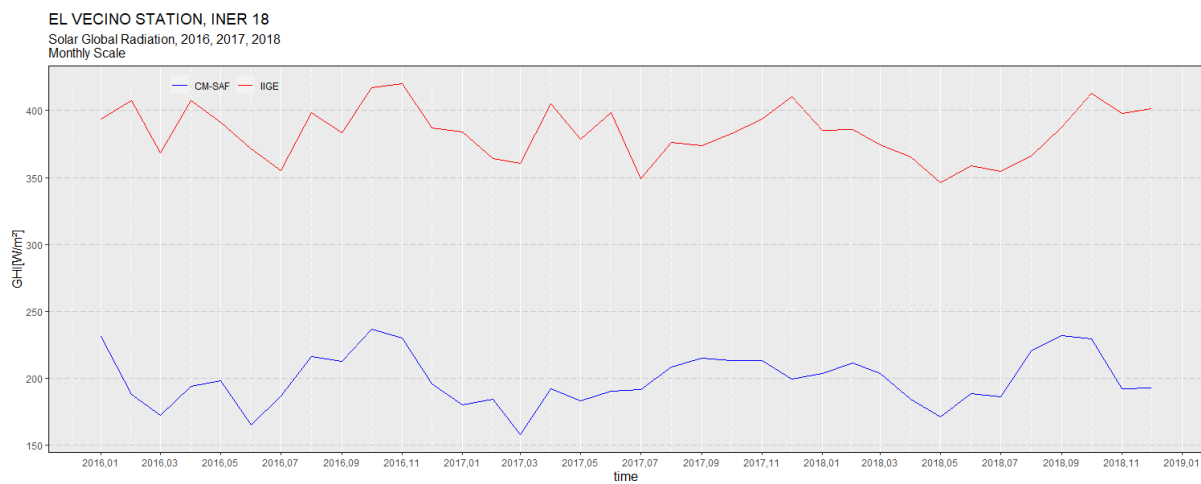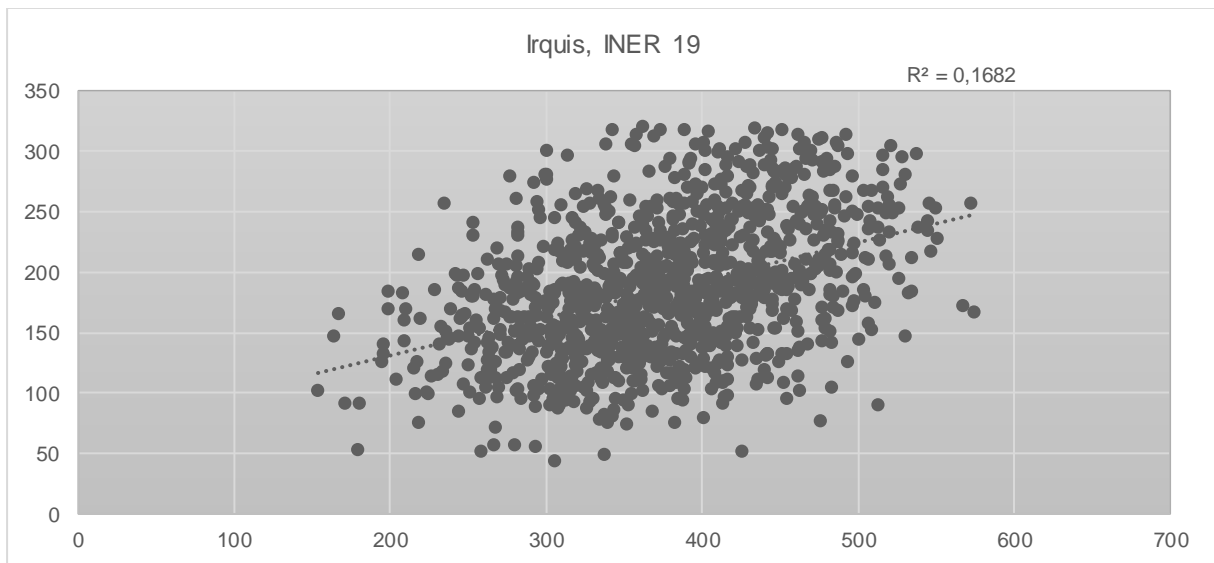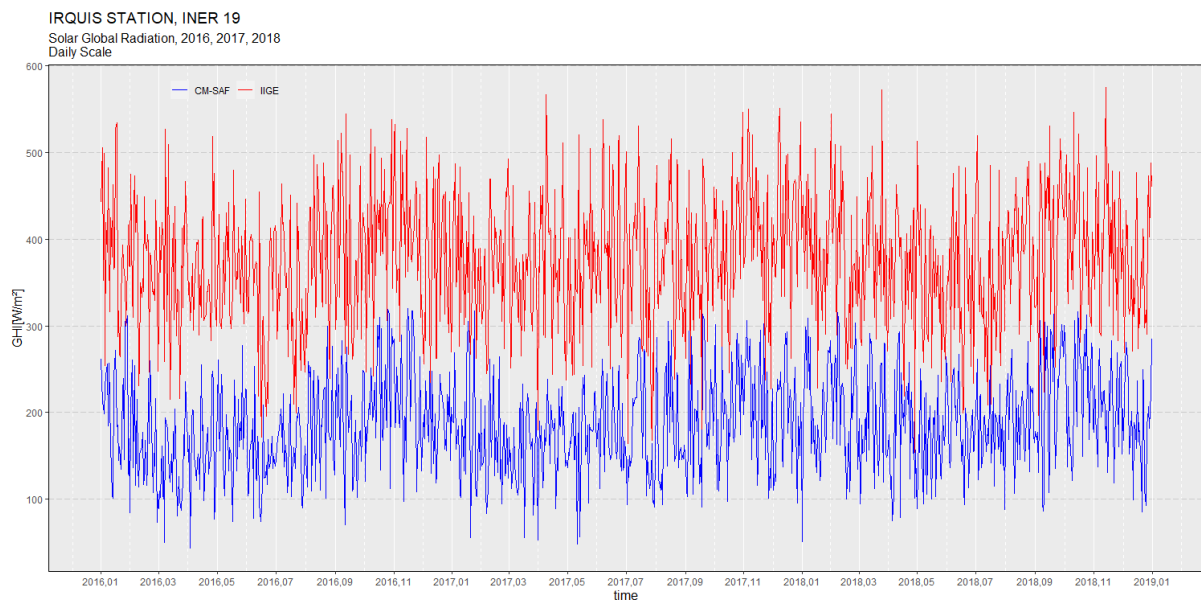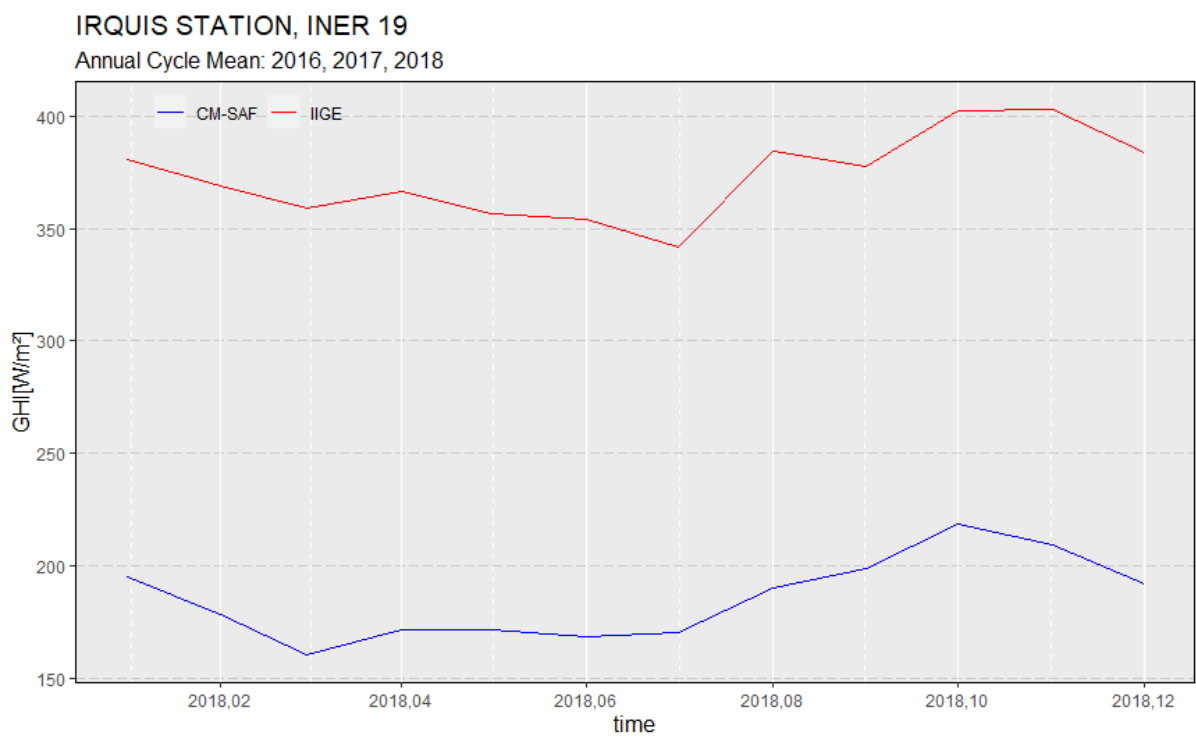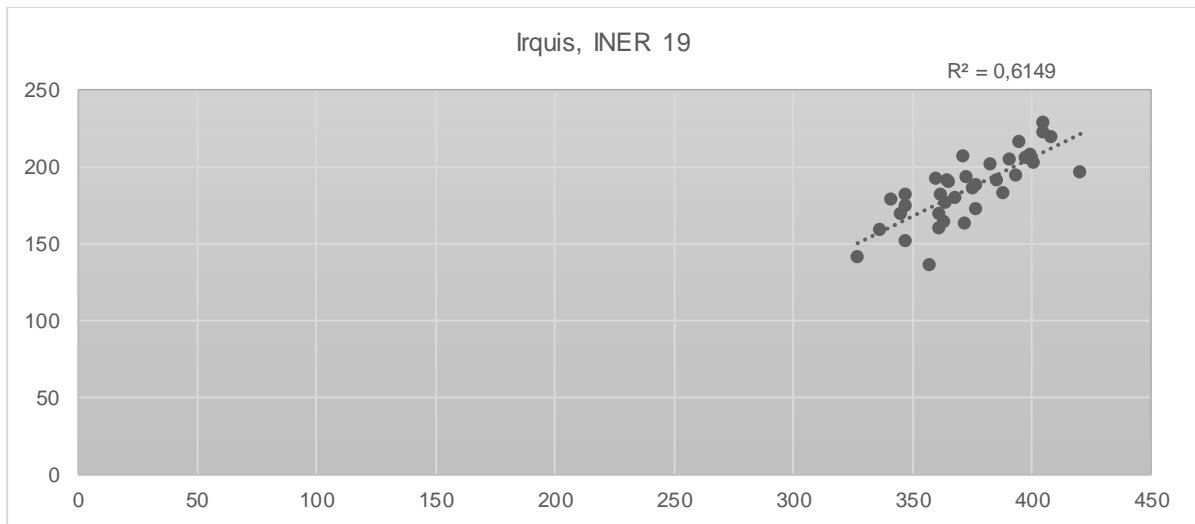
Quingeo Station

QUINGEO STATION, INER 20
Solar Global Radiation, 2016, 2017, 2018
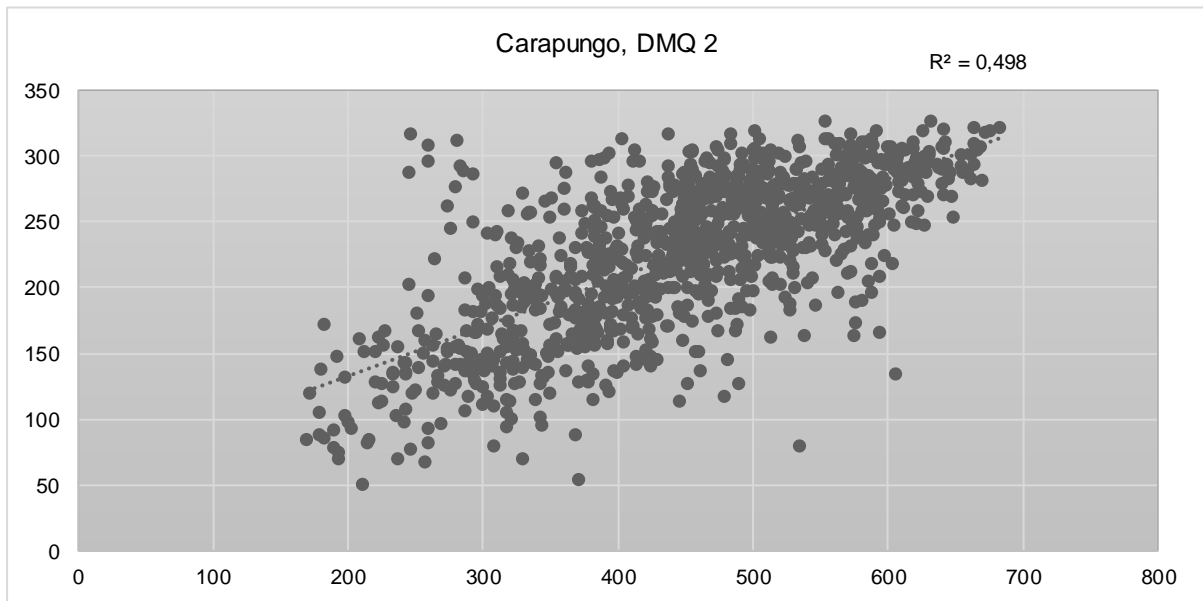Daily Scale

Quingeo, INER 20

R² = 0,0681
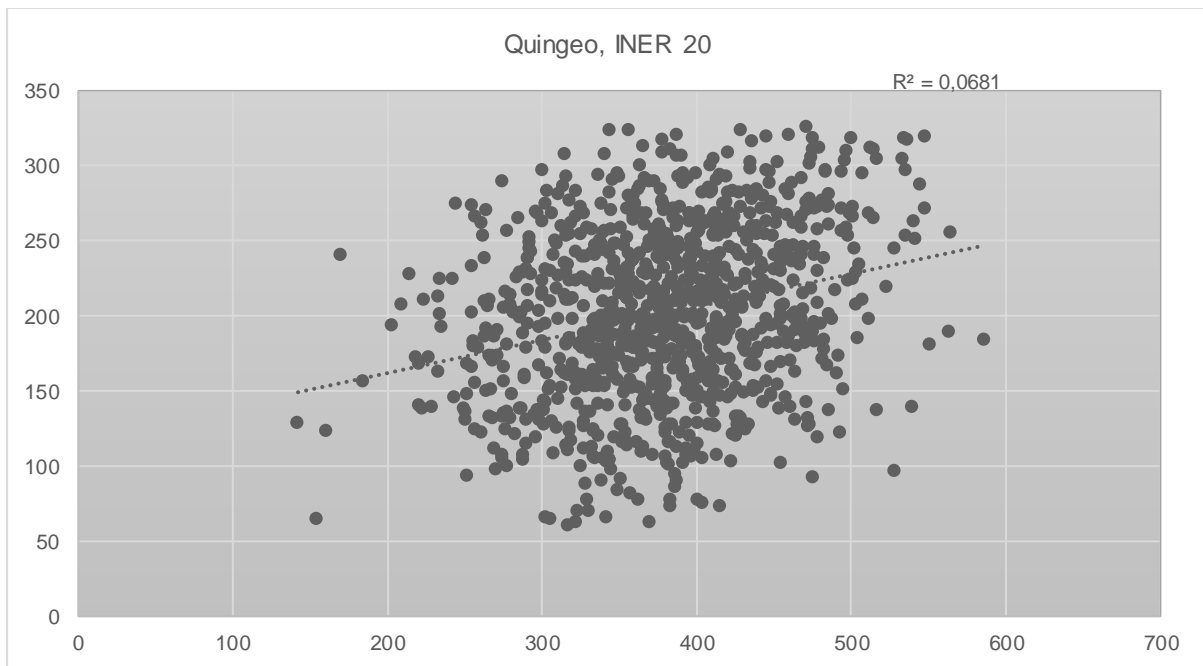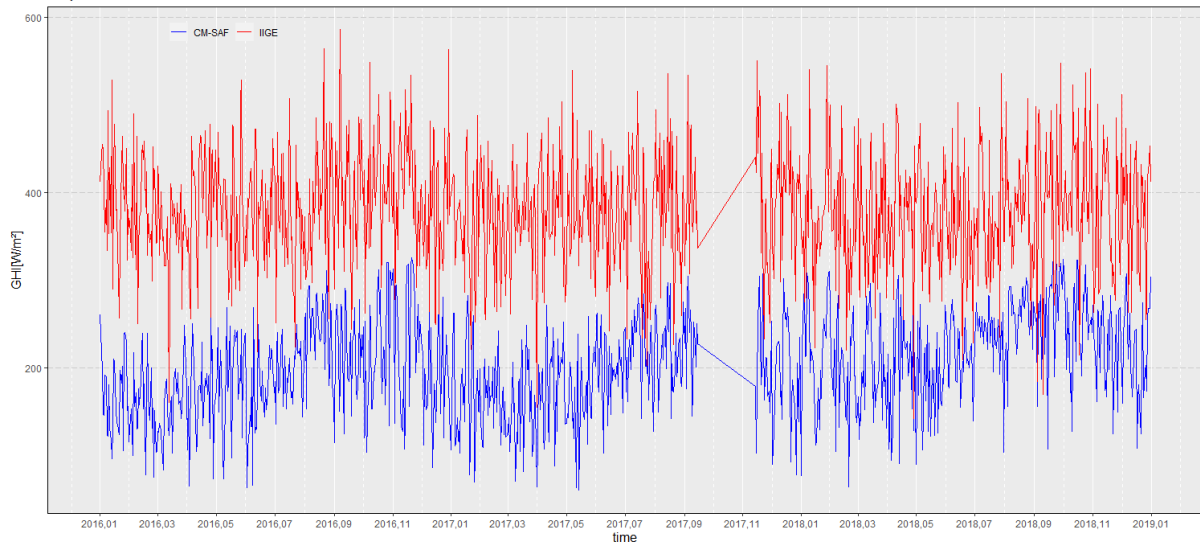
QUINGEO STATION, INER 20
Solar Global Radiation, 2016, 2017, 2018
Monthly Scale

Quingeo, INER 20

R² = 0,1107
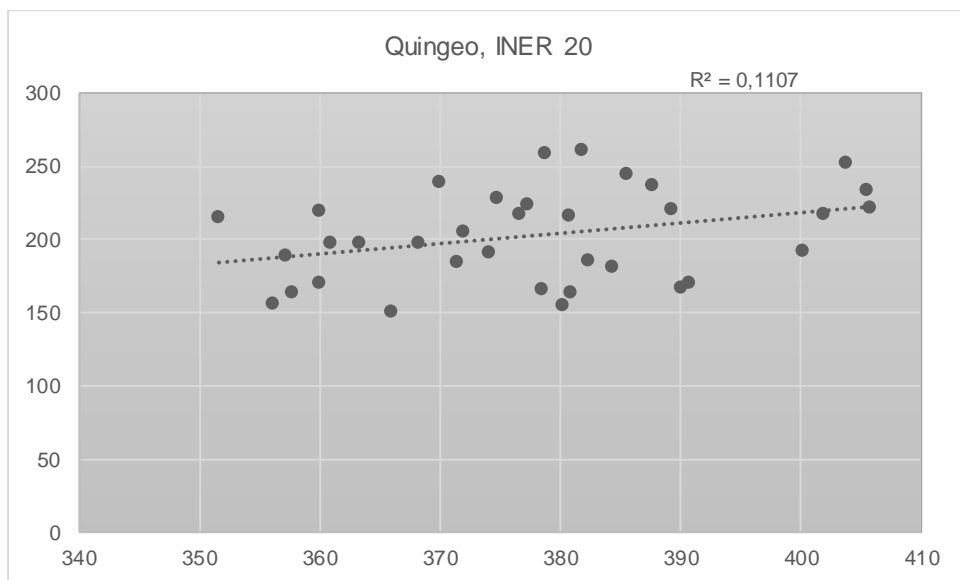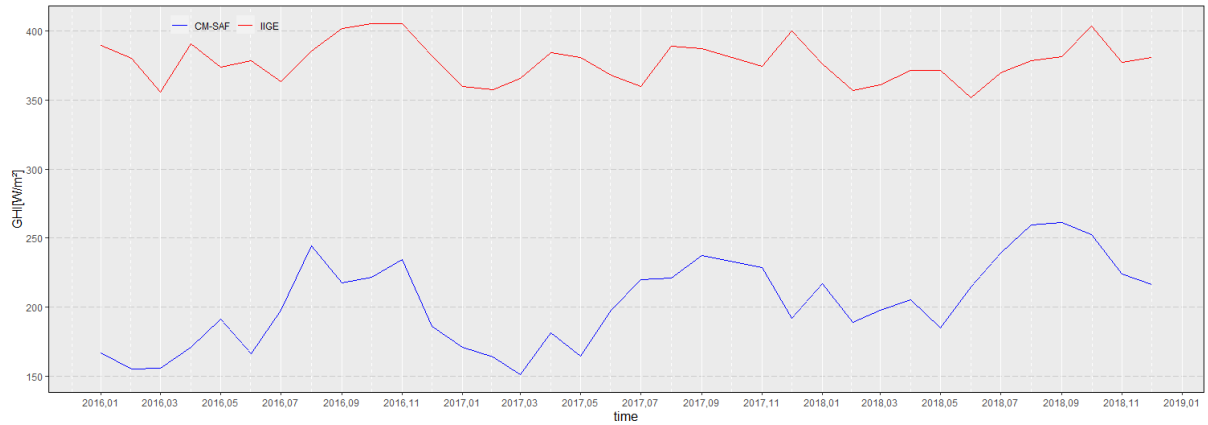
QUINGEO STATION, INER 20
Annual Cycle Mean: 2016, 2017, 2018
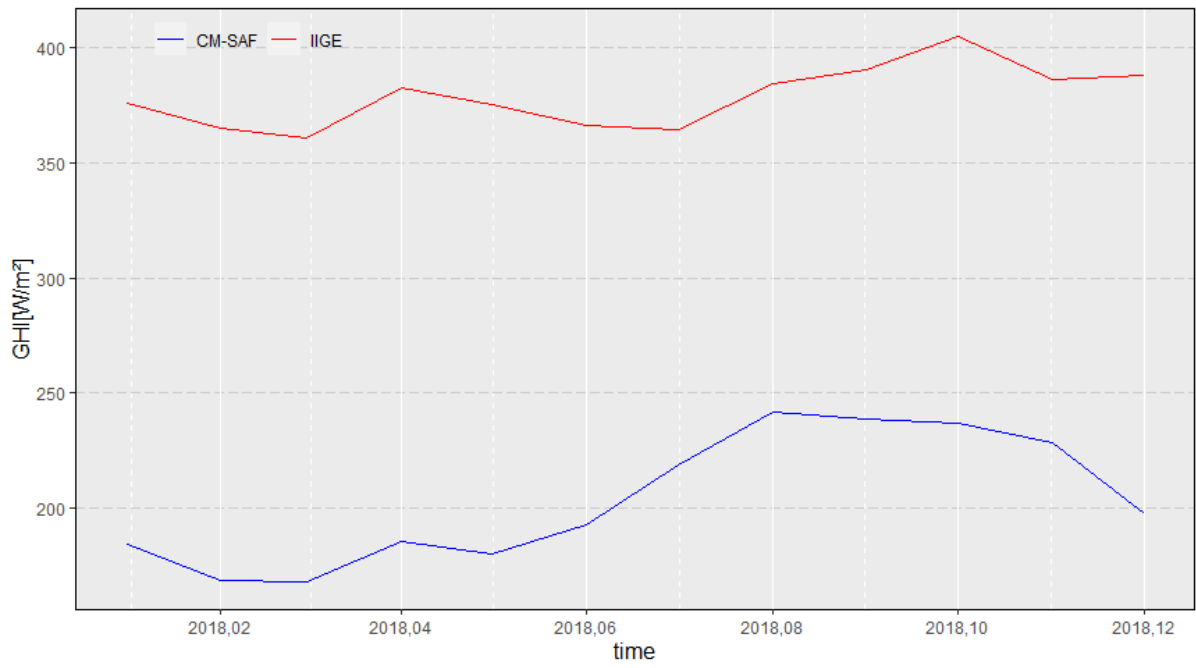
Cumbe Station

CUMBE STATION, INER 21
Solar Global Radiation, 2016, 2017, 2018
Daily Scale
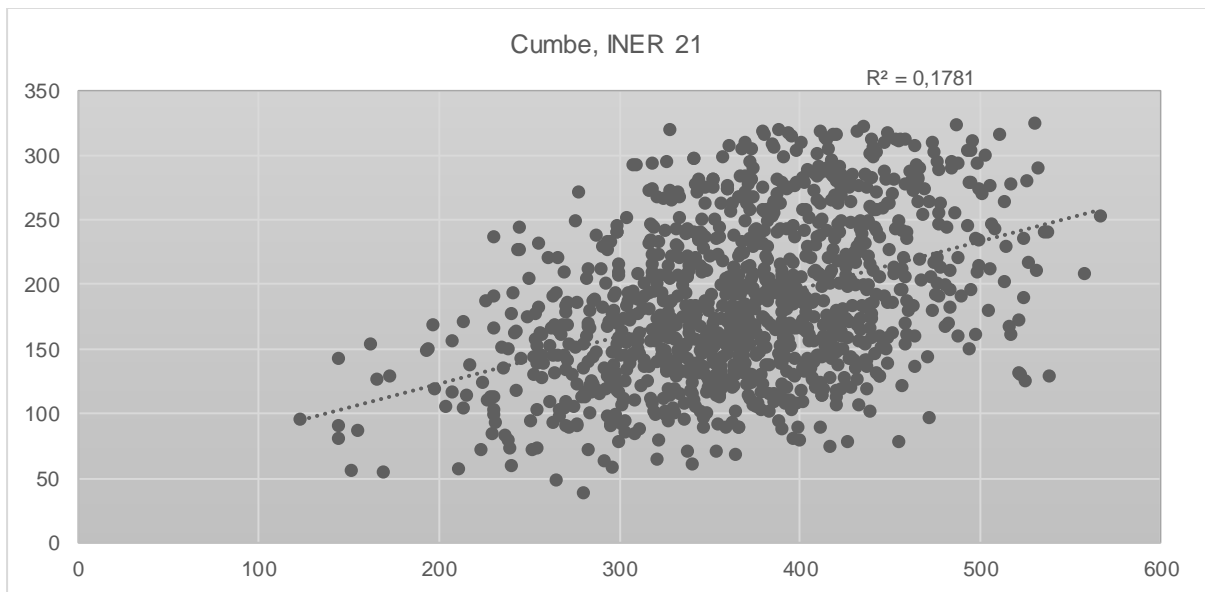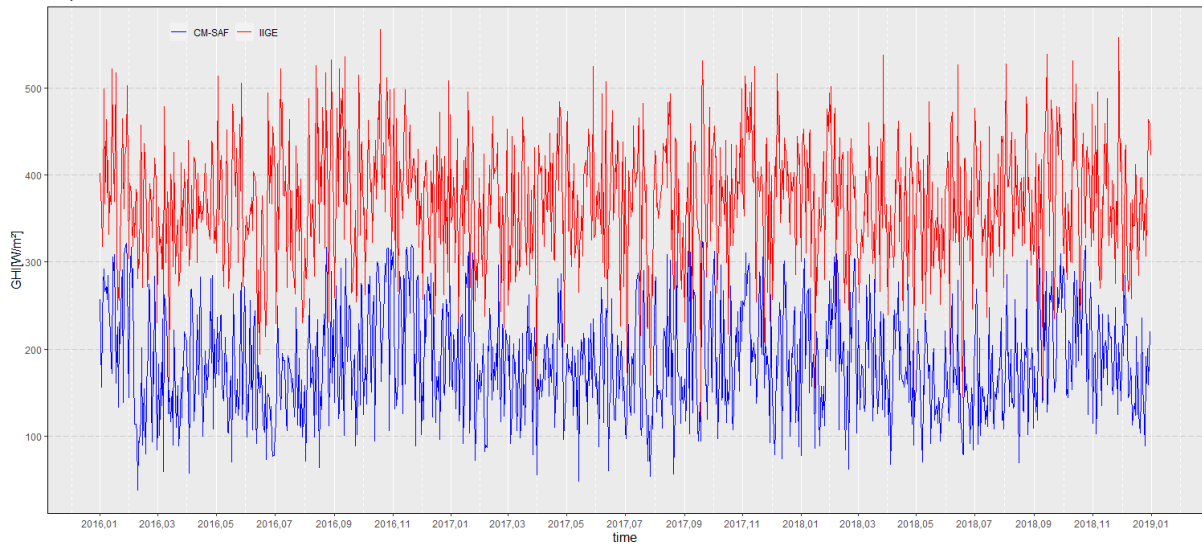
Cumbe, INER 21

R² = 0,1781

CUMBE STATION, INER 21
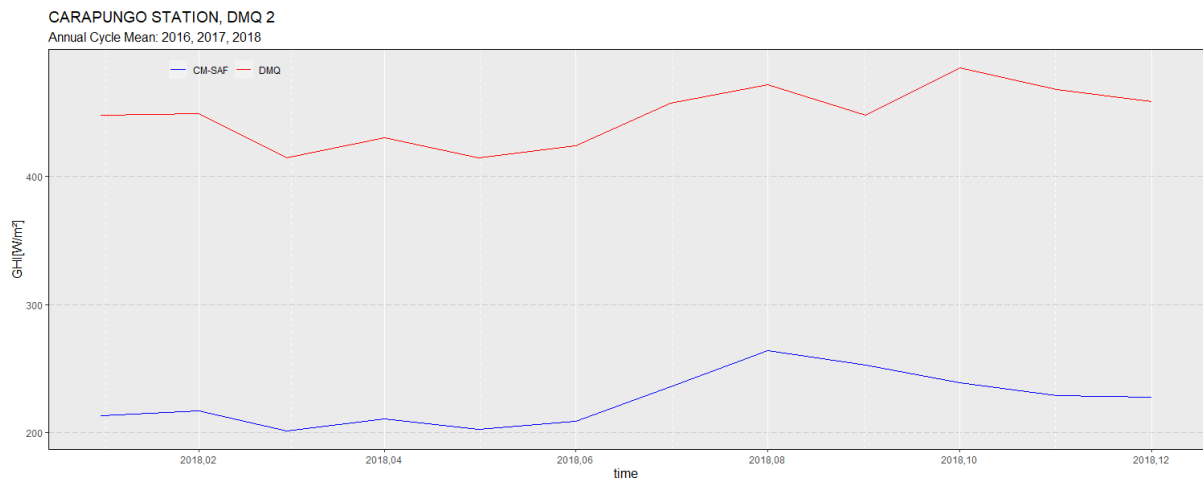Solar Global Radiation, 2016, 2017, 2018
Monthly Scale

Cumbe, INER 21

R² = 0,5029

CUMBE STATION, INER 21
Annual Cycle Mean: 2016, 2017, 2018
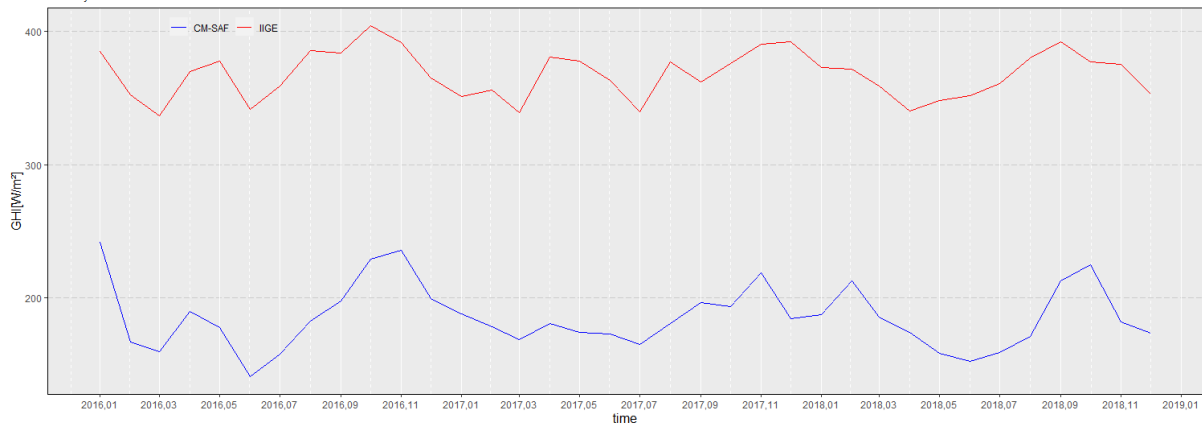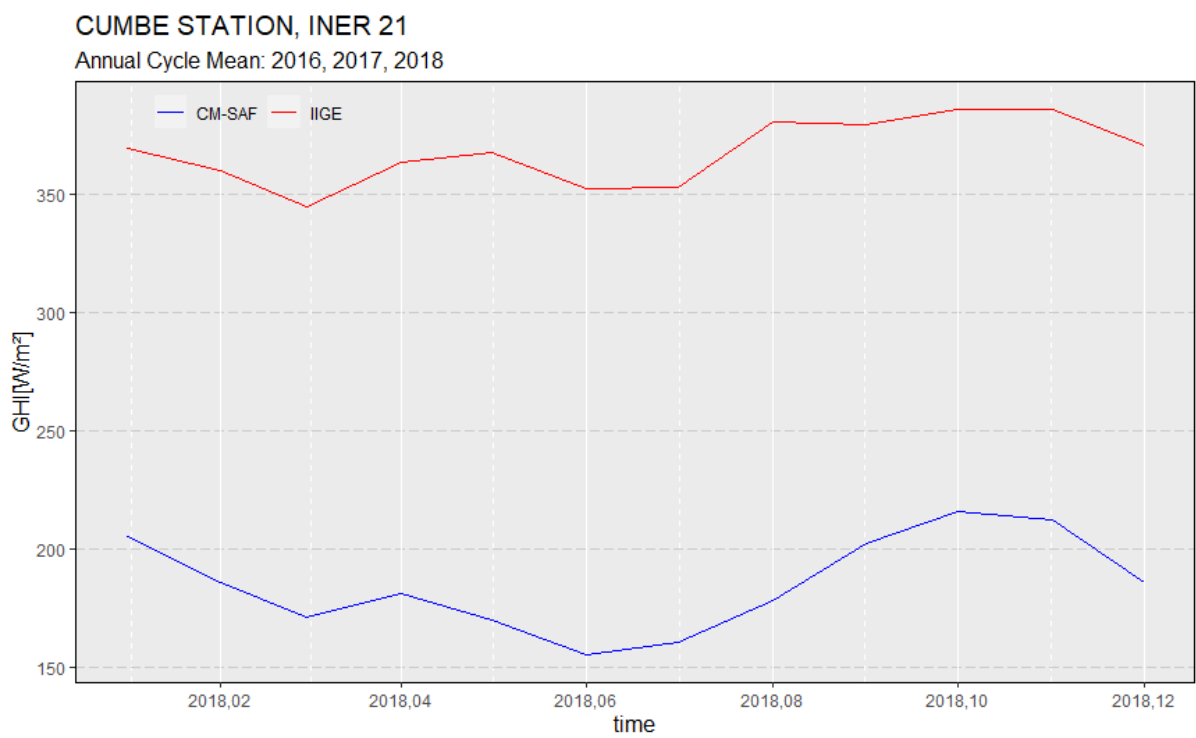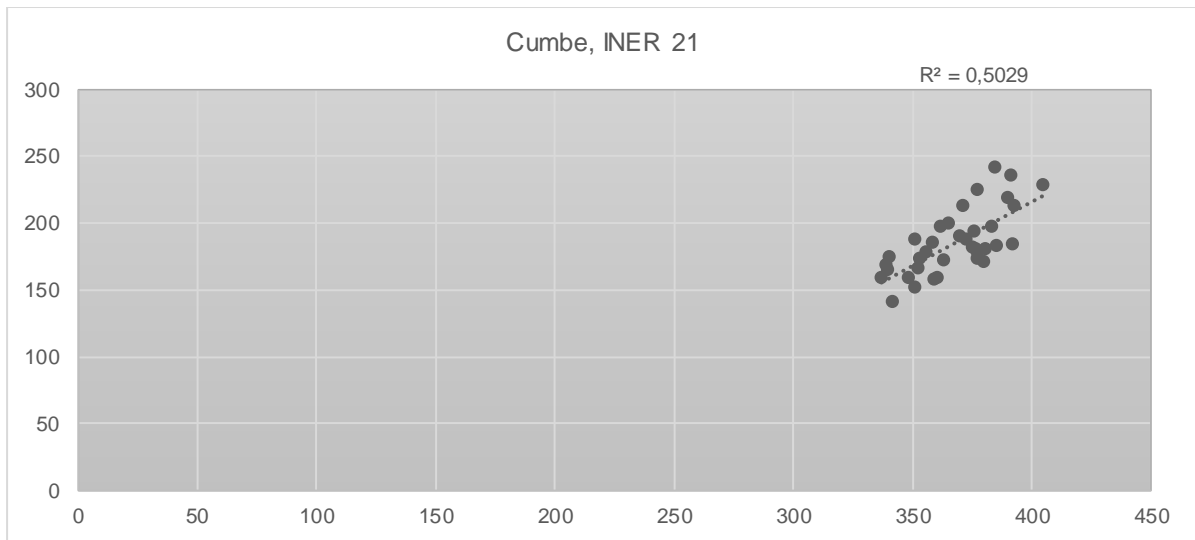
San Joaquín Station

San Joaquin, INER 22
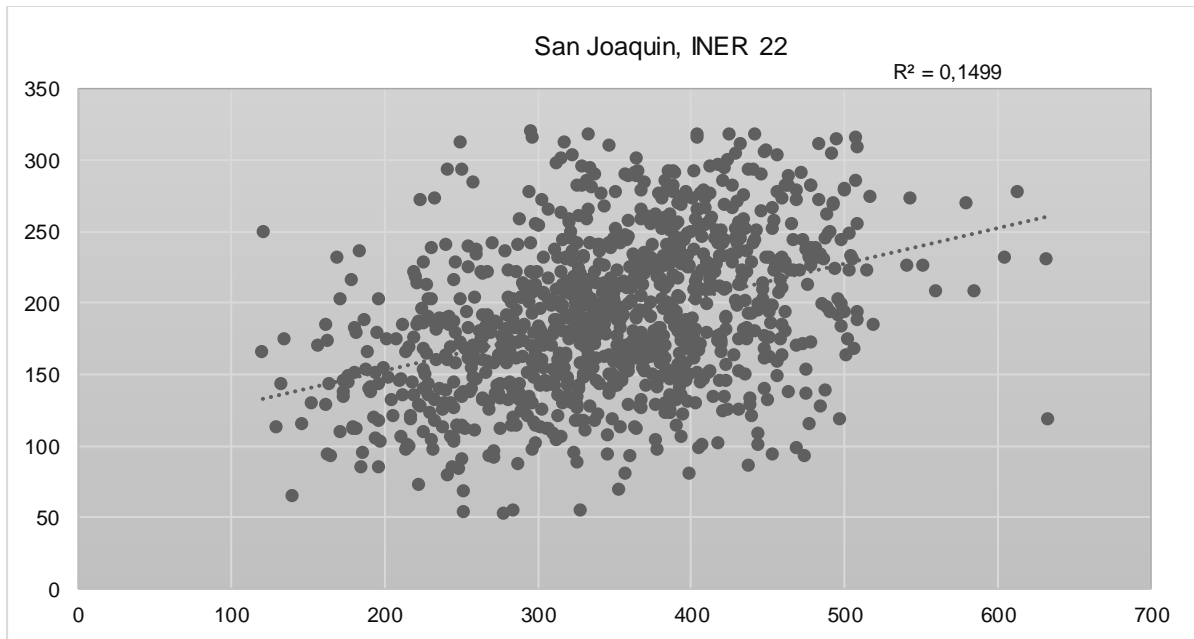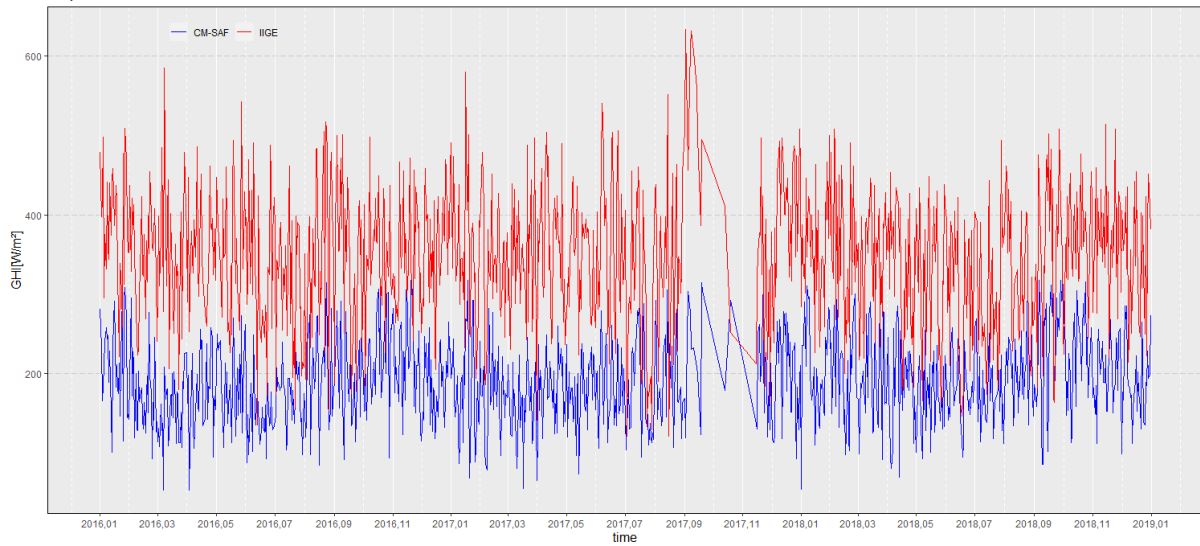
$R^2 = 0,1499$

San Joaquin, INER 22

R² = 0,1067

SAN JOAQUIN STATION, INER 22
Annual Cycle Mean: 2016, 2017, 2018
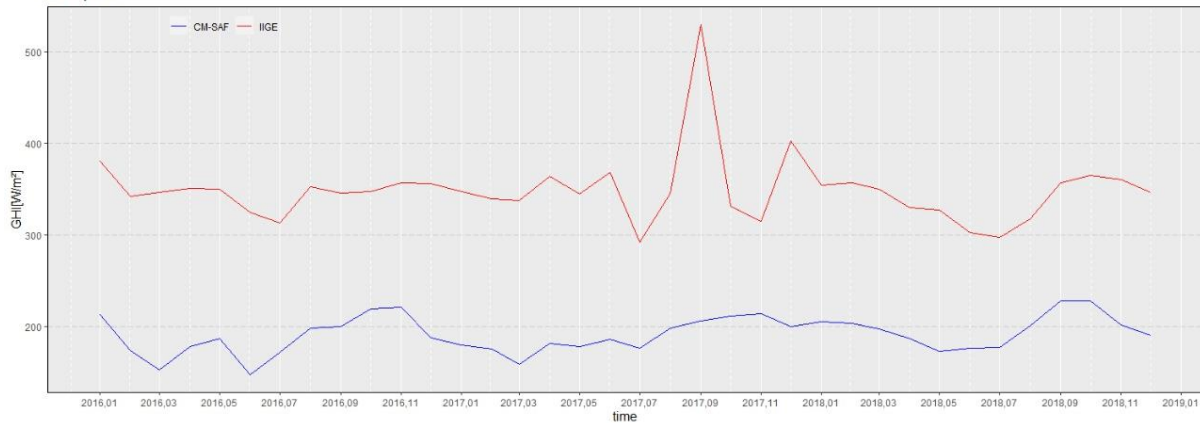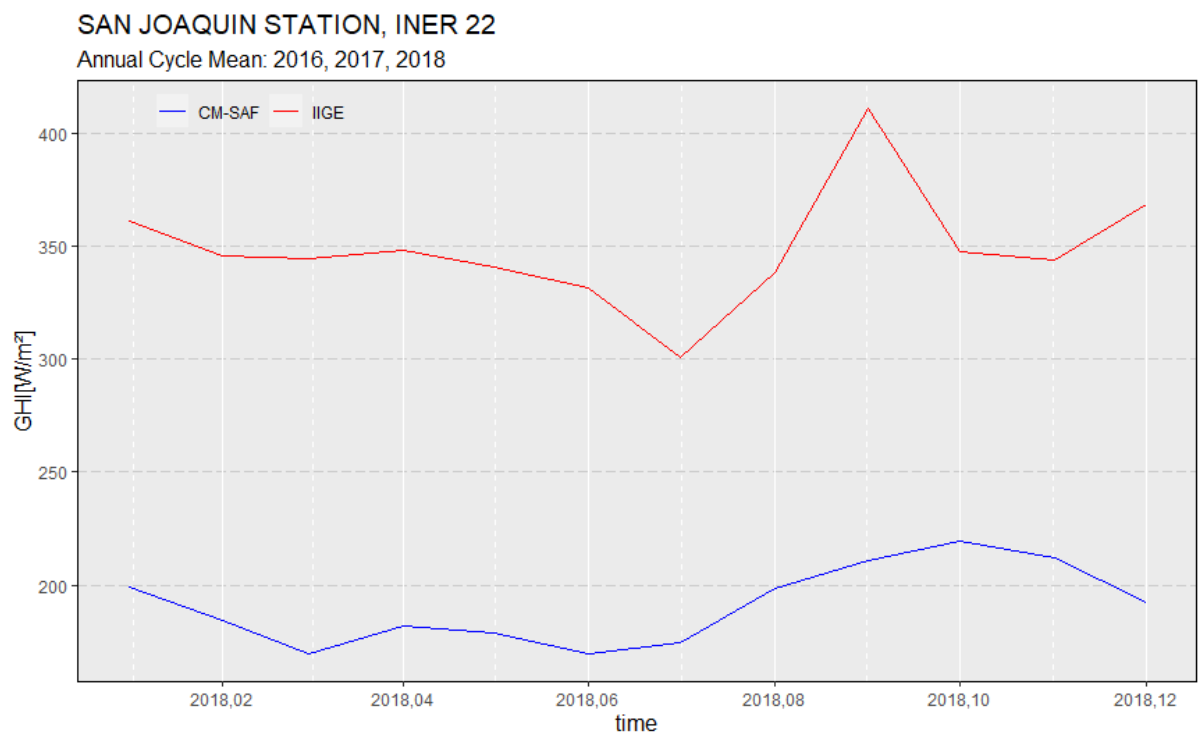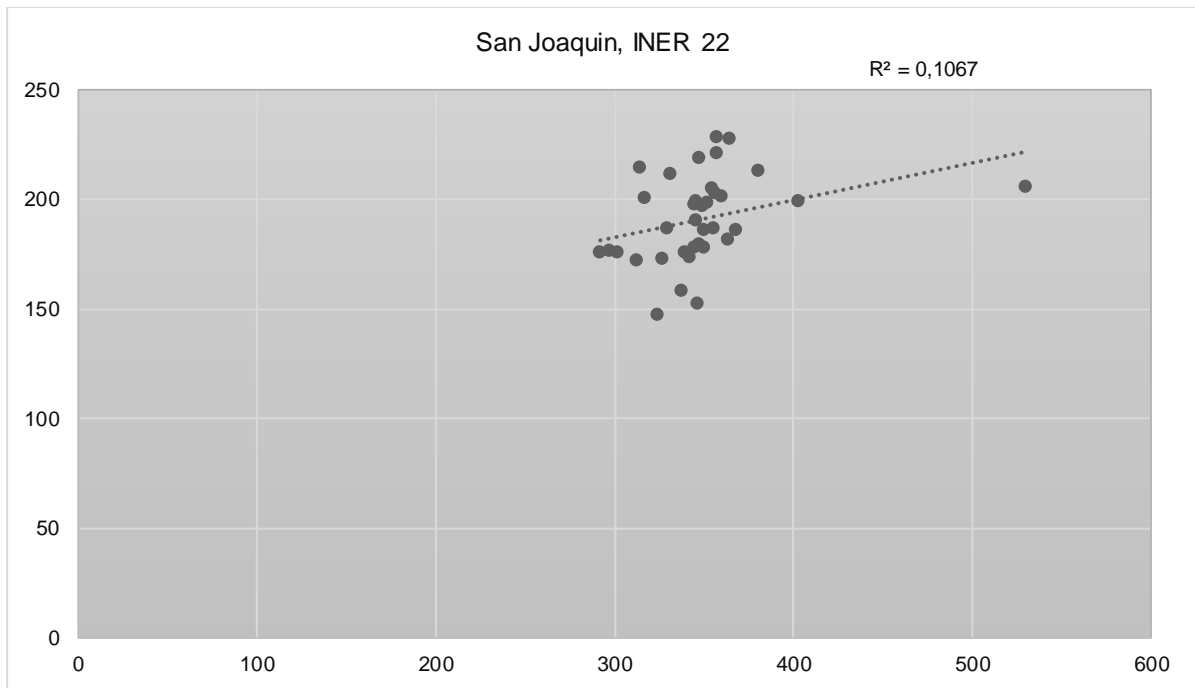
Sayausí Station

Sayausi, INER 23

R² = 0,049

SAYAUSI STATION, INER 23
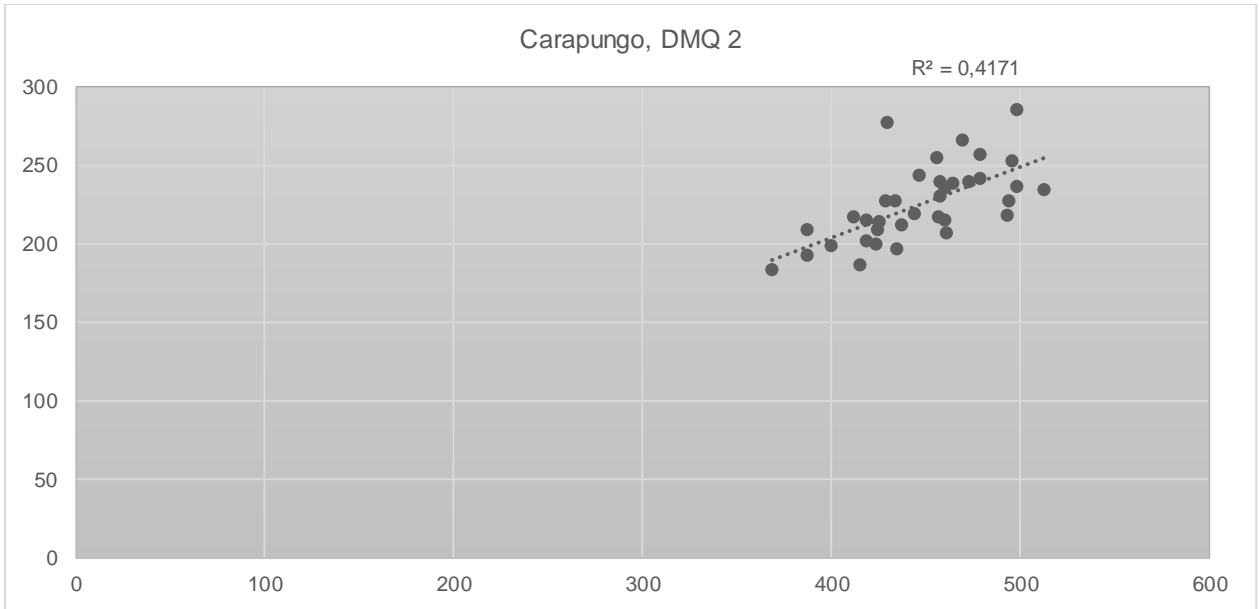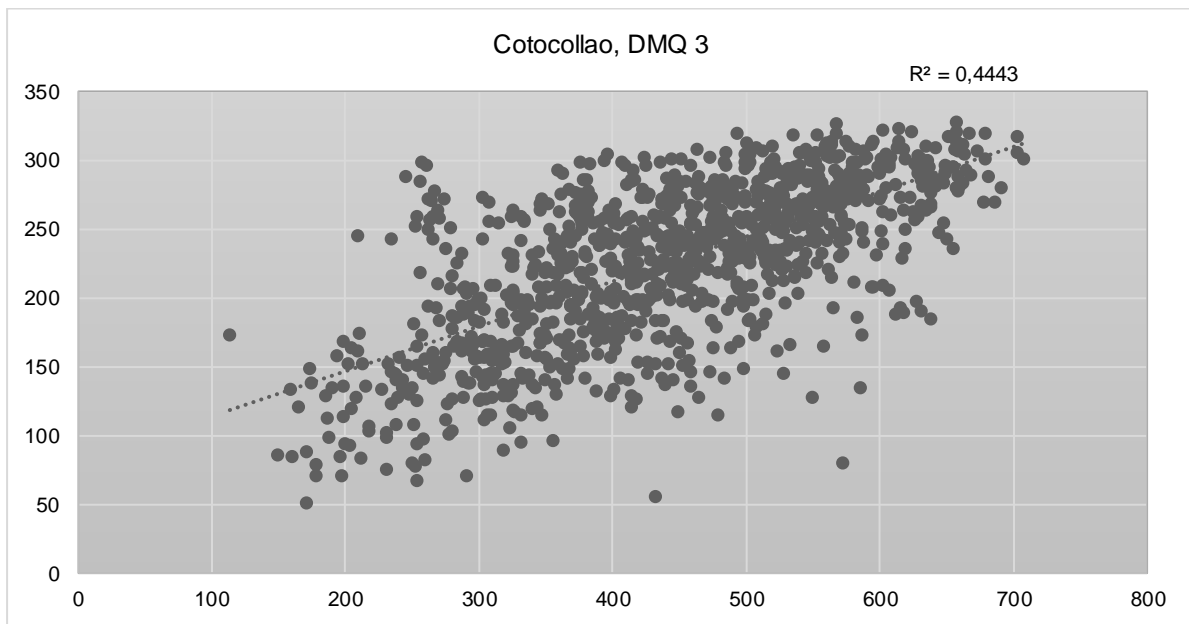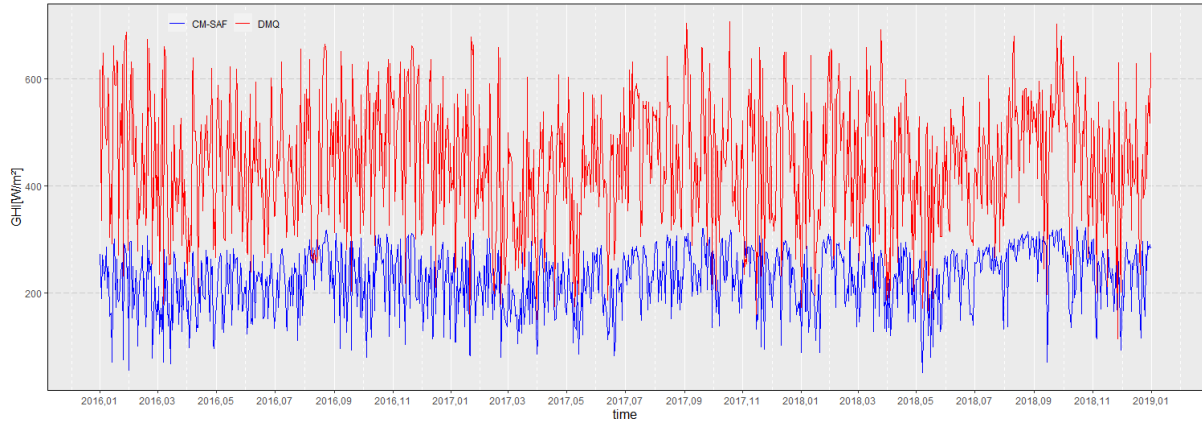Solar Global Radiation, 2016, 2017, 2018
Monthly Scale

Sayausi, INER 23

R² = 0,0296
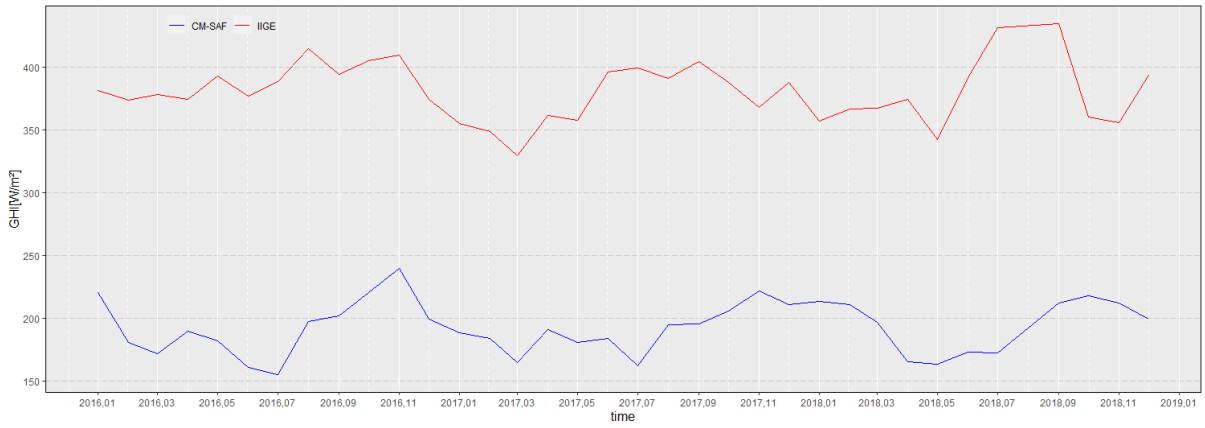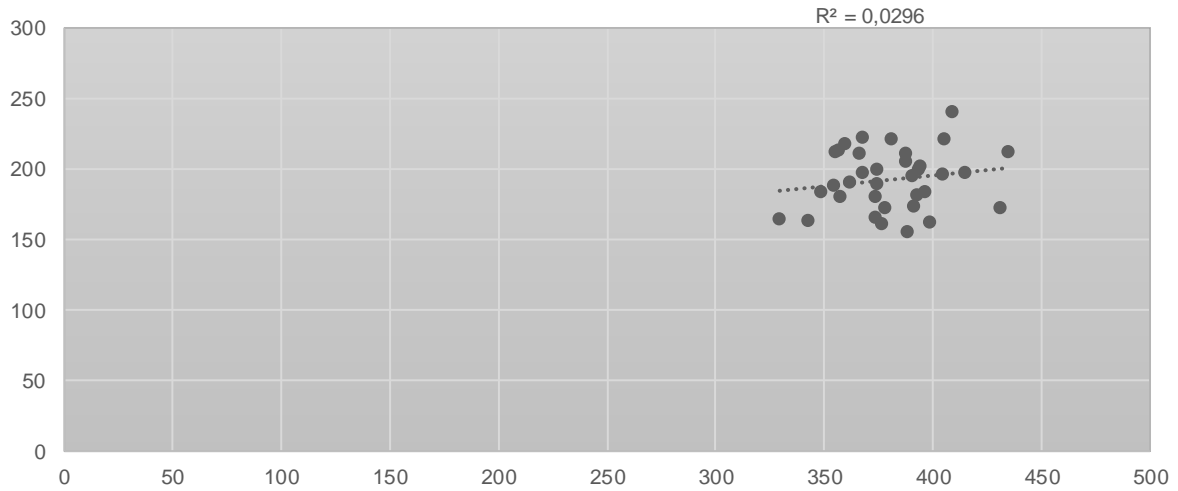
SAYAUSI STATION, INER 23
Annual Cycle Mean: 2016, 2017, 2018

Turi Station

TURI STATION, INER 24
Solar Global Radiation, 2016, 2017, 2018
Daily Scale

Turi Station, Iner 24

R² = 0,0856

TURI STATION, INER 24
Solar Global Radiation, 2016, 2017, 2018
Monthly Scale

Turi, INER 24

R² = 0,0756

TURI STATION, INER 24
Annual Cycle Mean: 2016, 2017, 2018
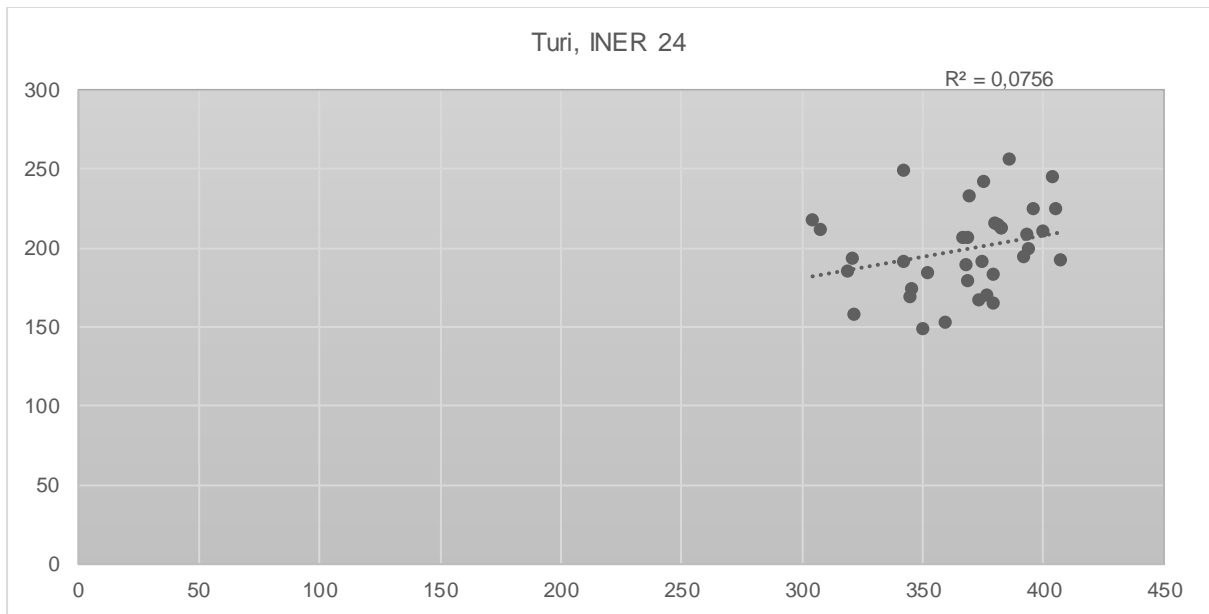
Belisario Station
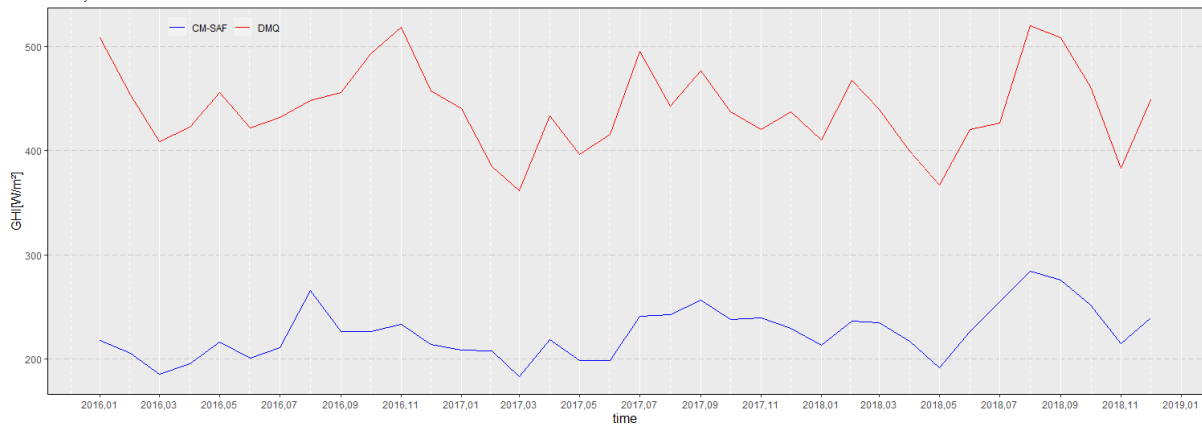

BELISARIO STATION, DMQ 1
Solar Global Radiation, 2016, 2017, 2018
Daily Scale

Belisario, DMQ 1   R² = 0,523

BELISARIO STATION, DMQ 1
Solar Global Radiation, 2016, 2017, 2018
Monthly Scale

Belisario, DMQ 1

R² = 0,6069

BELISARIO STATION, DMQ 1
Annual Cycle Mean: 2016, 2017, 2018
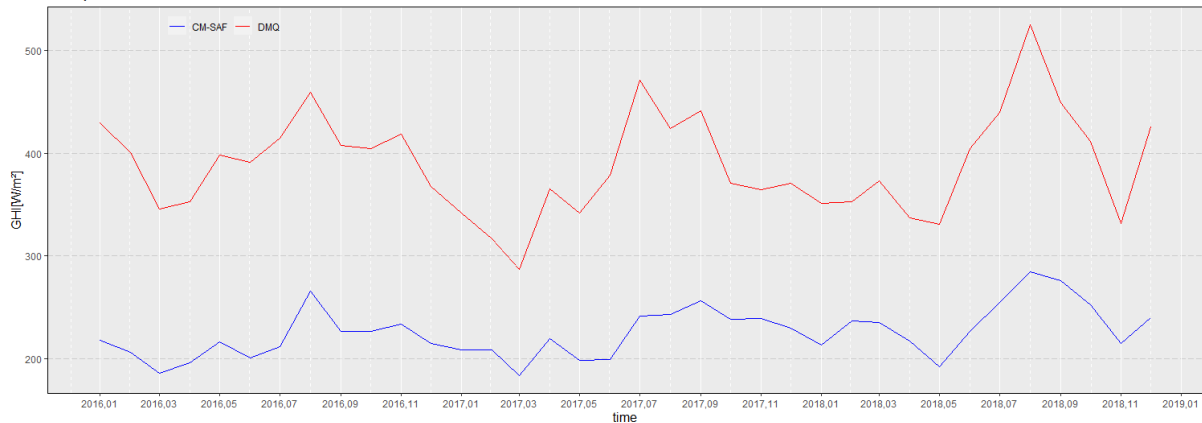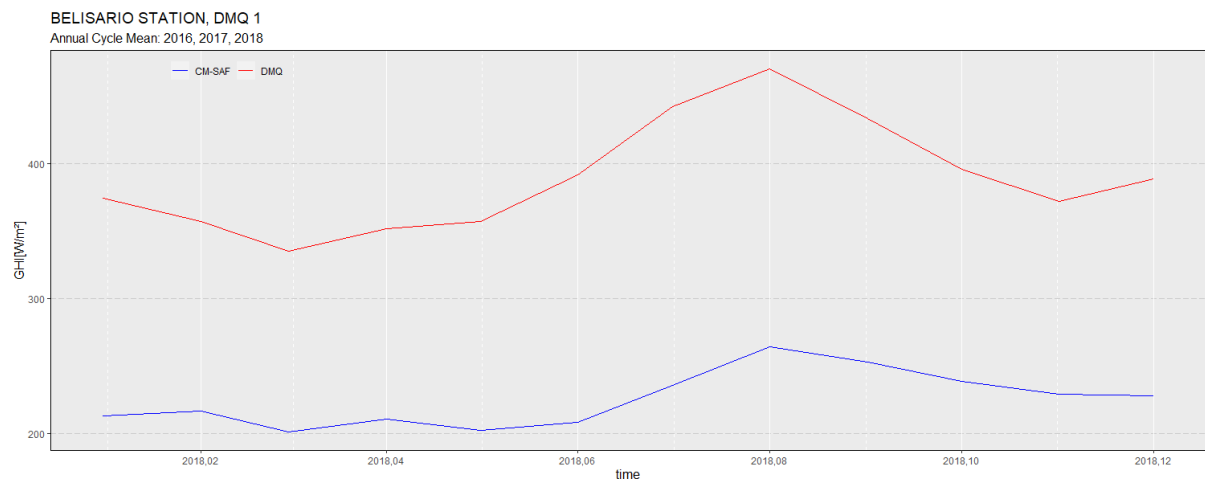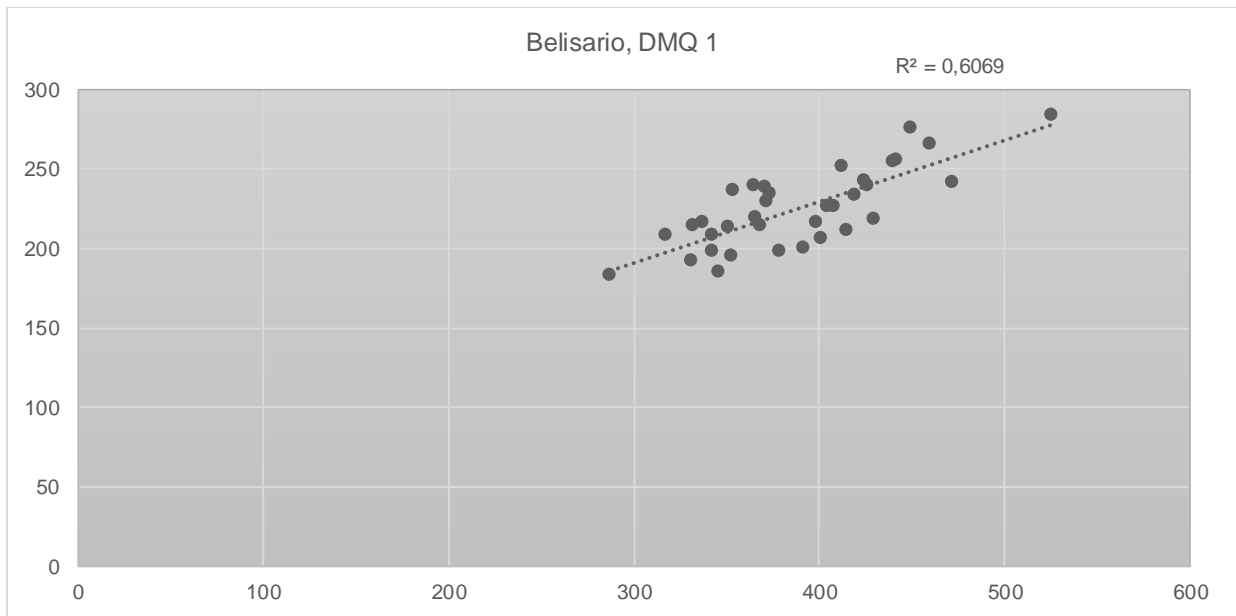
Carapungo Station

CARAPUNGO STATION, DMQ 2
Solar Global Radiation, 2016, 2017, 2018
Daily Scale
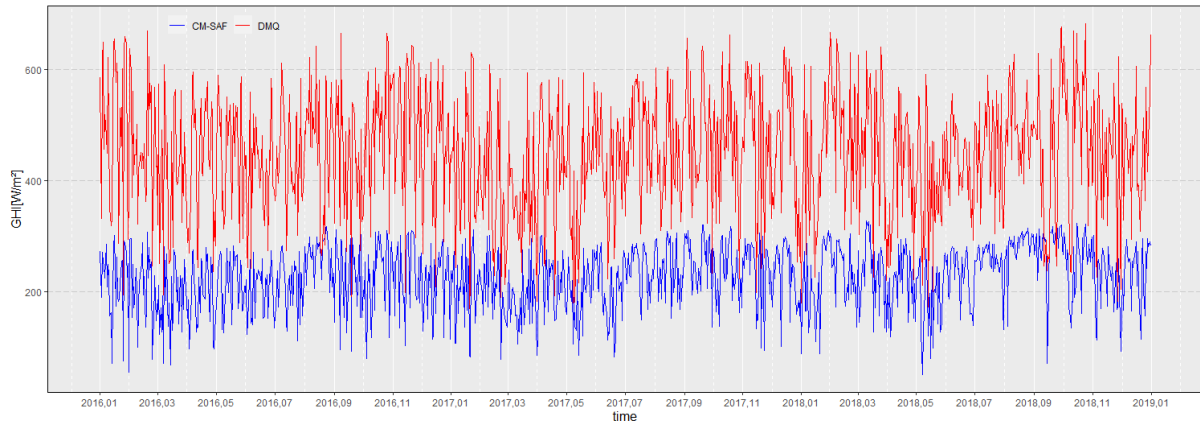
Carapungo, DMQ 2

R² = 0,498

CARAPUNGO STATION, DMQ 2
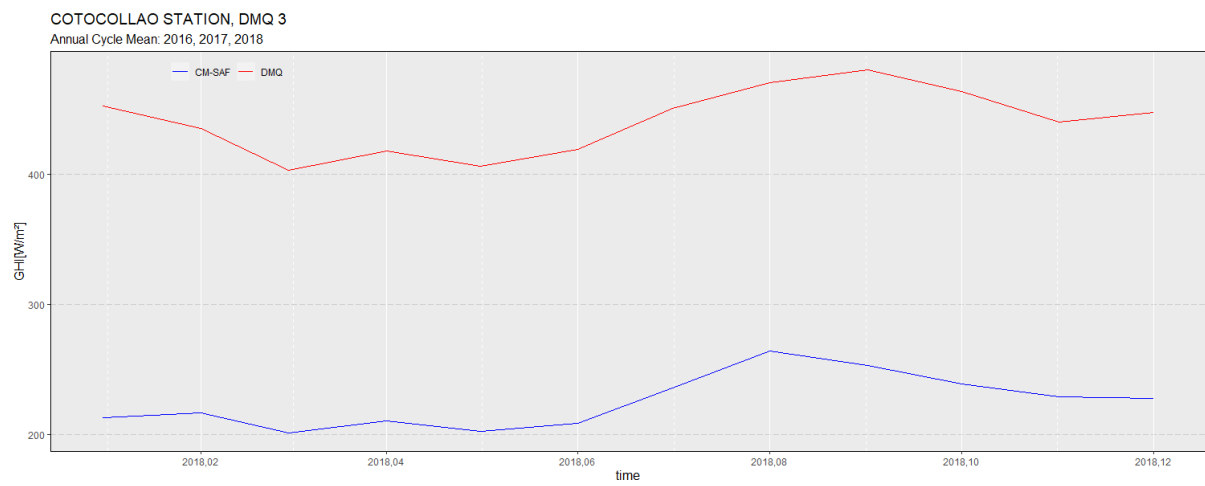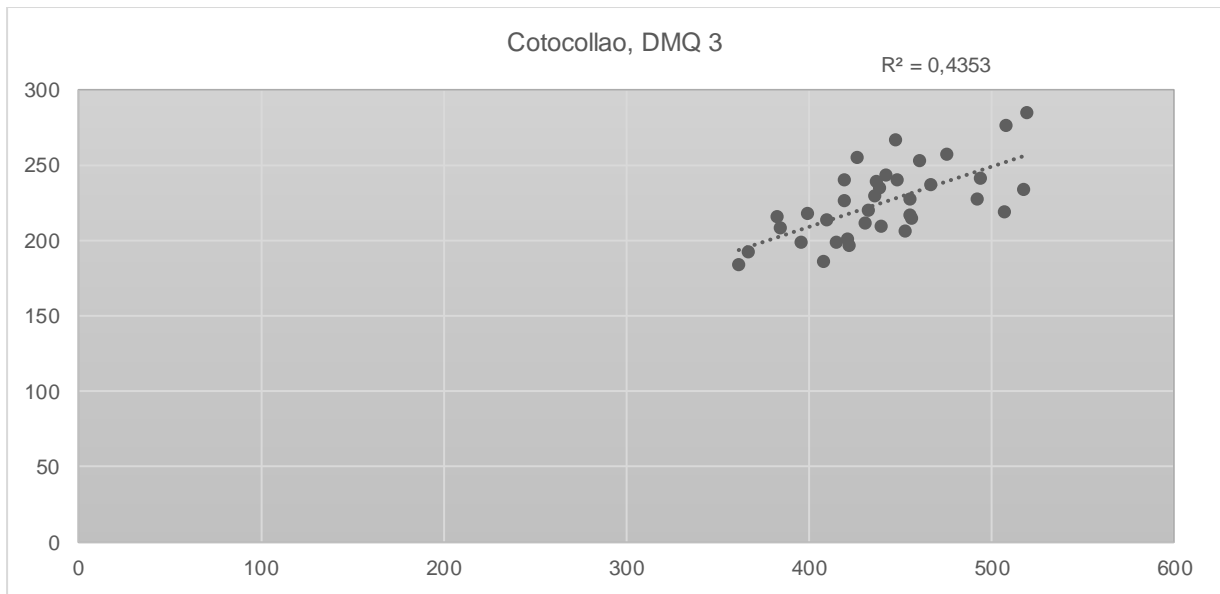Solar Global Radiation, 2016, 2017, 2018
Monthly Scale

Carapungo, DMQ 2

R² = 0,4171

CARAPUNGO STATION, DMQ 2
Annual Cycle Mean: 2016, 2017, 2018

CM-SAF — DMQ

GHI[W/m²]

time
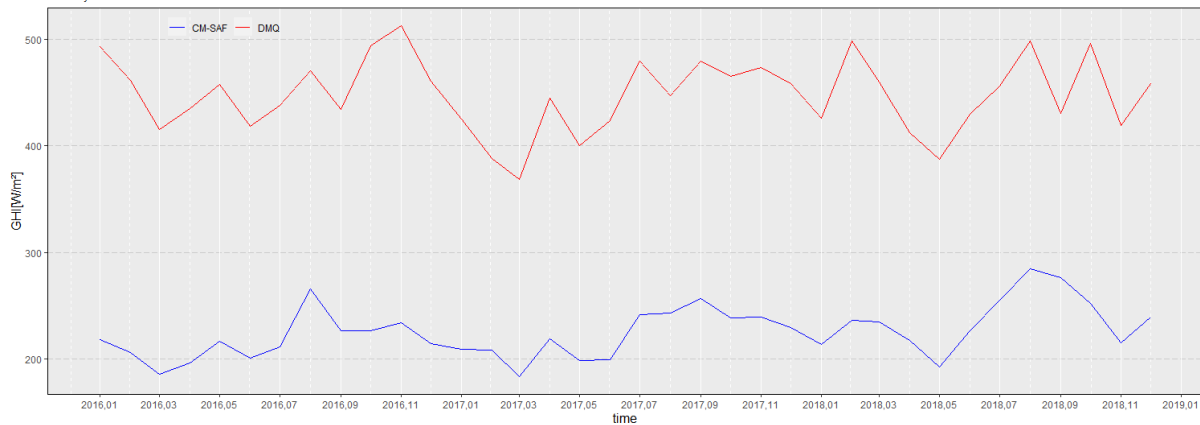
Cotocollao Station

COTOCOLLAO STATION, DMQ 3
Solar Global Radiation, 2016, 2017, 2018
Daily Scale
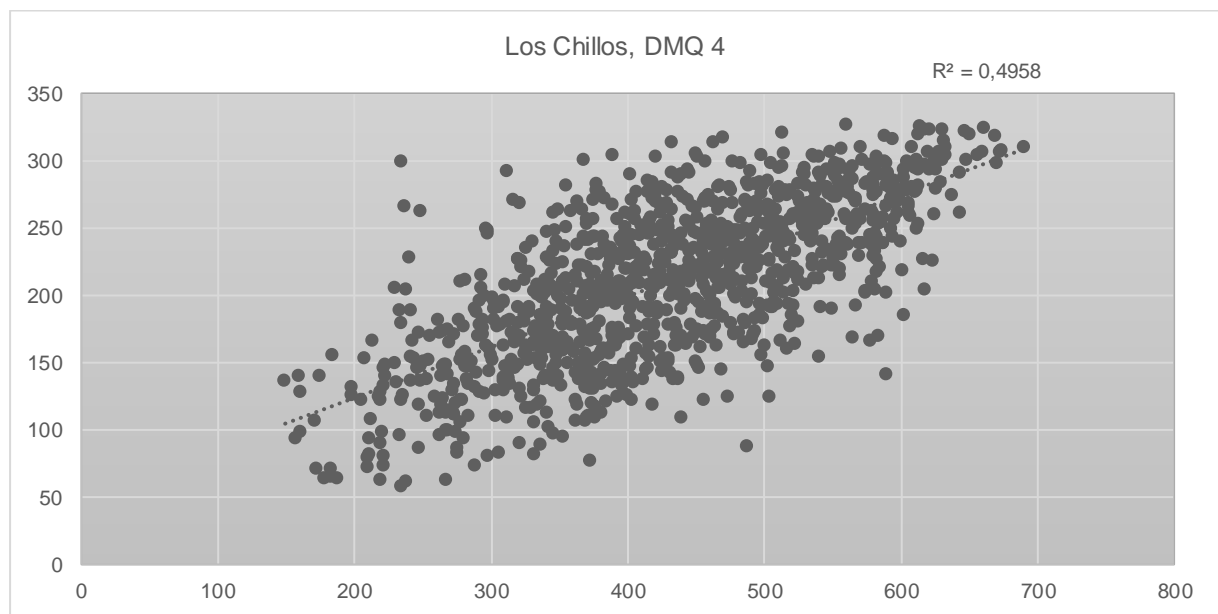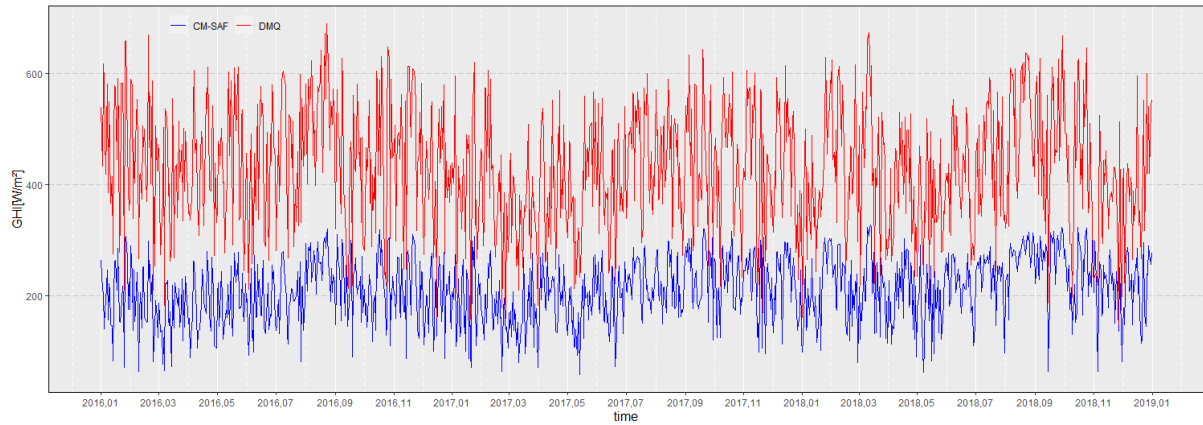

Cotocollao, DMQ 3

R² = 0,4443

COTOCOLLAO STATION, DMQ 3
Solar Global Radiation, 2016, 2017, 2018
Monthly Scale

School of Earth Sciences, Energy and Environment   Yachay Tech University

Cotocollao, DMQ 3

R² = 0,4353

COTOCOLLAO STATION, DMQ 3
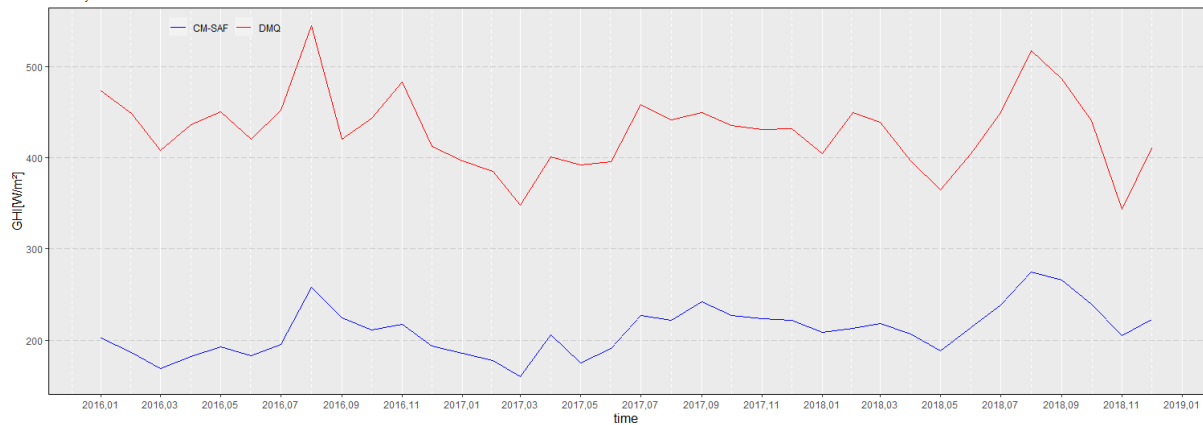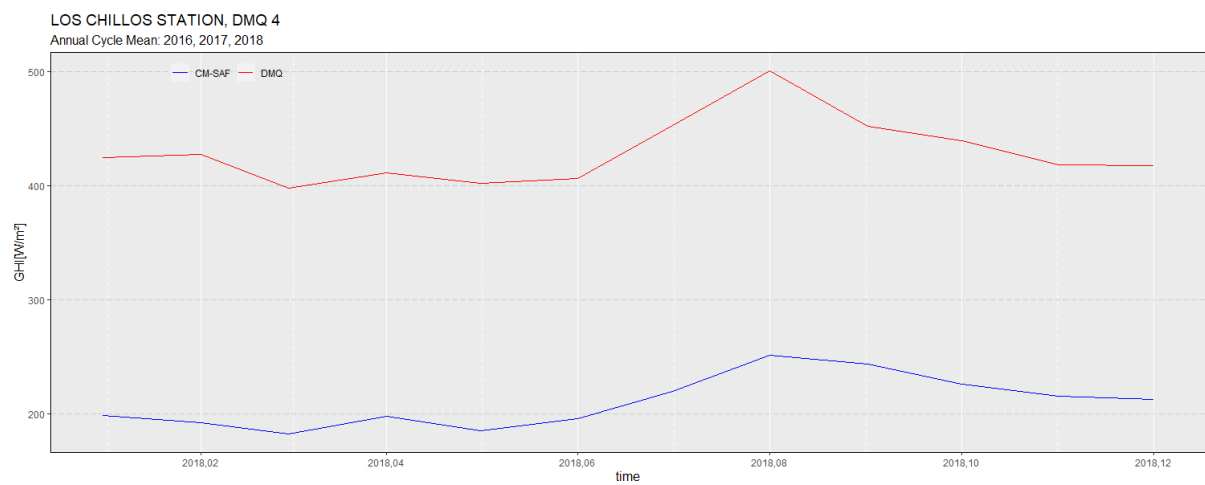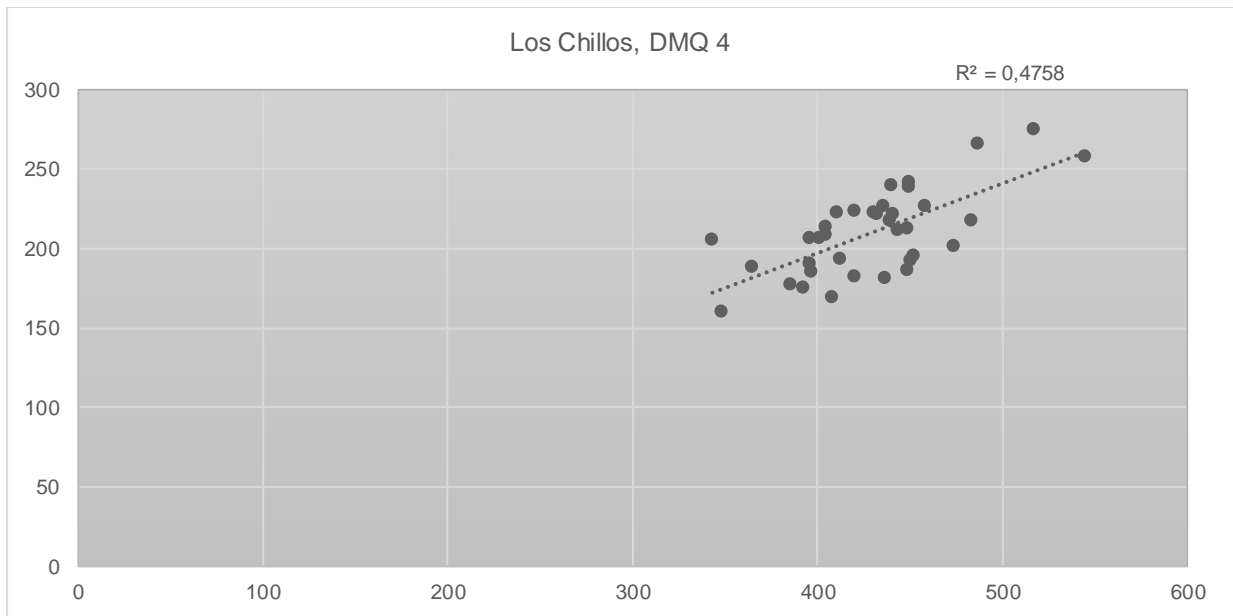Annual Cycle Mean: 2016, 2017, 2018

Los Chillos Station

LOS CHILLOS STATION, DMQ 4
Solar Global Radiation, 2016, 2017, 2018
Daily Scale

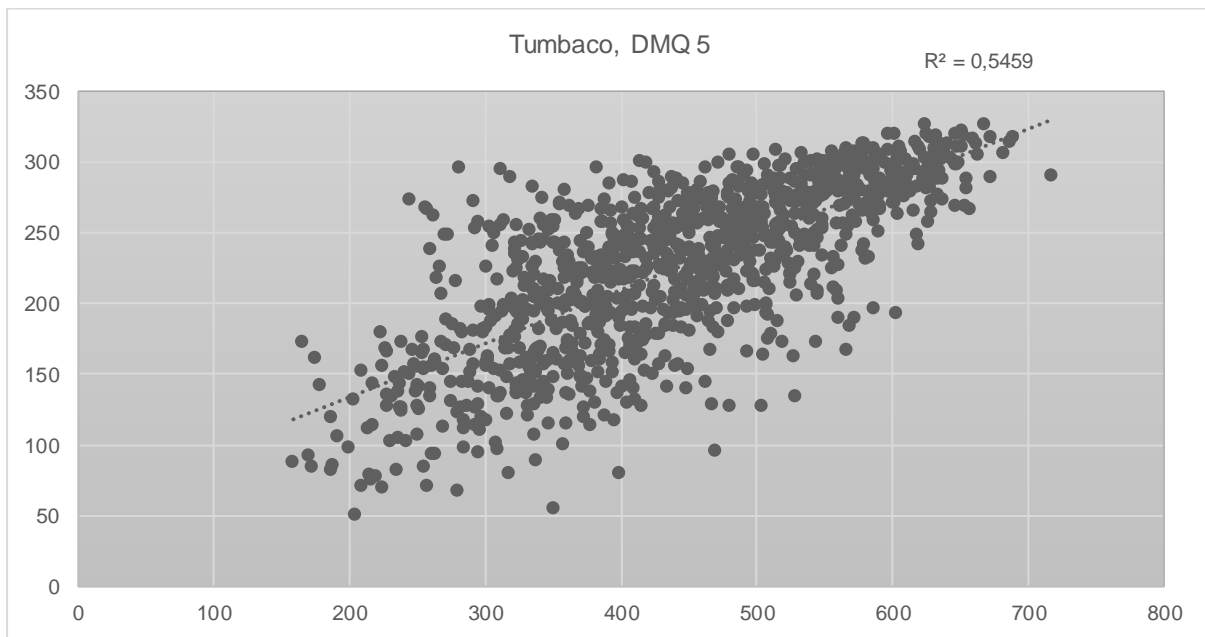

Los Chillos, DMQ 4

R² = 0,4958
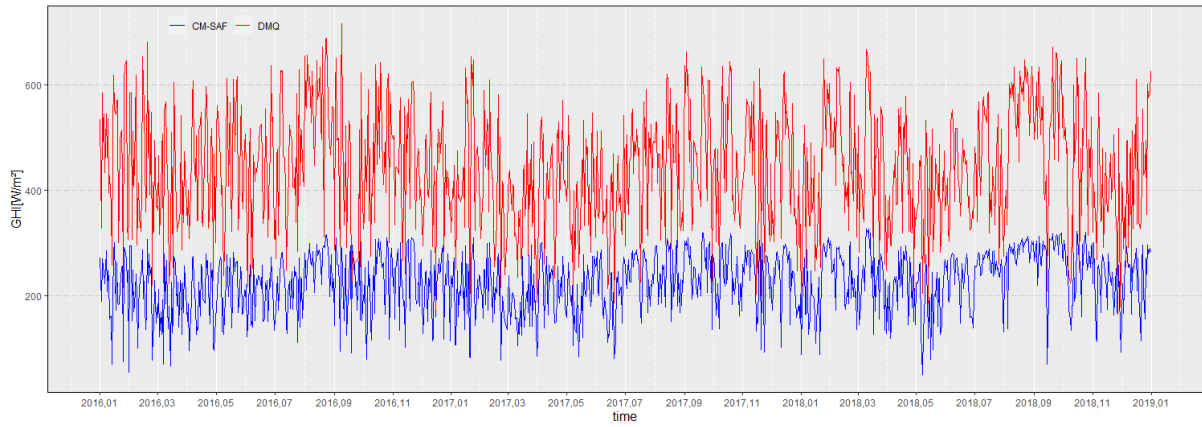

LOS CHILLOS STATION, DMQ 4
Solar Global Radiation, 2016, 2017, 2018
Monthly Scale

Los Chillos, DMQ 4

R² = 0,4758

LOS CHILLOS STATION, DMQ 4
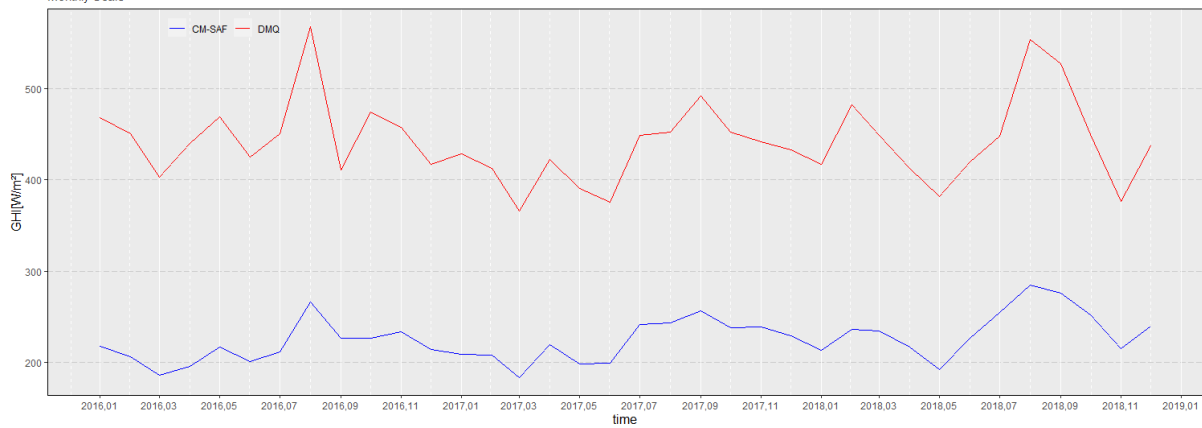Annual Cycle Mean: 2016, 2017, 2018

Tumbaco Station

TUMBACO STATION, DMQ 5
Solar Global Radiation, 2016, 2017, 2018
Daily Scale

Tumbaco, DMQ 5

R² = 0,5459

TUMBACO STATION, DMQ 5
Solar Global Radiation, 2016, 2017, 2018
Monthly Scale

Tumbaco, DMQ 5

R² = 0,6508

TUMBACO STATION, DMQ 5
Annual Cycle Mean: 2016, 2017, 2018
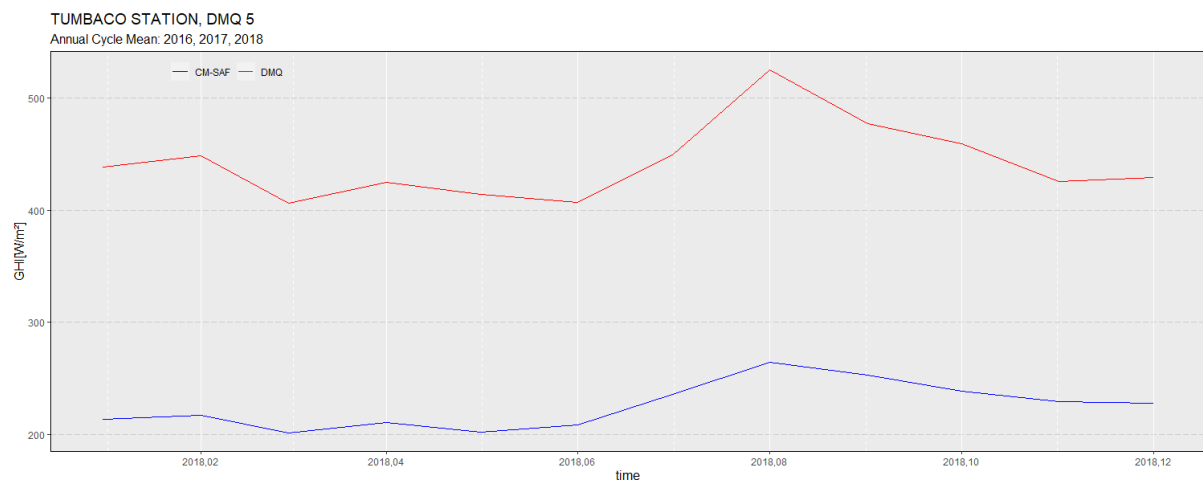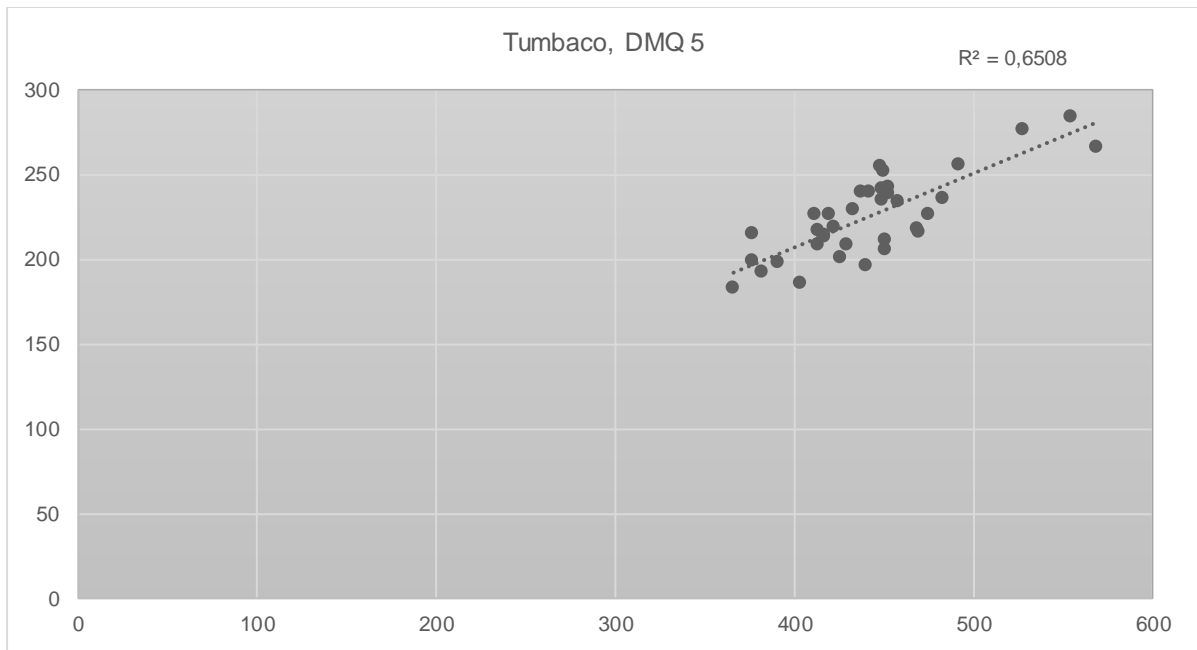
Annex 4

Solar radiation maps of each month of Ecuador

Surface Downwelling Shortwave Radiation (January)

Galapagos

Surface Downwelling Shortwave Radiation (February)

Galapagos

Surface Downwelling Shortwave Radiation (March)

Galapagos

Surface Downwelling Shortwave Radiation (April)

Galapagos

Surface Downwelling Shortwave Radiation (May)

Galapagos

Surface Downwelling Shortwave Radiation (June)
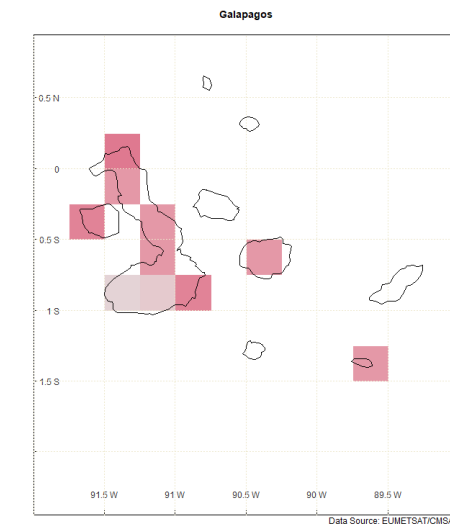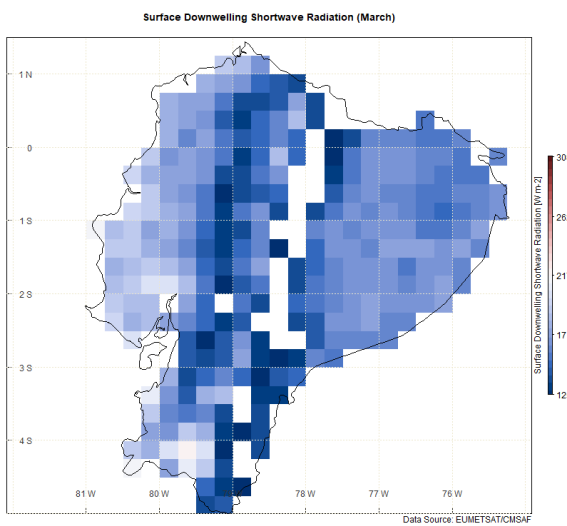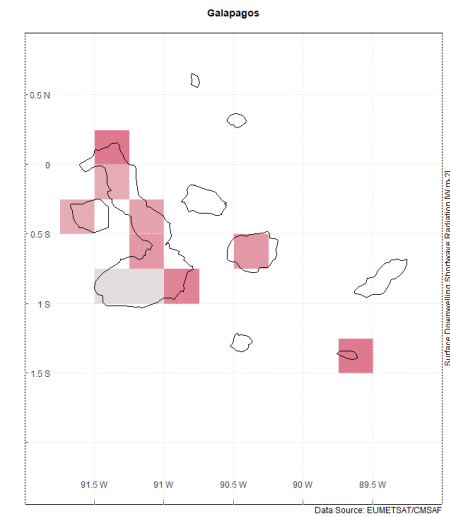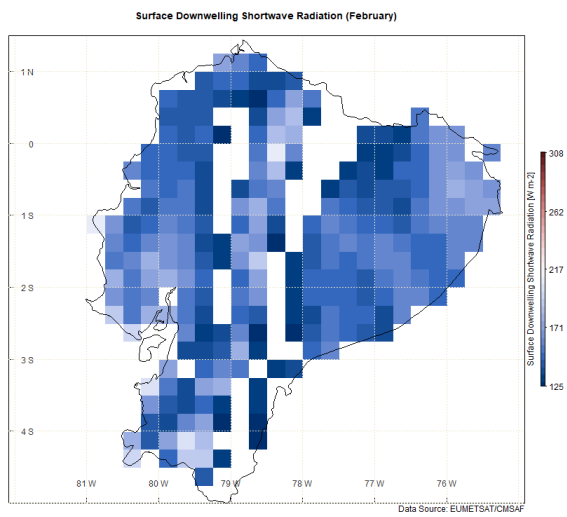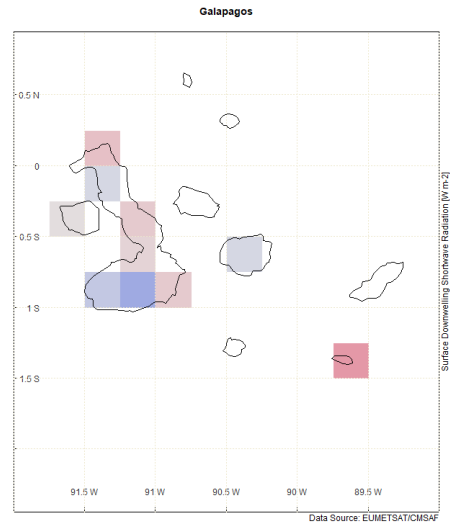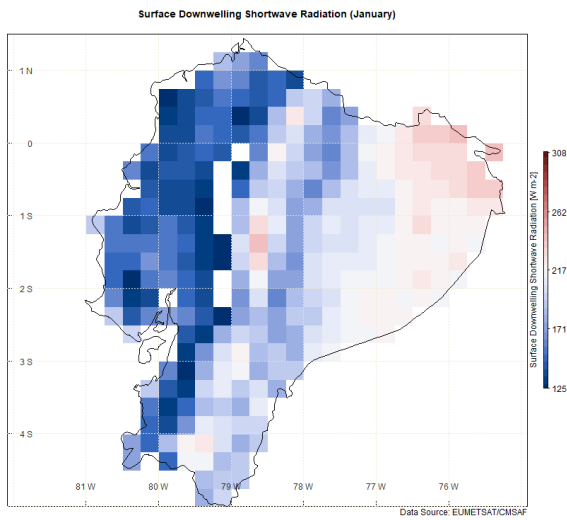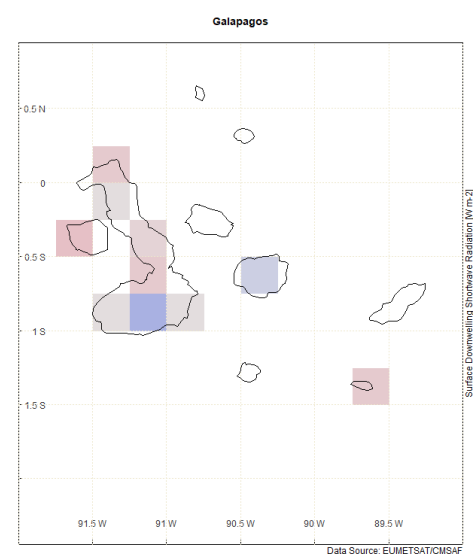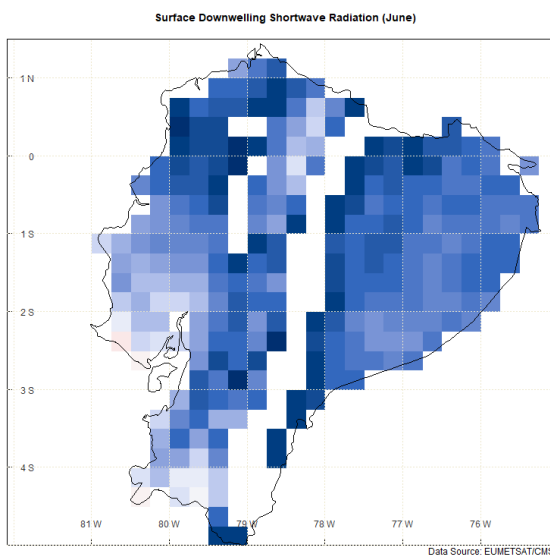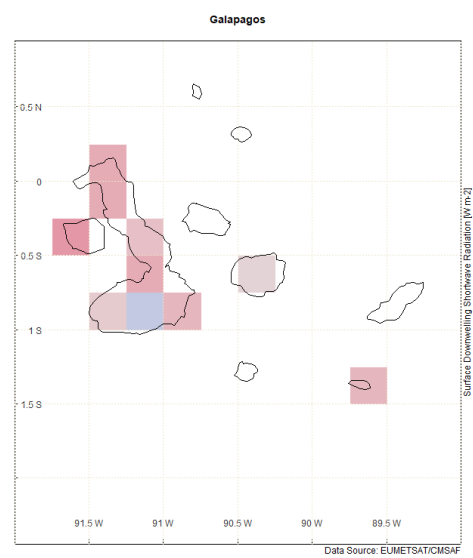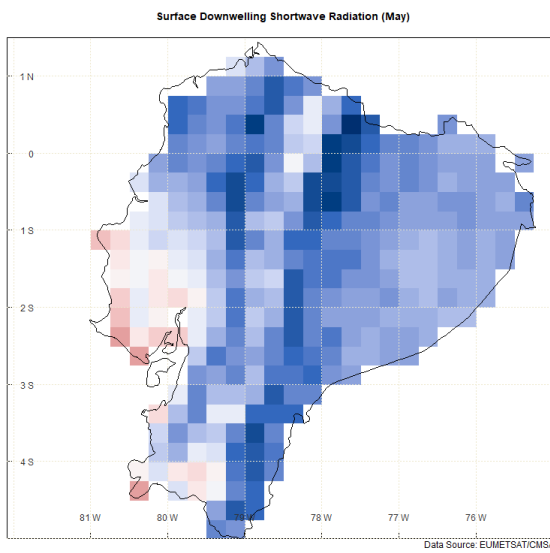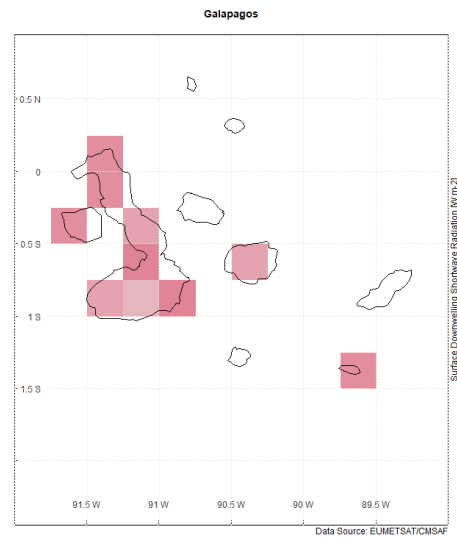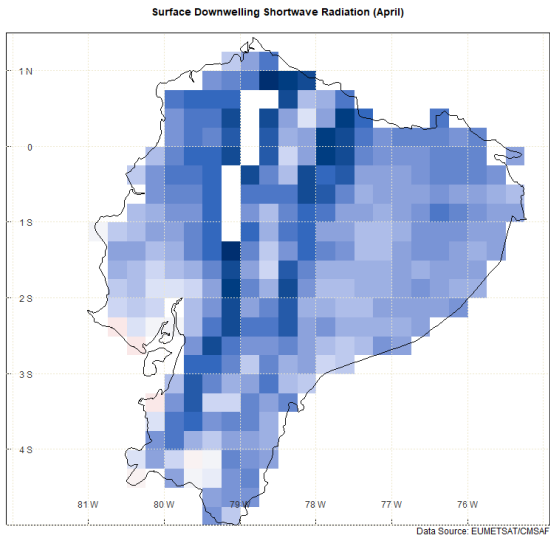
Galapagos

Surface Downwelling Shortwave Radiation (July)
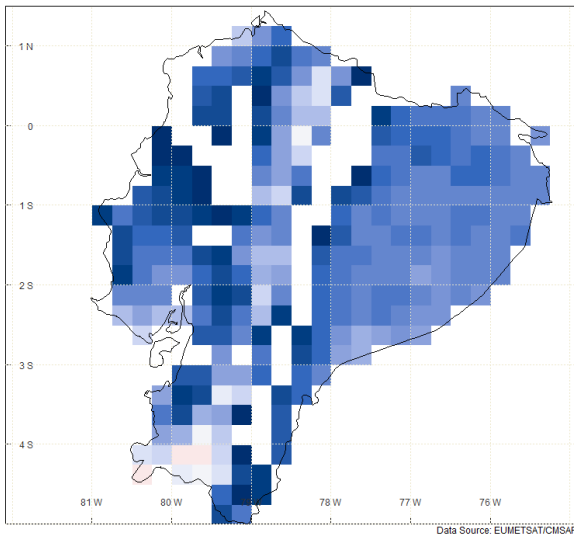
Galapagos
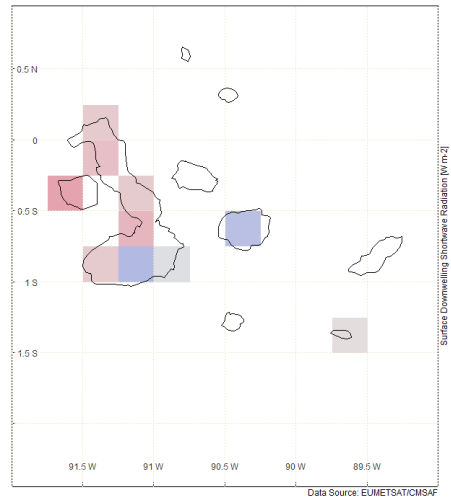
Surface Downwelling Shortwave Radiation (August)
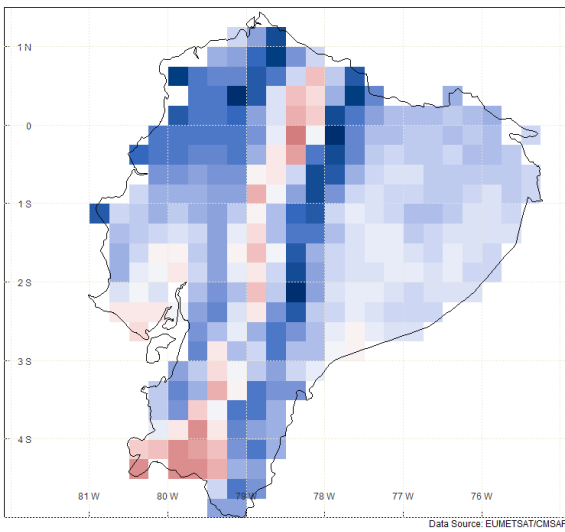
Galapagos
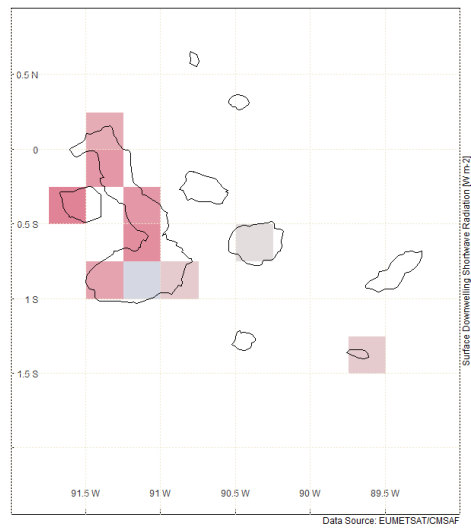
Surface Downwelling Shortwave Radiation (September)
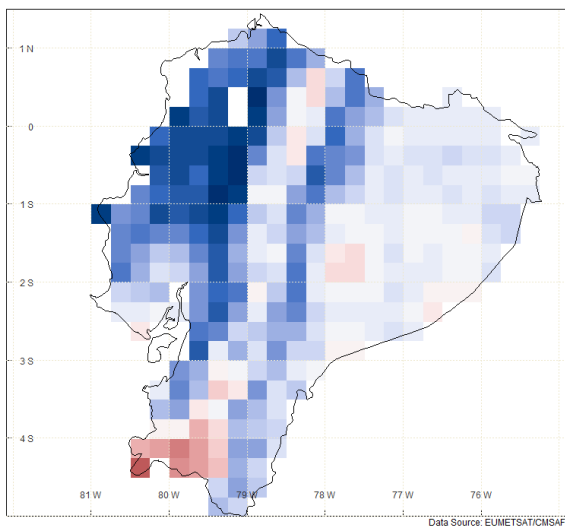
Galapagos
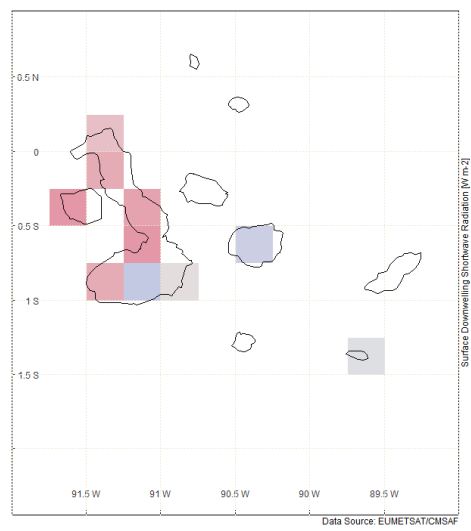
Surface Downwelling Shortwave Radiation (October)
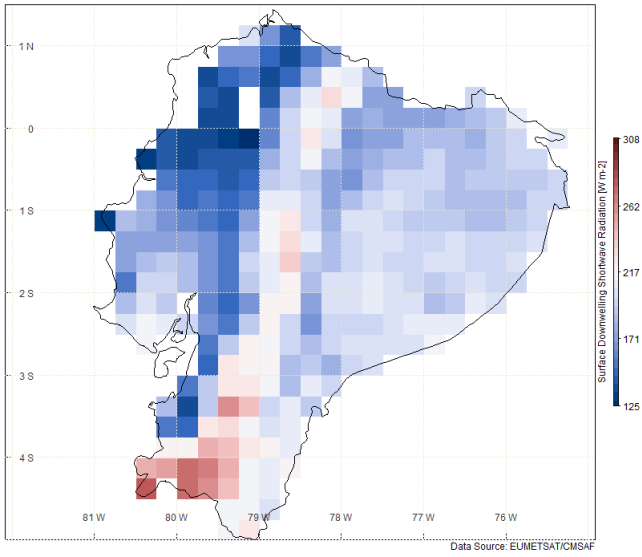
Galapagos
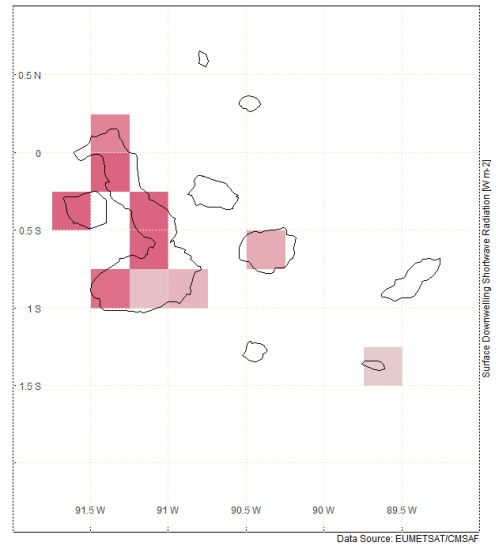
Surface Downwelling Shortwave Radiation (November)
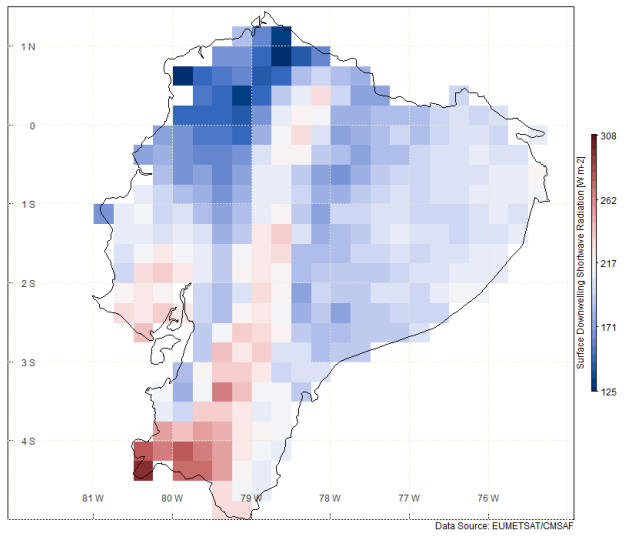
Galapagos
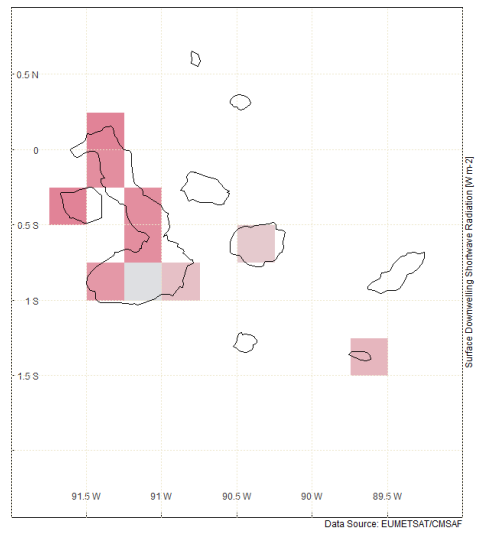
Surface Downwelling Shortwave Radiation (December)
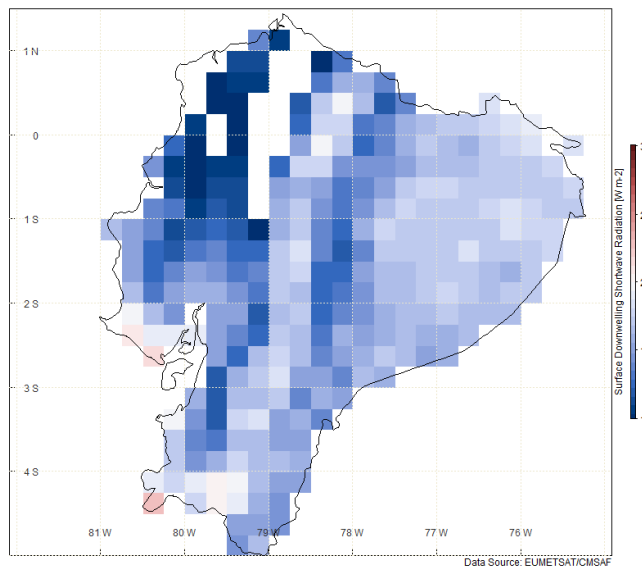
Galapagos
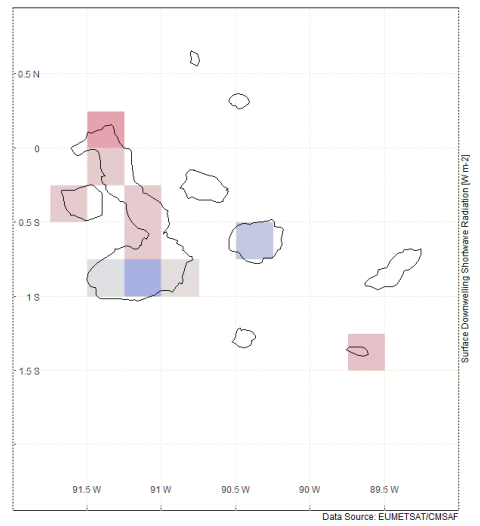
ANNEX 5

Results of statistical comparison of each year for INER and DMQ stations

Station	Year	D/M	RMSE	RMSE%	MBE	MBE%	R	R2	KS indicator
BAÑOS	2016	D	171.826	48.952	-157.497	-44.870	0.567	0.321	0.354
		M	156.267	44.799	-157.497	-44.870	0.879	0.773	0.536
	2017	D	170.032	50.531	-154.097	-45.796	0.521	0.271	0.388
		M	149.786	45.205	-154.097	-45.796	0.323	0.104	0.126
	2018	D	184.847	50.797	-172.491	-47.401	0.557	0.310	0.514
		M	171.568	47.250	-172.491	-47.401	0.826	0.682	0.869
ALTILLO	2016	D	178.639	48.915	-162.769	-44.570	0.515	0.265	0.030
		M	163.202	44.873	-162.769	-44.570	0.706	0.499	0.869
	2017	D	186.412	51.093	-170.802	-46.815	0.471	0.222	0.010
		M	169.654	46.856	-170.802	-46.815	0.183	0.033	0.256
	2018	D	182.187	50.273	-159.856	-44.111	0.328	0.108	0.354
		M	168.378	46.218	-159.856	-44.111	-0.328	0.107	0.869
TIXAN PISTILLI	2016	D	212.301	54.319	-197.327	-50.488	0.210	0.044	0.030
		M	196.551	50.571	-197.327	-50.488	0.515	0.265	0.536
	2017	D	200.580	53.385	-185.568	-49.390	0.284	0.081	0.023
		M	185.414	49.583	-185.568	-49.390	0.260	0.068	0.256
	2018	D	205.838	54.609	-187.636	-49.780	0.149	0.022	0.430
		M	188.937	49.783	-187.636	-49.780	-0.093	0.009	0.833
SANTA ANA	2016	D	210.785	56.751	-199.186	-53.628	0.493	0.243	0.009
		M	200.102	54.053	-199.186	-53.628	0.759	0.576	0.536
	2017	D	209.282	55.726	-200.300	-53.335	0.580	0.336	0.101

		M	197.400	53.029	-200.300	-53.335	0.726	0.527	0.256
	2018	D	208.009	56.123	-190.719	-51.458	0.256	0.065	0.125
		M	188.129	51.107	-190.719	-51.458	0.598	0.358	0.869
YANUNCAY	2016	D	214.854	57.240	-203.398	-54.188	0.538	0.289	0.015
		M	202.488	54.355	-203.398	-54.188	0.724	0.525	0.536
	2017	D	210.194	56.135	-199.188	-53.196	0.542	0.294	0.144
		M	197.324	53.047	-199.188	-53.196	0.743	0.552	0.256
	2018	D	199.543	52.351	-186.645	-48.967	0.456	0.208	0.944
		M	178.912	48.347	-186.645	-48.967	0.823	0.678	0.600
EL VECINO	2016	D	206.144	52.407	-190.923	-48.537	0.262	0.069	0.098
		M	190.210	48.555	-190.923	-48.537	0.676	0.457	0.869
	2017	D	202.491	52.874	-188.783	-49.295	0.313	0.098	0.031
		M	188.314	49.369	-188.783	-49.295	0.306	0.093	0.256
	2018	D	194.176	51.151	-178.042	-46.901	0.317	0.100	0.157
		M	177.512	46.946	-178.042	-46.901	0.590	0.348	0.536
IRQUIS	2016	D	205.077	55.281	-191.239	-51.551	0.385	0.148	0.001
		M	190.484	51.584	-191.239	-51.551	0.893	0.797	0.536
	2017	D	208.930	55.096	-197.471	-52.075	0.489	0.239	0.031
		M	195.088	51.858	-197.471	-52.075	0.720	0.518	0.256
	2018	D	194.953	51.868	-180.424	-48.003	0.362	0.131	0.313
		M	178.955	47.832	-180.424	-48.003	0.865	0.747	0.536
QUINGEO	2016	D	207.744	53.875	-193.042	-50.062	0.214	0.046	0.000
		M	193.870	50.425	-193.042	-50.062	0.561	0.315	0.256
	2017	D	202.588	53.631	-189.926	-50.279	0.307	0.095	0.000
		M	183.986	49.023	-189.926	-50.279	0.340	0.116	0.211
	2018	D	168.990	45.069	-153.062	-40.821	0.336	0.113	0.000
		M	153.088	40.991	-153.062	-40.821	0.624	0.389	0.256
CUMBE	2016	D	197.898	53.071	-182.649	-48.982	0.379	0.144	0.081
		M	182.230	49.099	-182.649	-48.982	0.830	0.690	0.869

	2017	D	197.463	53.450	-186.138	-50.385	0.500	0.250	0.120
		M	184.405	50.230	-186.138	-50.385	0.564	0.318	0.536
	2018	D	196.440	53.699	-183.221	-50.085	0.388	0.151	0.521
		M	183.216	50.160	-183.221	-50.085	0.661	0.437	0.536
SAN JOAQUIN	2016	D	180.257	51.626	-161.674	-46.304	0.324	0.105	0.009
		M	160.845	46.353	-161.674	-46.304	0.614	0.377	0.536
	2017	D	193.376	54.054	-173.985	-48.633	0.444	0.197	0.120
		M	179.806	49.988	-173.985	-48.633	0.309	0.095	0.256
	2018	D	161.730	47.500	-143.496	-42.145	0.431	0.186	0.463
		M	142.057	41.982	-143.496	-42.145	0.764	0.584	0.869
SAYAUSI	2016	D	188.228	50.523	-170.077	-45.651	0.344	0.118	0.116
		M	169.078	45.617	-170.077	-45.651	0.721	0.520	0.869
	2017	D	188.612	51.495	-172.093	-46.985	0.410	0.168	0.100
		M	170.621	47.004	-172.093	-46.985	0.206	0.042	0.256
	2018	D	177.275	49.087	-159.712	-44.224	0.416	0.173	0.269
		M	157.474	44.028	-159.712	-44.224	0.441	0.194	0.869
TURI	2016	D	200.748	53.564	-183.703	-49.016	0.310	0.096	0.002
		M	182.602	49.125	-183.703	-49.016	0.566	0.321	0.536
	2017	D	194.447	52.451	-177.737	-47.944	0.305	0.093	0.000
		M	178.376	48.429	-177.737	-47.944	0.179	0.032	0.100
	2018	D	169.979	46.797	-149.548	-41.173	0.311	0.097	0.003
		M	151.509	41.876	-149.548	-41.173	0.331	0.109	0.536

Station	Year	D/M	RMSE	RMSE%	MBE	MBE%	R	R2	KS indicator
BELISARIO	2016	D	200.002	50.137	-181.876	-45.593	0.686	0.471	0.001
		M	183.236	45.891	-181.876	-45.593	0.850	0.722	0.536
	2017	D	170.400	45.560	-151.821	-40.593	0.755	0.570	0.000
		M	154.812	41.515	-151.821	-40.593	0.797	0.635	0.100
	2018	D	179.671	45.341	-159.336	-40.209	0.756	0.572	0.000
		M	161.519	40.946	-159.336	-40.209	0.905	0.819	0.256
CARAPUNGO	2016	D	252.749	55.284	-239.946	-52.483	0.686	0.470	0.015
		M	241.705	52.845	-239.946	-52.483	0.593	0.351	0.536
	2017	D	227.184	51.903	-215.519	-49.238	0.797	0.636	0.000
		M	216.091	49.398	-215.519	-49.238	0.913	0.833	0.100
	2018	D	225.846	50.449	-210.742	-47.075	0.674	0.454	0.000
		M	212.110	47.405	-210.553	-47.075	0.866	0.751	0.256
COTOCOLLAO	2016	D	256.478	56.212	-239.032	-52.388	0.614	0.377	0.012
		M	240.848	52.817	-239.032	-52.388	0.506	0.256	0.536
	2017	D	224.495	52.249	-207.476	-48.288	0.718	0.515	0.000
		M	207.324	48.408	-207.476	-48.288	0.809	0.654	0.100
	2018	D	219.253	49.952	-201.993	-46.020	0.718	0.515	0.000
		M	202.019	46.163	-201.993	-46.020	0.930	0.865	0.256
LOS CHILLOS	2016	D	260.174	57.855	-248.167	-55.185	0.722	0.522	0.001
		M	249.330	55.485	-248.167	-55.185	0.767	0.589	0.256
	2017	D	220.532	53.312	-208.816	-50.480	0.748	0.560	0.000
		M	209.397	50.604	-208.816	-50.480	0.952	0.906	0.100
	2018	D	216.030	50.776	-200.820	-47.201	0.722	0.521	0.000
		M	202.708	47.651	-200.820	-47.201	0.891	0.793	0.256
TUMBACO	2016	D	250.017	55.193	-235.746	-52.043	0.708	0.501	0.006
		M	237.706	52.486	-235.746	-52.043	0.806	0.649	0.536
	2017	D	216.009	50.709	-203.789	-47.840	0.778	0.606	0.000
		M	204.846	48.041	-203.789	-47.840	0.956	0.914	0.100

2018	D	223.505	50.095	-209.230	-46.896	0.768	0.589	0.000
	M	211.476	47.384	-209.230	-46.896	0.915	0.837	0.256

ANNEX 6

Annual averages of statistical comparison for each station

Station	D/M	RMSE	RMSE%	MBE	MBE%	R	R2	KS
BAÑOS	D	175.568	50.093	-161.362	-46.022	0.552	0.304	0.418
	M	159.207	45.751	-161.362	-46.022	0.767	0.589	0.510
ALTILLO	D	182.413	50.094	-164.475	-45.165	0.439	0.193	0.131
	M	167.078	45.983	-164.475	-45.165	0.233	0.054	0.665
TIXAN PISTILLI	D	206.239	54.104	-190.177	-49.886	0.221	0.049	0.161
	M	190.300	49.979	-190.177	-49.886	0.172	0.030	0.541
SANTA ANA	D	209.359	56.200	-196.735	-52.807	0.442	0.195	0.078
	M	195.210	52.730	-196.735	-52.807	0.663	0.439	0.554
YANUNCAY	D	208.197	55.242	-196.410	-52.117	0.533	0.284	0.367
	M	192.908	51.916	-196.410	-52.117	0.670	0.449	0.464
EL VECINO	D	200.937	52.144	-185.916	-48.244	0.297	0.088	0.095
	M	185.345	48.290	-185.916	-48.244	0.532	0.283	0.554
IRQUIS	D	202.987	54.082	-189.711	-50.543	0.410	0.168	0.115
	M	188.176	50.425	-189.711	-50.543	0.784	0.615	0.443
QUINGEO	D	193.107	50.858	-178.677	-47.054	0.261	0.068	0.000
	M	176.982	46.813	-178.677	-47.054	0.333	0.111	0.241
CUMBE	D	197.267	53.407	-184.002	-49.817	0.422	0.178	0.241
	M	183.284	49.830	-184.002	-49.817	0.709	0.503	0.647
SAN JOAQUIN	D	178.454	51.060	-159.718	-45.694	0.387	0.150	0.198
	M	160.903	46.108	-159.718	-45.694	0.327	0.107	0.554
SAYAUSI	D	184.705	50.368	-167.294	-45.620	0.221	0.049	0.162
	M	165.724	45.550	-167.294	-45.620	0.172	0.030	0.665
TURI	D	188.391	50.937	-170.329	-46.044	0.293	0.086	0.002
	M	170.829	46.477	-170.329	-46.044	0.275	0.076	0.391

STATION	D/M	RMSE%	MBE%	R2	KS
	D	47.013	-42.132	0.537	0.000
BELISARIO	M	42.784	-42.132	0.725	0.297
	D	52.545	-49.599	0.520	0.005
CARAPUNGO	M	49.883	-49.599	0.645	0.297
	D	52.804	-48.899	0.469	0.004
COTOCOLLAO	M	49.129	-48.899	0.592	0.297
	D	53.981	-50.955	0.534	0.000
LOS CHILLOS	M	51.247	-50.955	0.763	0.204
	D	51.999	-48.926	0.566	0.002
TUMBACO	M	49.303	-48.926	0.800	0.297